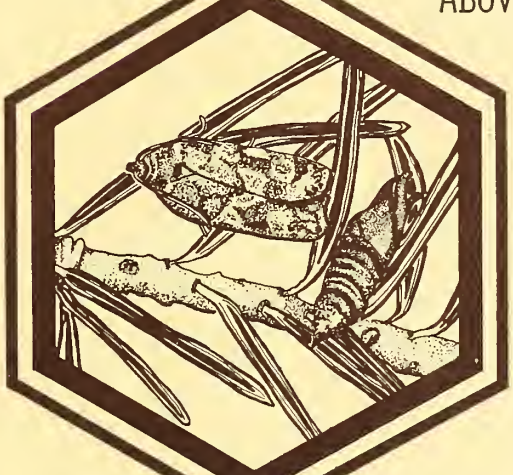

PREDICTION OF SPRAY BEHAVIOR ABOVE AND WITHIN A FOREST CANOPY

SPECIAL REPORT

DECEMBER 1977

Methods Application Group
Forest Insect and Disease Management
Forest Service, USDA
Davis, California

PREFACE

This material is reproduced with the permission of the USDA Expanded Douglas-fir Tussock Moth Research and Development Program, which provided funding for this study.

John W. Barry, USDA Forest Service Forest Insect and Disease Management (FI&DM) Methods Application Group; Bruce Grim, U.S. Army Dugway Proving Ground; and Robert Ekblad, USDA Forest Service Missoula Equipment Development Center, provided technical assistance during this study. John W. Barry provided FI&DM pilot project data for model validation and field notes.

DISCLAIMER STATEMENTS

The use of trade, firm, or corporation names is for the information and convenience of the reader. Such use does not constitute an official evaluation, conclusion, recommendation, endorsement, or approval of any produce or service to the exclusion of others which may be suitable.

This publication reports research involving pesticides. It does not contain recommendations for their use, nor does it imply that the uses discussed here have been registered. All uses of pesticides must be registered by appropriate state and/or federal agencies before they can be recommended.

TR-77-308-01

PREDICTION OF SPRAY BEHAVIOR ABOVE AND WITHIN A FOREST CANOPY

Prepared by

R. K. Dumbauld, J. E. Rafferty and J. R. Bjorklund

December 1977

Prepared for

U. S. DEPARTMENT OF AGRICULTURE
FOREST SERVICE
Pacific N. W. Forest and Range Experiment Station
P. O. Box 3141
Portland, Oregon 97208

Contract No. 19-276

H. E. CRAMER COMPANY, INC.
University of Utah Research Park
P. O. Box 8049
Salt Lake City, Utah 84108

TABLE OF CONTENTS

SECTION 1
INTRODUCTION

1.1 BACKGROUND

A major activity of the U. S. Forest Service is the use of aerial spray applications to control the tussock moth, spruce budworm and other forest defoliators. In recent years, the types of spray materials and spray application methods that may be used by the Forest Service have been constrained by regulations and requirements for precluding adverse environmental effects. The Douglas-Fir Tussock Moth Research Program (DFTM) was chartered by the USDA in 1974 to use all available technology to reduce losses caused by the Douglas-fir tussock moth and to develop and evaluate new short- and long-term forest and pest management systems designed to prevent or suppress infestations. Under this charter, DFTM has sponsored programs to evaluate the effectiveness of aerially applied insecticides in control projects and to determine the extent of insecticidal drift beyond the sprayed areas. Although forest spray operations and pilot projects have been carried out for many years, quantitative generalizations of the results of these activities have proved to be difficult. The principal difficulty stems from the inherent complexity of spray behavior and the many factors that must be taken into account when comparing the results from different projects and when evaluating basic relationships among the various factors affecting the results from individual projects. Because mathematical dispersion models are potentially very useful in determining the interactions of the many factors affecting spray behavior, DFTM contracted with the H. E. Cramer Company to study the effectiveness of models in predicting spray behavior above and within the forest canopy.

1.2 STUDY OBJECTIVES AND PURPOSE

The principle objectives of this study were to:

- Begin construction of a technical data base that can be used to evaluate and improve aerial spray applications for controlling the Douglas-fir tussock moth and spruce budworm, using data from selected pilot spray projects including the 1976 Region 1 Pilot Project data

- Use the existing data base in refining and adapting existing mathematical models, including the Grim-Barry Model (Grim and Barry, 1975) to predict spray behavior above and within the forest canopy

- Use the mathematical models of spray dispersion, deposition and drift to evaluate the results of measurements made during the 1976 Region 1 Pilot Project and to demonstrate the potential usefulness of these modeling techniques

The Forest Service supplied the data listed in Table 1-1 for use in the study. The decision was made early in the study, with the concurrence of the Forest Service and DFTM, to limit the research effort to the use of data from the Rennic Creek and the 1976 Region 1 Pilot Projects. This decision was made because the data sets for these projects were most complete and because it had become evident that adaptation of the dispersion and Grim-Barry canopy penetration models for use in the study would require a significant fraction of the total effort under the contract.

This technical report describes the dispersion model, the Grim-Barry canopy penetration model, the procedures used to combine the models in computer programs for predicting deposition and drift from aerial sprays, and the results of applying the models to predict deposition and drift for the Rennic Creek and 1976 Region 1 Pilot Projects.

TABLE 1-1

SPRAY BEHAVIOR DATA SUPPLIED BY THE FOREST SERVICE
FOR USE IN THE STUDY

Date	Project Name	Maps, Charts, Sampling Positions	Forest Description	Spray Deposit Data	Meteorological Data	Aircraft Data
1973	Pine Butterfly Pilot Project	X	X	X	X	
1974	Rennic Creek	X	X	X	X	X
1975	Region 1 Pilot Project (Gallatin/ Beaverhead)	X	X	X	X	
1976	Region 1 Pilot Project (Townsend, Montana)	X	X	X	X	X

1.3 ORGANIZATION OF THE REPORT

Section 2 of the report contains a description of the mathematical models used in the this study for predicting spray behavior in and above the forest canopy. The procedures used in developing model inputs and the inputs used in predicting spray behavior for the Rennic Creek Trials and for Plots 1 through 3 of the 1976 Region 1 Pilot Project are given in Section 3. Section 4 contains a comparison of model estimates with spray measurements and Section 5 provides a summary of results and recommendations for future studies.

SECTION 2

DESCRIPTION OF THE DISPERSION AND CANOPY PENETRATION MODELS

The spray dispersion models described in this section are similar to the aircraft spray models described by Dumbauld, Rafferty and Cramer (1976). These models were developed previously for the U. S. Army Dugway Proving Ground and are based on generalized diffusion models described by Cramer, et al. (1972). We originally planned to use computer programs incorporating the models developed for Dugway in the DFTM research study. After studying the maps showing the complex aircraft spray patterns for the 1976 Region 1 Pilot Programs, we decided that the use of these programs would result in computer calculation costs beyond funds available under the contract. The only practical alternative was to develop a new computer program that, unlike the Dugway Program (which simulates line sources not oriented perpendicular to the mean wind direction by using a large number of volume sources), uses an analytical solution to the line source problem. The new computer program developed under the contract, which contains the models described in Section 2.1, significantly reduces the computation time. Also, we believe the analytical dispersion models developed under the contract represent an important advance in modeling techniques.

A computer program incorporating the Grim-Barry canopy penetration model was supplied to us by Mr. Bruce Grim, Dugway Proving Ground, and by Mr. John Barry, Methods Application Group, U. S. Forest Service. In adapting the Grim-Barry canopy penetration model for use in conjunction with the dispersion models and recoding the program for use on our HP 9640-A Multiprogramming System, we discovered some errors in the original program coding. After consulting with Mr. Grim and Mr. Barry, we made some small changes in the computation procedures used in their program (Grim and Barry, 1975). The basic modeling techniques, which are briefly described in Section 2.2, are unchanged. A description of

the effect of aircraft wake vortices and the techniques used to define the source geometry are given in Section 2.3.

2.1 DRIFT AND DEPOSITION MODELS

The drift and deposition models described below are designed for use with nearly-instantaneous elevated line sources oriented at an arbitrary angle with respect to the mean wind direction. In the models, the axis of the spray cloud is assumed to intersect the ground at a downwind distance from the source that is proportional to the product of the effective release height H' and the mean cloud transport speed $\bar{u}$ divided by the drop settling velocity V_j for the j^{th} drop-size category. The inclination of the cloud axis from the horizontal for a given drop-size category j is thus equal to $\tan^{-1}(V_j/\bar{u})$. It is assumed that drops dispersed upwards by turbulence are totally reflected downwards at the top of the surface mixing layer, but the fraction of drops reflected at the boundary layer represented by the ground is a variable input parameter for each j^{th} category. The models use the Cartesian coordinate system shown in Figure 2-1 for a line source of length L at a height H' and a calculation point at R(ε, δ, z), where H' and z are measured above the top of the canopy when the models are used in conjunction with the canopy penetration model described in Section 2.2.

The model for drift, expressed in terms of dosage units (i.e., mass x time/volume), is given by the following expressions:

$$D_L = \frac{S}{k\,\sigma'_A \sin\theta\,\bar{u}} \sum_{j=1}^{J} f_j \left\{ \sum_{i=0}^{\infty} \left[\gamma_j^{\,i} \left(\frac{\pi}{2Y}\right)^{1/2} \left\{ \exp\left(\frac{O^2}{4Y} - P\right) \right\} \right. \right. \quad (2\text{-}1)$$

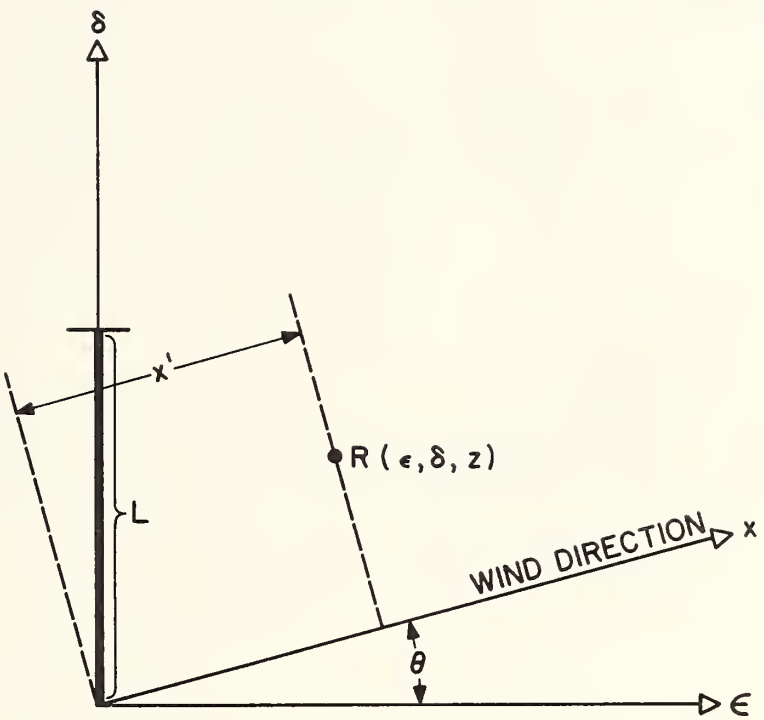

FIGURE 2-1. Schematic diagram showing the line source geometry with respect to a calculation point at R(ϵ, δ, z) and wind direction θ.

$$\left\{\operatorname{erf}\left(Y^{1/2}\left(\frac{k}{a}+\frac{O}{2Y}\right)\right)-\operatorname{erf}\left(Y^{1/2}\left(\frac{k}{b}+\frac{O}{2Y}\right)\right)\right\} \qquad \text{(2-1) (Continued)}$$

$$+\gamma_j^{\,i+1}\left(\frac{\pi}{2Z}\right)^{1/2}\left\{\exp\left(\frac{R^2}{4Z}-P\right)\right\}\left\{\operatorname{erf}\left(Z^{1/2}\left(\frac{k}{a}+\frac{R}{2Z}\right)\right)-\operatorname{erf}\left(Z^{1/2}\left(\frac{k}{b}+\frac{R}{2Z}\right)\right)\right\}\Bigg]$$

$$+\sum_{i=1}^{\infty}\Bigg[\gamma_j^{\,i}\left(\frac{\pi}{2T}\right)^{1/2}\left\{\exp\left(\frac{U^2}{4T}-P\right)\right\}\left\{\operatorname{erf}\left(T^{1/2}\left(\frac{k}{a}+\frac{U}{2T}\right)\right)-\operatorname{erf}\left(T^{1/2}\left(\frac{k}{a}+\frac{U}{2T}\right)\right)\right\}$$

$$+\gamma_j^{\,i-1}\left(\frac{\pi}{2W}\right)^{1/2}\left\{\exp\left(\frac{X}{4W}-P\right)\right\}\left\{\operatorname{erf}\left(W^{1/2}\left(\frac{k}{a}+\frac{X}{2W}\right)\right)-\operatorname{erf}\left(W^{1/2}\left(\frac{k}{b}+\frac{X}{2W}\right)\right)\right\}\Bigg]\Bigg\}$$

where

$$S = Qk/2\pi L \qquad (2\text{-}2)$$

$$Y = \frac{1}{k^2}\left[n-\frac{\delta}{\cos\theta}\right]^2+\left[C+z\right]^2 \qquad (2\text{-}3)$$

$$O = \frac{2^{1/2}}{\sigma_A' k}\left[\frac{k^2 V_j}{\bar{u}}\left(C+z\right)-\left(n-\frac{y}{\cos\theta}\right)\cot\theta\right] \qquad (2\text{-}4)$$

$$P = \left[\frac{kV_j}{2^{1/2}\sigma_A'\,\bar{u}}\right]^2+\left[\frac{\cot\theta}{2^{1/2}\sigma_A'}\right]^2 \qquad (2\text{-}5)$$

$$Z = \frac{1}{k^2}\left[n-\frac{\delta}{\cos\theta}\right]^2+\left[D+z\right]^2 \qquad (2\text{-}6)$$

$$R = -\frac{2^{1/2}}{\sigma'_A k}\left[\frac{k^2 V_j}{\bar{u}}\left(D + z\right) + \left(n - \frac{\delta}{\cos\theta}\right)\cot\theta\right] \qquad (2\text{-}7)$$

$$T = \frac{1}{k^2}\left[n - \frac{\delta}{\cos\theta}\right]^2 + \left[D - z\right]^2 \qquad (2\text{-}8)$$

$$U = -\frac{2^{1/2}}{\sigma'_A k}\left[\frac{k^2 V_j}{\bar{u}}\left(D - z\right) + \left(n - \frac{\delta}{\cos\theta}\right)\cot\theta\right] \qquad (2\text{-}9)$$

$$W = \frac{1}{k^2}\left[n - \frac{\delta}{\cos\theta}\right]^2 + \left[C - z\right]^2 \qquad (2\text{-}10)$$

$$X = \frac{2^{1/2}}{\sigma'_A k}\left[\frac{k^2 V_j}{\bar{u}}\left(C - z\right) - \left(n - \frac{\delta}{\cos\theta}\right)\cot\theta\right] \qquad (2\text{-}11)$$

$$C = 2iH_m - H' - \left(V_j x_V/\bar{u}\right) \qquad (2\text{-}12)$$

$$D = 2iH_m + H' + \left(V_j x_V/\bar{u}\right) \qquad (2\text{-}13)$$

$$a = 2^{1/2}\,\sigma'_A\left(x' + x_V - \ell\,\sin\theta\right) \qquad (2\text{-}14)$$

$$b = 2^{1/2}\,\sigma'_A\left(x' + x_V\right) \qquad (2\text{-}15)$$

$$n = \left(x' + x_V\right)\cot\theta + x'\tan\theta = \left(\varepsilon/\sin\theta\right) + \left(\delta/\cos\theta\right) + x_V\cot\theta \quad (2\text{-}16)$$

$$x' = \left(\varepsilon + \delta\,\tan\theta\right)\cos\theta = \varepsilon\,\cos\theta + \delta\,\sin\theta \quad (2\text{-}17)$$

x_V = virtual distance

$$= \frac{k\sigma_o}{\sigma'_A} - x_R \quad (2\text{-}18)$$

ℓ = effective line length

$$= \begin{cases} \delta + \varepsilon\,\cot\theta & ; \quad \delta + \varepsilon\,\cot\theta \leq L \\ L & ; \quad \delta + \varepsilon\,\cot\theta > L \end{cases} \quad (2\text{-}19)$$

The following parameters used in the preceding equations are based on meteorological measurements or inferred from meteorological measurements:

σ'_A = standard deviation of the wind azimuth angle in radians

k = constant relating σ'_A and σ'_E

$$= \sigma'_A/\sigma'_E \quad (2\text{-}20)$$

σ'_E = standard deviation of the wind elevation angle in radians

H_m = depth of the surface mixing layer below a capping inversion

$\bar{u}$ = mean transport wind speed

$$= \begin{cases} \dfrac{\bar{u}_R \left[z_2^{1+p} - z_1^{1+p} \right]}{(z_2 - z_1)(z_R)^p (1+p)} & ; \quad \bar{u} > \bar{u}_R \\ \bar{u}_R & ; \quad \bar{u} \leq \bar{u}_R \end{cases} \qquad (2\text{-}21)$$

$\bar{u}_R$ = mean wind at the reference height z_R

p = wind power-law coefficient

z_2 = effective upper bound of the cloud

$$= \begin{cases} H' + 2.15\left(\dfrac{kx'}{\sigma_A} + x_V\right) & ; \quad z_2 < H_m \\ H_m & ; \quad z_2 \geq H_m \end{cases} \qquad (2\text{-}22)$$

z_1 = effective lower bound of the cloud

$$= \begin{cases} H' - 2.15\left(\dfrac{kx'}{\sigma_A} + x_V\right) & ; \quad z_1 > 2 \\ 2 & ; \quad z_1 \leq 2 \end{cases} \qquad (2\text{-}23)$$

θ = angle between a line perpendicular to the line source and the mean wind direction (see Figure 2-1)

The following parameters are source inputs required for use in the model:

Q = total source strength emitted along the length L of the line source

H' = effective release height

V_j = gravitational settling velocity for the median drop by mass in the j^{th} drop-size category

f_j = fraction of the total source strength in the j^{th} drop-size category

γ_j = reflection coefficient for the median drop by mass in the j^{th} drop-size category

σ_o = standard deviation of the cloud distribution at the distance x_R

x_R = distance from the line source to cloud stabilization

L = length of the line source

The model for deposition, expressed in units of mass per unit area, at the point (ε, δ, 0) is given by the expression

$$
\begin{aligned}
Dep_L = \frac{2S}{\sin\theta} \sum_{j=1}^{J} f_j (1-\gamma_j) \Bigg\{ & \frac{B\exp\left(\frac{G^2}{4F} - P\right)}{2F} \left[\exp\left[-\left(F^{1/2} \left(\frac{1}{a} - \frac{G}{2F} \right) \right)^2 \right] \right. \\
& \left. - \exp\left[-\left(F^{1/2} \left(\frac{1}{b} - \frac{G}{2F} \right) \right)^2 \right] \right] + \frac{GB\pi^{1/2} \exp\left(\frac{G^2}{4F} - P\right)}{4F^{3/2}} \\
& \left[\operatorname{erf}\left(F^{1/2} \left(\frac{1}{b} - \frac{G}{2F} \right) \right) - \operatorname{erf}\left(F^{1/2} \left(\frac{1}{a} - \frac{G}{2F} \right) \right) \right] \\
+ \sum_{i=1}^{\infty} \gamma_j^{\,i-1} \Bigg\{ & \frac{C\exp\left(\frac{J^2}{4I} - P\right)}{2I} \left[\exp\left[-\left(I^{1/2} \left(\frac{1}{a} - \frac{J}{2I} \right) \right)^2 \right] \right. \\
& \left. - \exp\left[-\left(I^{1/2} \left(\frac{1}{b} - \frac{J}{2I} \right) \right)^2 \right] \right] + \frac{JC\pi^{1/2} \exp\left(\frac{J^2}{4I} - E\right)}{4I^{3/2}} \\
& \left[\operatorname{erf}\left(I^{1/2} \left(\frac{1}{b} - \frac{J}{2I} \right) \right) - \operatorname{erf}\left(I^{1/2} \left(\frac{1}{a} - \frac{J}{2I} \right) \right) \right] \\
& + \gamma_j \frac{D\exp\left(\frac{K^2}{4E} - P\right)}{2E} \left[\exp\left[-\left(E^{1/2} \left(\frac{1}{a} - \frac{K}{2E} \right) \right)^2 \right] - \exp\left[-\left(E^{1/2} \left(\frac{1}{b} - \frac{K}{2E} \right) \right)^2 \right] \right] \\
& + \gamma_j \frac{KD\pi^{1/2} \exp\left(\frac{K^2}{4E} - P\right)}{4E^{3/2}} \left[\operatorname{erf}\left(E^{1/2} \left(\frac{1}{b} - \frac{K}{2E} \right) \right) - \operatorname{erf}\left(E^{1/2} \left(\frac{1}{a} - \frac{K}{2E} \right) \right) \right] \Bigg\} \Bigg\}
\end{aligned}
\qquad (2\text{-}24)
$$

where

$$B = H' + \frac{V_j \, x_V}{\bar{u}} \tag{2-25}$$

$$G = \frac{2^{1/2}}{\sigma'_A} \left[\frac{V_j B k^2}{\bar{u}} + \left(n - \frac{\delta}{\cos\theta} \right) \cot\theta \right] \tag{2-26}$$

$$F = k^2 B^2 + \left(n - \frac{\delta}{\cos\theta} \right)^2 \tag{2-27}$$

$$J = \frac{-2^{1/2}}{\sigma'_A} \left[\frac{V_j C k^2}{\bar{u}} + \left(n - \frac{\delta}{\cos\theta} \right) \cot\theta \right] \tag{2-28}$$

$$I = k^2 C^2 + \left(n - \frac{\delta}{\cos\theta} \right)^2 \tag{2-29}$$

$$K = \frac{2^{1/2}}{\sigma'_A} \left[\frac{V_j D k^2}{\bar{u}} + \left(n - \frac{\delta}{\cos\theta} \right) \cot\theta \right] \tag{2-30}$$

$$E = k^2 D^2 + \left(n - \frac{\delta}{\cos\theta} \right)^2 \tag{2-31}$$

The source and meteorological inputs required by the deposition model are identical to those required by the drift model. The mathematical basis of the drift and deposition models is explained in Appendix B.

We point out that care must be used in numerically evaluating the error functions appearing in the drift and deposition models, since

terms in the model equations may not balance if computational precision is not maintained. Double precision arithmetic routines and careful arrangement of the order in which terms are evaluated may be required in computerized techniques. Despite the apparent complexity of the models, solution times are relatively short because the summation for multiple reflection from i=0 to infinity usually can be terminated after less than 10 passes (by checking if succeeding passes result in significant increases in the calculated drift or deposition). Also, as inspection of the model equations indicates, the models cannot be used when the wind is exactly perpendicular to the line source (θ=0 degrees) or when the wind direction is exactly parallel to the line source (θ=90 degrees). Exact solutions for these angles are easily derived, but in practice the computer program changes these angles by a small fraction (0.01 degrees) and computes the drift and deposition with little or no loss in accuracy.

2.2 GRIM-BARRY CANOPY PENETRATION MODEL

Grim and Barry (1975) developed a mathematical model to calculate the percentage material of a given drop-size category j which, after entering the forest at the top of the canopy, is retained at various levels within the canopy. The model is based on a Monte Carlo technique where a large number of drops in each size category are passed along a trajectory through a simulated forest with trees assigned to equal areas according to the density (stems per acre) in the forest being simulated. The drop trajectory is a function of the gravitational settling velocity V_j and the mean wind speed at various levels within the forest canopy. As a drop proceeds along the trajectory, each tree is randomly displaced within the assigned area in the plane of the horizon and calculations are made to determine if the drop intersects the tree envelope and, if an intersection occurs, whether the drop strikes a tree element. When the drop strikes a tree element, a tally is recorded for the height

interval within the canopy where the "hit" occurs and for all greater height intervals. Drops proceed along the trajectory until a hit occurs or until the trajectory intersects the ground. After the specified total number of drops in the size category have passed along the trajectory, the tally number within each height interval is divided by the total number of drops to obtain the percentage of drops reaching the given height interval. The total number of drops passed along the trajectory required to achieve a stabilized solution (percentage penetration) is a function of the steepness of the trajectory, with more drops being required for size categories with large settling velocities.

Figure 2-2 is a schematic diagram showing an example drop trajectory and forest construct. The drop trajectory in each of k height intervals is defined by the following piecewise linear function:

$$x_k = \left\{ \begin{array}{ll} 0 & ; \quad k = 0 \\ \dfrac{0.25(k-1)H_c}{\tan \phi_k} + x_{k-1} & ; \quad k = 1, 2, 3, 4 \end{array} \right\} \qquad (2\text{-}32)$$

$$y_k = 0 \qquad (2\text{-}33)$$

$$z_k = 0.25kH_c \quad ; \quad k = 0, 1, 2, 3, 4 \qquad (2\text{-}34)$$

where

ϕ_k = angle, measured in radians, defining the declination of the trajectory with respect to the plane of the horizon

$$= \left\{ \begin{array}{ll} \tan^{-1} \dfrac{V_j}{\bar{u}_{c;k}} & ; \quad \phi \leq 1.4 \text{ radians} \\ 1.4 \text{ radians} & ; \quad \phi > 1.4 \text{ radians} \end{array} \right\} \qquad (2\text{-}35)$$

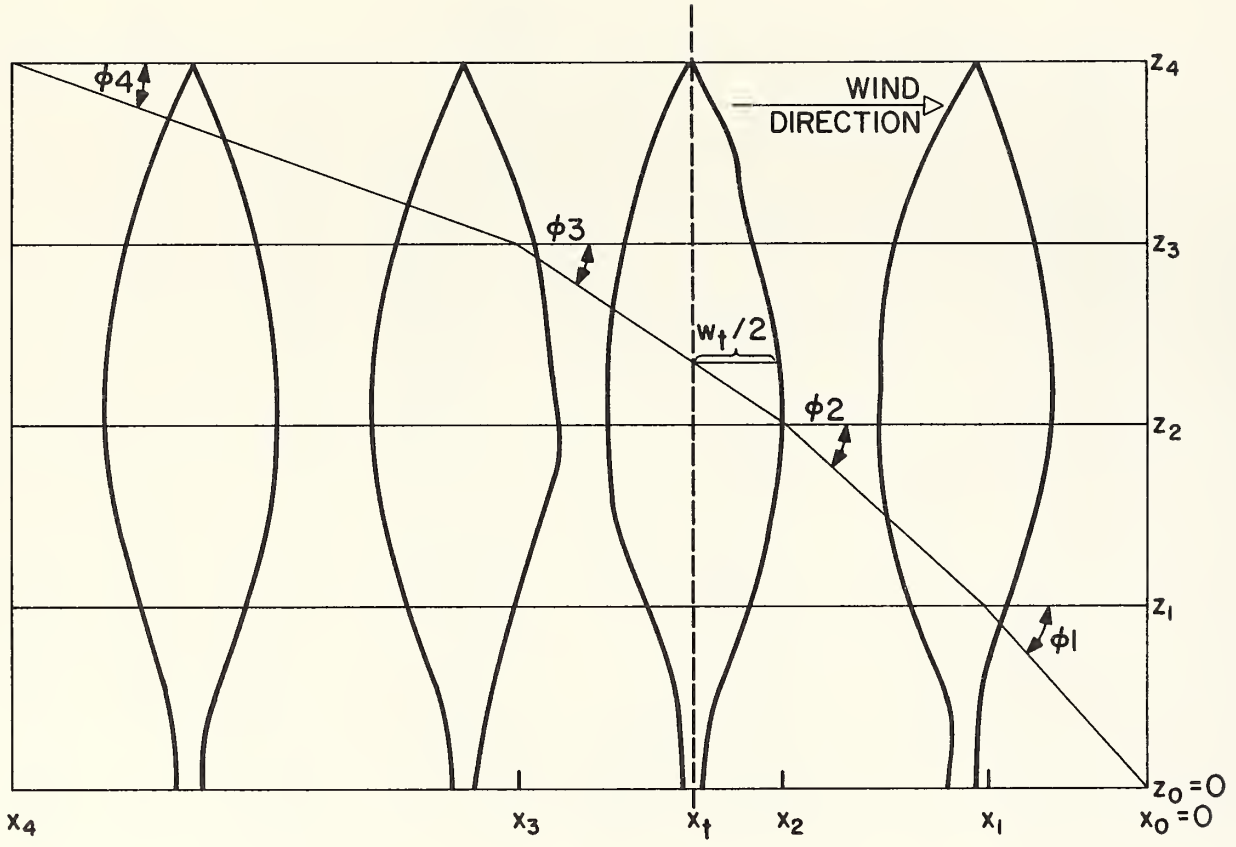

FIGURE 2-2. Schematic diagram showing an example drop trajectory and simulated forest.

H_c = height of the forest canopy

$\bar{u}_{c;k}$ = mean wind speed in the k^{th} height interval within the canopy

The number of trees placed along the trajectory path in the simulated forest is given by the expression

$$N_t = x_4/\Delta x_t \tag{2-36}$$

where

x_4 = maximum horizontal travel distance in meters of the drop within the forest canopy

Δx_t = alongwind tree spacing within the simulated forest

$$= 63.8/\sqrt{D_t} \tag{2-37}$$

D_t = tree density in units of stems per acre

As shown in Figure 2-3, each tree stem is given the following location along the trajectory:

$$x_t = (N_t - n)\,\Delta x_t + (R - 0.5)\,\Delta x_t \quad ; \quad n=1,2,....N_t \tag{2-38}$$

$$y_t = \left| (R' - 0.5)\,\Delta x_t \right| \tag{2-39}$$

where

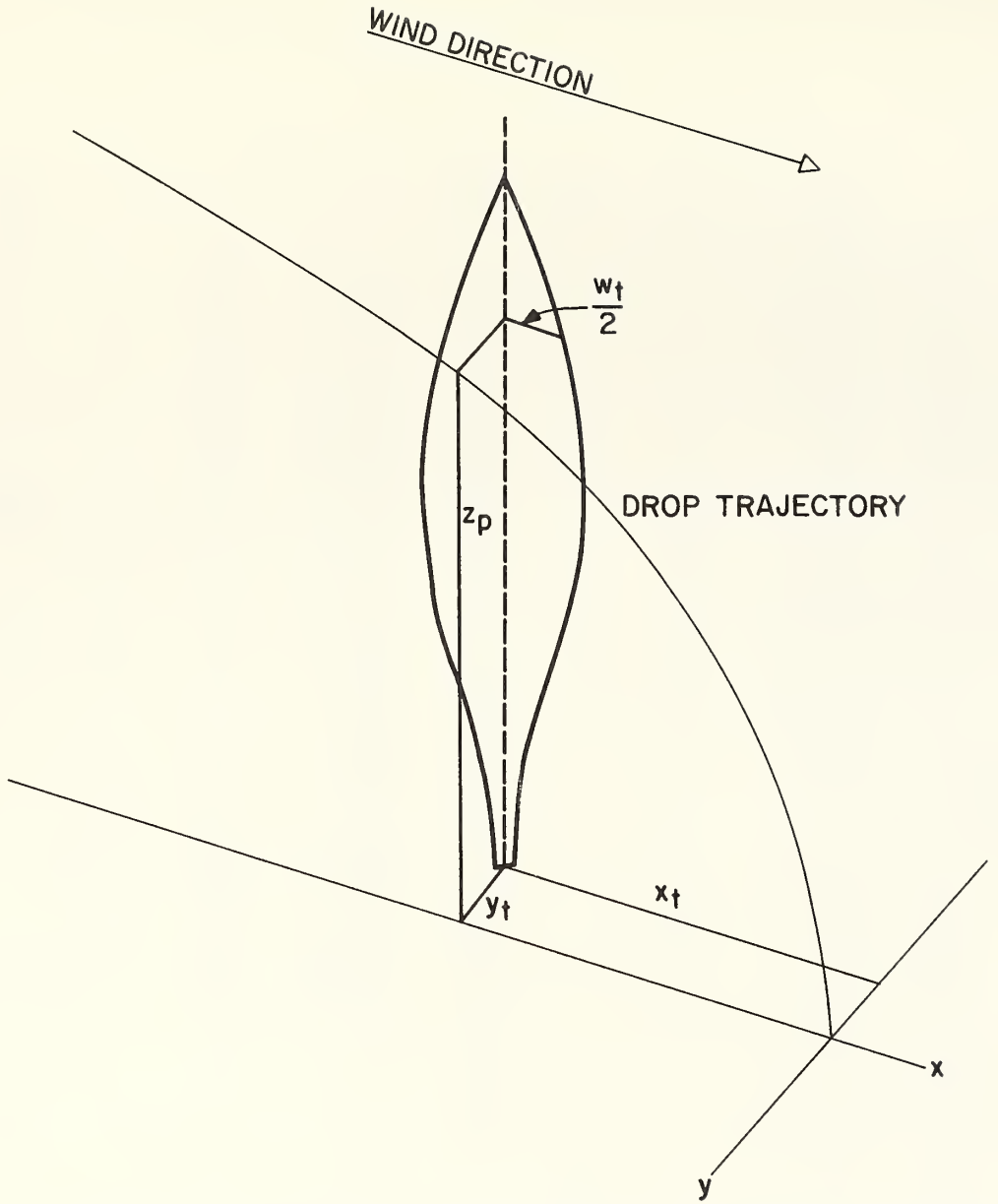

FIGURE 2-3. Schematic diagram showing the coordinate location of the "random tree".

n = tree number

and R and R' are uniform random numbers between 0 and 1. The possibility of the drop trajectory intersecting the tree envelope is determined by comparing the distance y_t with the radius of the tree envelope $(W_t/2)$ at the height z_p where the trajectory passes through the distance x_t. The tree widths W_t are specified by the program user at one-meter intervals and the program calculates the radius $(W_t/2)$ at z_p by linear interpolation. If y_t is greater than $(W_t/2)$, no intersection occurs and the computer program proceeds to the next tree along the trajectory.

If the drop trajectory intersects the tree envelope, the program calculates the probability that the drop impacts on a tree element from the expression

$$P_j = E_j(1 - PRPEN^{\zeta}) \tag{2-40}$$

where

E_j = impaction efficiency of the tree element for the j^{th} drop-size category

PRPEN = probability of penetration for the population of drops and for a horizontal trajectory through the tree

ζ = path length correction factor for a non-horizontal trajectory

$$\zeta = \begin{cases} \dfrac{1}{\cos_k} & ; \quad \zeta \leq \dfrac{H_c}{W_m} \\ \dfrac{H_c}{W_m} & ; \quad \zeta > \dfrac{H_c}{W_m} \end{cases} \tag{2-41}$$

W_m = maximum width of the tree envelope

A particular drop of the population of drops is assumed to intersect the tree element when the value of P_j from Equation (2-40) is greater than a uniform random number R" between 0 and 1. Each tree is divided into ten height-class intervals, and an intersection with a tree element is recorded as a "hit" in the class interval in which z_p occurs and in every higher class interval.

The process described above is repeated for every drop passed along the trajectory and the final percentage of material penetrating to a given height interval determined by dividing the number of recorded hits in the height interval by the total number of drops in all j^{th} size categories passed along the trajectory.

The inputs required by the canopy-penetration model are:

PRPEN = probability of penetration

$\bar{u}_{c;k}$ = mean wind speed in the k^{th} height interval within the forest canopy

V_j = gravitational settling velocity in meters per second for the median drop by mass in the j^{th} drop-size category

E_j = impaction collection efficiency for the j^{th} drop-size category

D_t = tree density in stems per acre

H_c = tree height in meters

W_i = tree width at one-meter height intervals

M = total number of drops to be passed along the trajectory

The computer program also permits the user to simulate a multi-storied canopy of up to three tree heights, with a different value of PRPEN possible for each tree or story height. The authors vary the values of PRPEN as a function of the four foliage types illustrated in Figure 2-4.

The output from the canopy penetration model includes, in addition to the percentage of material in the j^{th} drop size category penetrating to each of ten levels within the canopy, the maximum horizontal travel distance of the drop within the forest canopy (x_4). When the deposition model given by Equation (2-24) is used in conjunction with the canopy penetration model to calculate ground-level deposition within the canopy, the distance from the line source to the target is adjusted so that the deposition model calculates the deposition at the top of the forest canopy at a distance x_4 upwind from the target. The deposition at the target is then determined by multiplying the deposition predicted from Equation (2-24) by the percentage of material reaching the ground from the canopy penetration model.

2.3 SOURCE GEOMETRY AND WAKE VORTICES

During the first few minutes after spray is released from an aircraft, the vortices formed by the wing, helicopter rotor tips or propellers principally control the growth of the spray cloud and except for the lateral translation of the vortex system by a crosswind, the position of the cloud in space as well as the amount of material deposited on the underlying surface directly below the flight path. As pointed out by Jones (1970) and others, the descent of the vortex system from low-flying aircraft has frequently been observed to stop when the cloud is about one-half wingspan above the surface. Jones also notes (after Prandtl and Tietjens, 1934) that the sink rate ω of the vortex system can be approximated by the expression

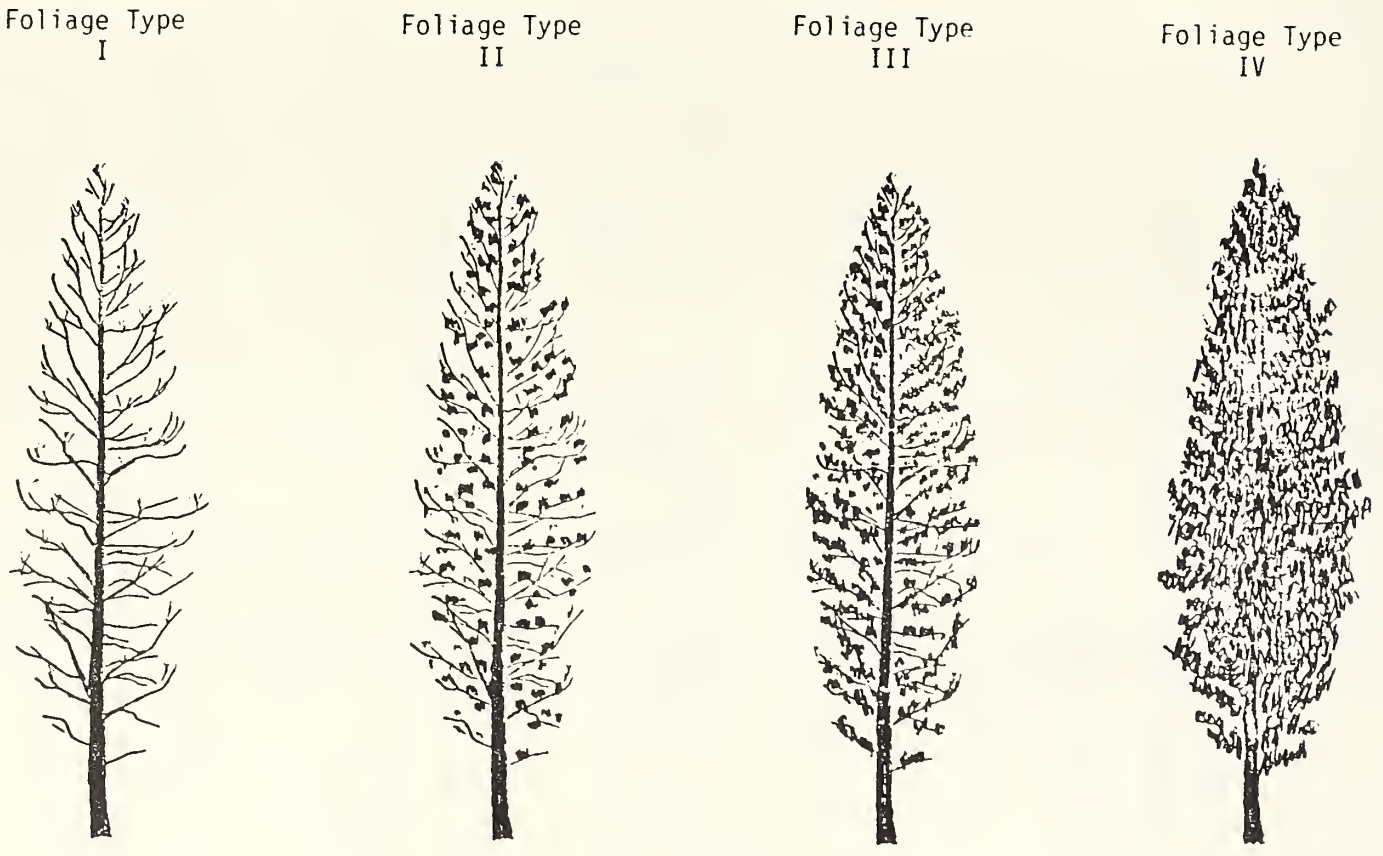

FIGURE 2-4. Diagram illustrating four foliage types suggested for use in classifying forests (after Grim and Barry, 1975).

$$\omega = \frac{8g\ W_a}{\pi^3 \rho_b^{\ 2} V_a} \qquad (2\text{-}42)$$

where

g = gravitational acceleration (9.8 m sec^{-2})

W_a = weight of aircraft

ρ = air density

V_a = aircraft speed

b = aircraft wingspan

Equation (2-42) is strictly applicable for use with fixed wing aircraft. However, as pointed out by the Bell Helicopter Company (1966 and updates), helicopter vortices resemble fixed-wing vortices at high forward speeds.

In the drift and deposition models described in Section 2.1 above, the source parameters correspond to the spray cloud properties when the cloud has reached approximate equilibrium. The vortex sink rate calculated from Equation (2-42) and the observations that the vortex tube stops descending at a distance (b/2) above the surface or above the forest canopy were used to calculate the source parameters for the drift and deposition models. Figure 2-5 is a schematic diagram showing the geometrical considerations used in specifying the source dimension σ_o, the distance downwind at which cloud stabilization occurs x_R, and the effective release height H'. As shown in Figure 2-5, the cloud descent from the aircraft at height H forms the angle $\tan^{-1}(\omega/\bar{u})$ with the horizontal. The distance downwind from the flight path where the cloud reaches a height b/2 above the surface is then

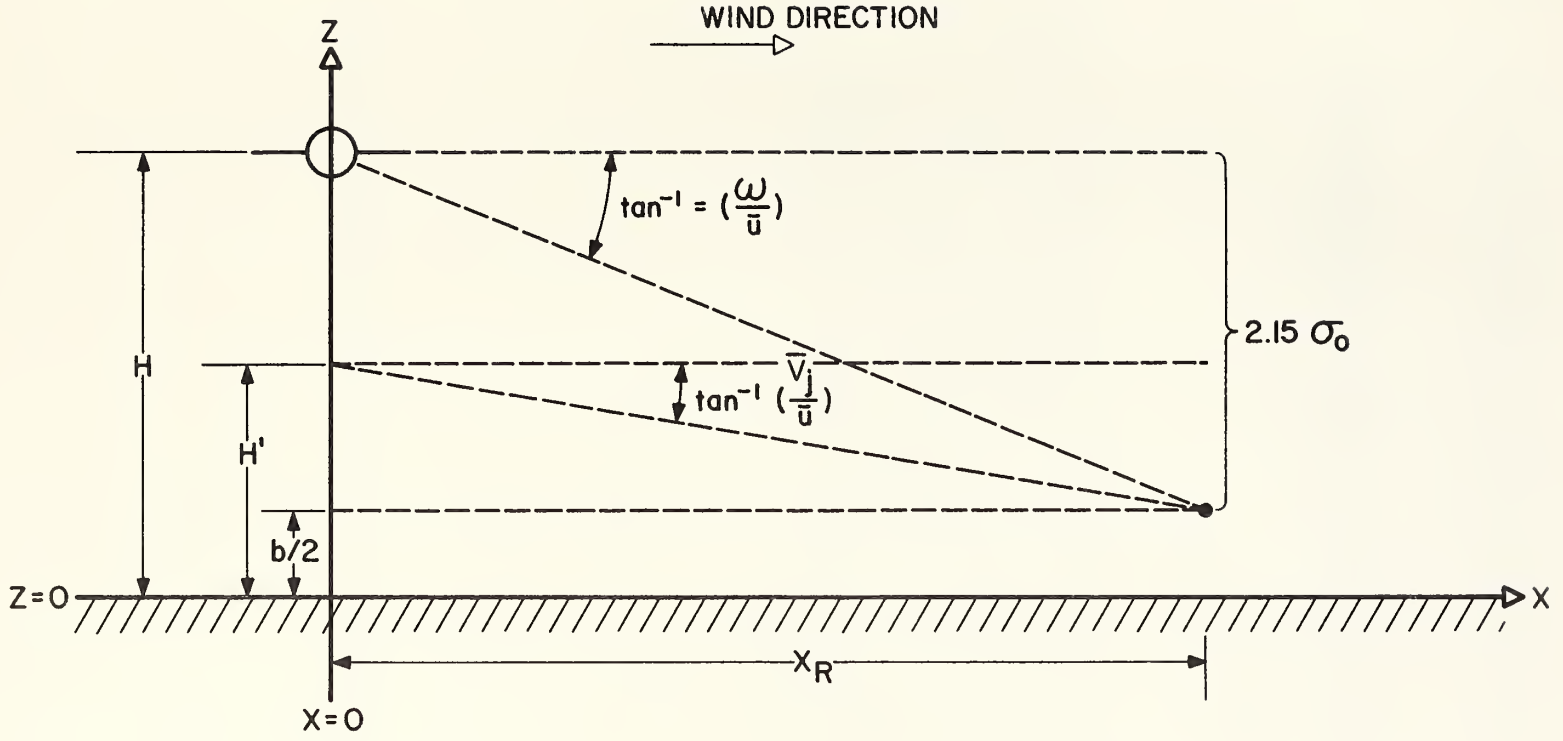

FIGURE 2-5. Schematic diagram showing geometry used in constructing the source dimension σ_o, distance x_R and effective source height H'.

$$x_R = \bar{u}\,\tau \qquad (2\text{-}43)$$

where

τ = time required for the cloud to descend to the height b/2 from the aircraft at height H

$$= \frac{H - b/2}{\omega} \qquad (2\text{-}44)$$

As noted in Section 2.1, the deposition and drift models are formulated under the assumption that the cloud centerline descends at an angle $\tan^{-1}(V_j/\bar{u})$ with the horizontal. We have therefore assumed that the effective declination of the cloud centerline downwind from an effective source height H' is given by the angle $\tan^{-1}(\bar{V}_j/\bar{u})$, where $\bar{V}_j$ is the gravitational settling velocity associated with the mass median drop diameter for the spray distribution. Based on this assumption, inspection of Figure 2-5 shows that

$$H' = \frac{\bar{V}_j}{\bar{u}}\,x_R + b/2$$

$$= \bar{V}_j\,\tau + b/2 \qquad (2\text{-}45)$$

Finally, the standard deviation of the cloud distribution at the distance x_R is given by

$$\sigma_o = \frac{H - b/2}{2.15} \qquad (2\text{-}46)$$

under the assumptions that

- The cloud at distance x_R is a folded Gaussian distribution in the vertical with the centroid at b/2

- The concentration at height H at distance x_R is one-tenth the concentration at the cloud centroid

SECTION 3

MODEL INPUTS FOR THE RENNIC CREEK AND 1976 REGION 1 PILOT PROJECT TRIALS

The source, meteorological and forest-description model inputs required to calculate the deposition for the Rennic Creek Trials and deposition and drift for the 1976 Region 1 Pilot Project Trials are respectively described in Sections 3.1 and 3.2.

3.1 MODEL INPUTS FOR THE RENNIC CREEK TRIALS

3.1.1 General

Five spray trials were conducted at the Rennic Creek site in the Lolo National Forest, Montana on 23 October 1974 using a Bell G-3 helicopter equipped with 41 Spraying System Number 80015 nozzles. The helicopter was equipped to spray fuel oil (with a density of 0.847 grams per cubic centimeter) containing Automate B Red Dye at a rate of 1 gallon per acre for a 60-foot swath width and a forward speed of 50 miles per hour. The pilot flew the G-3 over the deposition measurement grid shown in Figure 3-1. The grid consisted of six sampling rows of which three were located in the open and three were located beneath the forest canopy represented by the stipled area in the figure. Standard Kromekote card samplers were placed on the ground at 28 sampling positions along each row. Wind speed and direction were measured at heights of 2 meters and 18.6 meters on a crank-up tower, located at the position shown by the filled triangle in Figure 3-1, and on a 2-meter mast located within the forest as indicated by the open triangle in the figure. Temperature was measured within and above the canopy using a balloon-borne wiresonde located near the 2-meter mast as shown by the filled square in Figure 3-1.

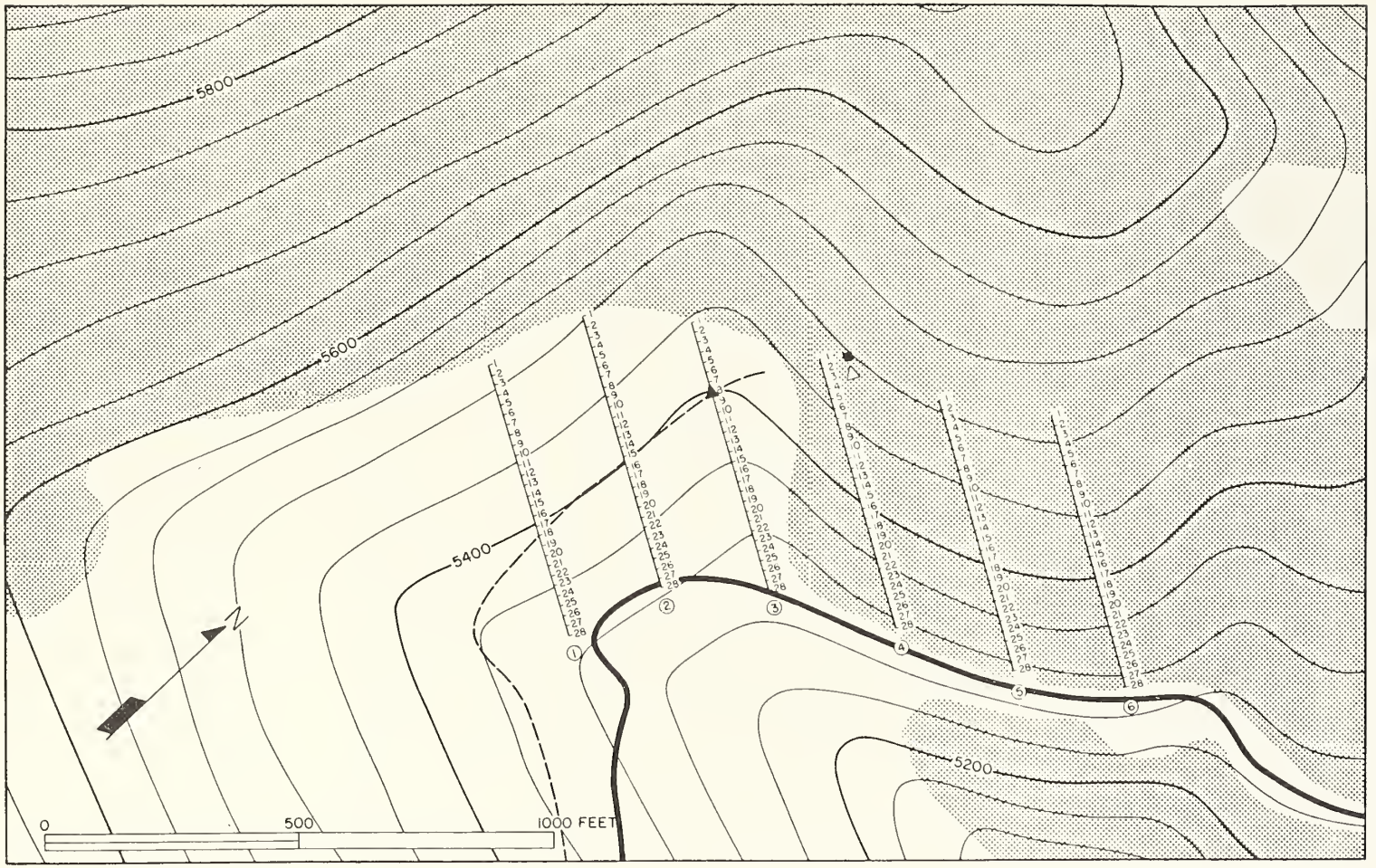

FIGURE 3-1. Sampling rows and meteorological measurement sites for the Rennic Creek Trials. Forest is shown by the stippled area.

The U. S. Forest Service supplied the H. E. Cramer Company with the average wind direction and average, maximum and minimum wind speed from the three wind instruments for three one-minute periods beginning one minute prior to spray operations, and with the wiresonde temperature profile for each trial. Standard surface weather observations of relative humidity, cloud cover and atmospheric pressure were also provided. The drop-size distribution and associated mass sampled on each Kromekote card was supplied, in the form of computer output from the ASCAS program, by the Methods Application Group, U. S. Forest Service at Davis, California.

3.1.2 Source Inputs

Table 3-1 gives the characteristics of the Bell G-3 helicopter required to calculate the sink rate ω of wake vortices and the emission rate of fuel oil per meter of flight path. The spray was released over a flight path of one-third mile centered on the third sampling row shown in Figure 3-1. The pilot was instructed to fly a single swath on each trial along the terrain contours. The position of the helicopter with respect to the ground-sampling network was noted only as the helicopter passed over the third sampling row. This position is given in Table 3-2 with respect to sampler location along Sampling Row 3.

The source characteristics σ_o, x_R, τ and H' calculated from the expressions for wake vortex effects in Section 2.3 and the aircraft release height H above the open and forested areas are given in Table 3-3.

The settling velocity $\bar{V}_j$ for the mass median drop is also given in Table 3-3. The cumulative mass distribution assumed representative of the aircraft spray distribution was obtained by averaging the distributions measured on the Kromekote cards in the open area (Sampling Rows

TABLE 3-1

BELL G-3 HELICOPTER CHARACTERISTICS

Parameter	Value
Rotor Diameter b (m)	11.28
Weight W_a (kg)	1050.0
Air Speed V_a (m sec^{-1})	22.3
Source Emission Rate Q/L (g m^{-1})	14.5

TABLE 3-2

HELICOPTER POSITION OVER SAMPLING ROW 3
OF THE RENNIC CREEK TRIALS

Trial Number	Sampler Number
1	14
2	21
3	21
4	23-24
5	26

TABLE 3-3

SOURCE INPUTS FOR THE RENNIC CREEK TRIALS

Trial Number	Location	σ_o (m)	X_R (m)	τ (sec)	H (m)	H' (m)	$\bar{V}_j$ (m sec^{-1})
1	Open	18.6	77.4	40.1	45.7	33.0	0.683
	Trees	9.8	50.0	25.9	15.2	23.3	0.683
2	Open	15.1	71.4	39.9	38.1	32.9	0.683
	Trees	6.3	29.6	16.5	7.6	16.9	0.683
3	Open	15.1	70.1	39.2	38.1	32.4	0.683
	Trees	6.3	29.0	16.2	7.6	16.7	0.683
4	Open	15.1	69.8	39.0	38.1	32.4	0.683
	Trees	6.3	28.9	16.2	7.6	16.7	0.683
5	Open	15.1	63.7	38.9	38.1	32.2	0.683
	Trees	6.3	26.4	16.1	7.6	16.6	0.683

1, 2 and 3) over all five trials. The value of $\bar{V}_j$ was calculated for the mass median drop diameter (211 μm) using procedures described by McDonald (1960). The fraction of mass f_i, settling velocities V_j, and reflection coefficients γ_j for this mass distribution are given in Table 3-4. The values of the reflection coefficient are based on the relationship between gravitational settling velocities and reflection coefficients shown in Figure 3-2. This relationship, postulated by Dumbauld, Rafferty and Cramer (1976), was shown by the authors to improve the correspondence between predicted and measured deposition patterns for the DC-7B spray trials conducted at Dugway Proving Ground, Utah.

The impaction efficiencies E_j shown in Table 3-4 and used in the canopy penetration model described in Section 2.2 were calculated from the following empirical relationship, recommended by Grim and Barry (1975) and attributed to Sell:

$$E_j = \begin{cases} \dfrac{2.8 \times 10^{-4} \, d_j^{\,2} \, u}{s} & ; \quad E \leq 1 \\ 1 & ; \quad E > 1 \end{cases} \qquad (3\text{-}1)$$

where

u = impaction velocity in meters per second

d_j = drop diameter for the j^{th} category in micrometers

s = diameter in meters of the element on which the drop impacts

TABLE 3-4

MASS DISTRIBUTION, SETTLING VELOCITIES, REFLECTION COEFFICIENTS, AND IMPACTION EFFICIENCIES FOR THE RENNIC CREEK TRIALS

Drop-size Category j	Mean Drop Diameter (μm)	Fraction of Mass f_j	Settling Velocity V_j ($m\ sec^{-1}$)	Reflection Coefficient γ_j	Impaction Efficiency E_j		
					Trial 1	Trials 2, 3 & 4	Trial 5
1	24.9	$1x10^{-3}$	$1.64x10^{-2}$	0.74	$2.22x10^{-2}$	$2.42x10^{-2}$	$2.61x10^{-2}$
2	43.0	$9x10^{-3}$	$4.89x10^{-2}$	0.62	$6.62x10^{-2}$	$7.23x10^{-2}$	$7.80x10^{-2}$
3	63.6	$2x10^{-2}$	$1.07x10^{-1}$	0.48	$1.45x10^{-1}$	$1.58x10^{-1}$	$1.71x10^{-1}$
4	81.6	$3x10^{-2}$	$1.76x10^{-1}$	0.31	$2.39x10^{-1}$	$2.60x10^{-1}$	$2.81x10^{-1}$
5	99.6	$4x10^{-2}$	$2.25x10^{-1}$	0.18	$3.55x10^{-1}$	$3.88x10^{-1}$	$4.18x10^{-1}$
6	123.0	$1x10^{-1}$	$2.94x10^{-1}$	0.01	$5.42x10^{-1}$	$5.92x10^{-1}$	$6.38x10^{-1}$
7	151.8	$1x10^{-1}$	$4.16x10^{-1}$	0	$8.26x10^{-1}$	$9.01x10^{-1}$	$9.72x10^{-1}$
8	176.3	$1x10^{-1}$	$5.16x10^{-1}$	0	1	1	1
9	211.3	$2x10^{-1}$	$6.83x10^{-1}$	0	1	1	1
10	246.8	$1x10^{-1}$	$8.13x10^{-1}$	0	1	1	1
11	274.2	$1x10^{-1}$	$9.09x10^{-1}$	0	1	1	1
12	310.5	$1x10^{-1}$	1.04	0	1	1	1
13	347.2	$4x10^{-2}$	1.20	0	1	1	1
14	386.5	$3x10^{-2}$	1.38	0	1	1	1
15	429.8	$2x10^{-2}$	1.56	0	1	1	1
16	459.0	$1x10^{-1}$	1.66	0	1	1	1

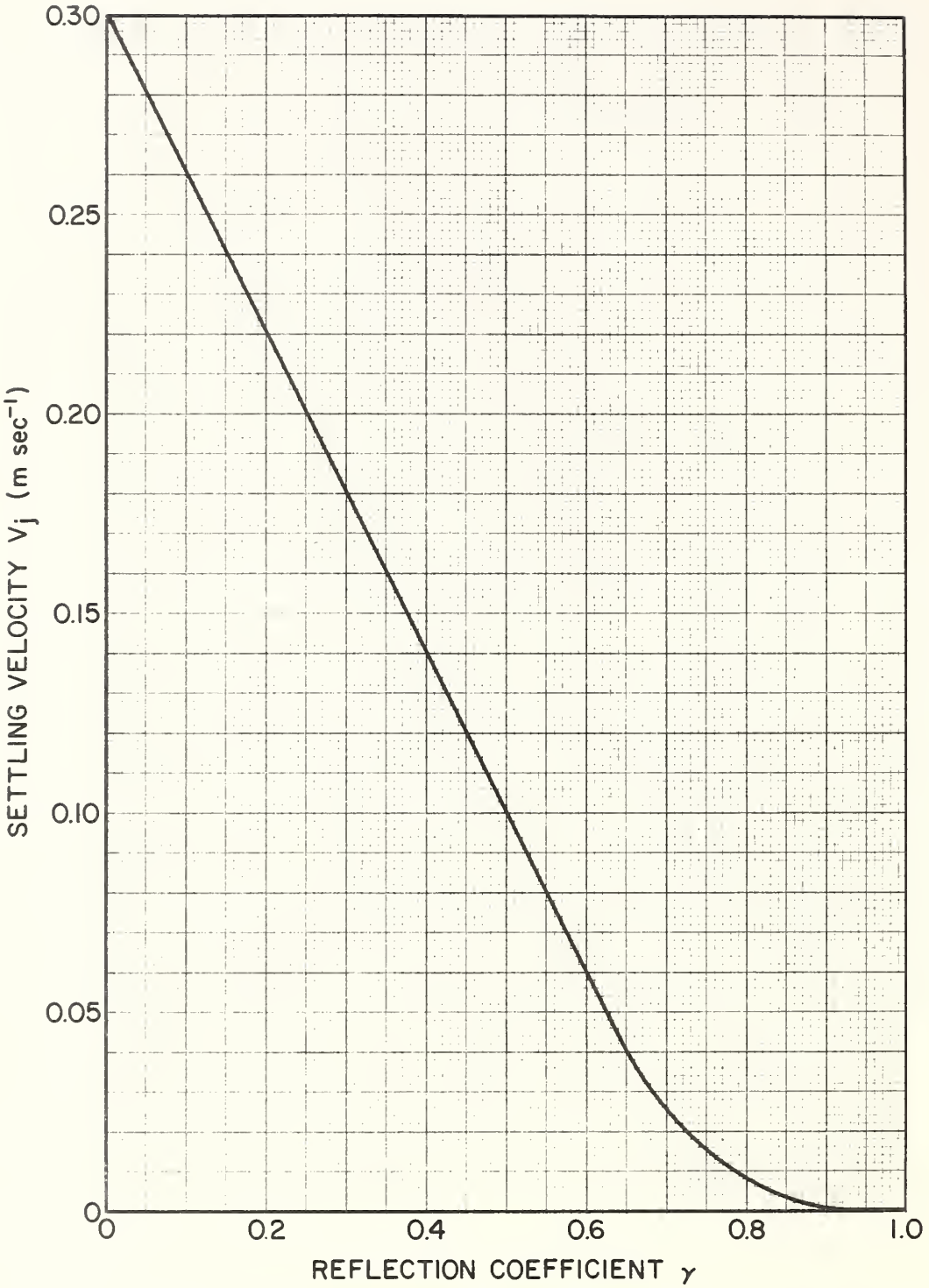

FIGURE 3-2. Relationship between the gravitational settling velocity V_j and the reflection coefficient γ at the ground surface.

Grim and Barry obtained a good fit to their deposition data within a similar forest canopy by using a value for s of 0.13 meters. This value of s was used to calculate the value of E_j shown in Table 3-4. The impaction velocity u in Equation (3-1) was set equal to the wind speed measured at a height of 2-meters within the forest canopy.

3.1.3 Meteorological Inputs

Meteorological inputs required by the deposition and canopy penetration models are presented in Table 3-5. The wind direction shown in the table is the average wind direction measured on the meteorological tower located in the open area. Although wind speed was measured at heights of 2- and 18.6 meters on the tower in the open area and at 2 meters within the forest canopy, the data supplied by the Forest Service indicate that the average wind speed was, for practical purposes, the same at all locations. For this reason, only a single value of wind speed is given in Table 3-5 for each trial, and this speed is assumed to be constant in the vertical (p=0) and in the plane of the horizon.

Measurements of σ_A and σ_E were not made during the Rennic Creek Trials. Therefore, values of σ_A for a sampling period of ten-minutes ($\sigma_A\{\tau$=600 seconds$\}$) were assigned to each trial based on previous experience in modeling spray deposition under the stability conditions indicated by the wiresonde temperature profiles. A value for σ_A of 10 degrees was assigned to Trials 1 and 2 and a value of 15 degrees was assigned to Trials 3, 4 and 5. These σ_A values were adjusted for the time τ required for the wake vortex to reach the stabilization height (b/2) above the ground in the open areas and the canopy top in the forested area by using the relationship

$$\sigma_A\{\tau\} = \sigma_A\{\tau_o=600 \text{ seconds}\} \left(\frac{\tau}{600}\right)^{1/5} \qquad (3\text{-}2)$$

TABLE 3-5

METEOROLOGICAL MODEL INPUTS FOR THE RENNIC CREEK TRIALS

Trial Number	Local Time	Wind Direction (deg)	Wind Speed At 2 Meters ($m\ sec^{-1}$)	p	$\sigma_A = \sigma_E$ (deg)		Air Density ρ ($g\ cm^{-3}$)	Air Pressure (Inches Hg)
					Open	Trees		
1	1032	130	1.93	0	5.82	5.33	1149	26.97
2	1149	140	1.79	0	5.81	4.88	1150	26.95
3	1300	142	1.79	0	8.69	7.29	1129	26.93
4	1406	136	1.79	0	8.68	7.28	1124	26.91
5	1457	147	1.64	0	8.68	7.28	1120	26.88

The value of σ_E was set equal to σ_A under the assumption that turbulence was isotropic in the vicinity of the flight path.

Values of air density and pressure, used in the calculation of the vortex sink rate ω and settling velocity V_j, are also shown in Table 3-5.

3.1.4 Forest Description

A detailed description of the trees--including the height, diameter at breast height (d.b.h.), crown width and crown height, in circular one-tenth acre plots on each of rows 4, 5 and 6--was supplied to the H. E. Cramer Company by the Forest Service. According to this description, 95 percent of the stand is Douglas-fir, with the remainder of the trees being larch, lodgepole pine, or ponderosa pine. The overall forest canopy is relatively uniform with only a few scattered openings. Ground cover is variable, ranging from patches of ninebark 3-feet in height to sparse pinegrass and low forbs. Although there are approximately 600 trees per acre, slightly more than half of the trees (315 stems per acre) had little or no foliage. We eliminated these trees from consideration, ordered the remaining trees by height, divided the distribution into thirds (95 stems per acre) and calculated the average height, d.b.h., crown width and crown height in each of three stories. Assuming the trees to be triangular in shape, we then calculated tree widths in one-meter height intervals assuming the base of the triangle was at the average crown height. The results of these calculations and the inputs used in the canopy penetration model are shown in Table 3-6. The value of the probability of penetration PRPEN was set equal to 0.38, the value suggested by Grim and Barry (1975) for a Foliage Type III tree (see Figure 2-4).

TABLE 3-6

FOREST CHARACTERISTICS AT RENNIC CREEK

Parameter	Story		
	1	2	3
Average Tree Height, H_c(m)	19	13	8
Average Stand Density, D_t (stems/acre)	95	95	95
Probability of Penetration, PRPEN	0.38	0.38	0.38
Tree Envelope Widths, W_i(m)			
i = 1	0.3	0.25	0.20
2	0.3	0.25	0.20
3	0.3	0.25	0.20
4	0.3	0.25	2.31
5	0.3	0.25	1.77
6	0.3	0.25	1.22
7	0.3	0.25	0.67
8	0.3	0.25	0.13
9	0.3	2.50	
10	0.3	1.88	
11	4.23	1.26	
12	3.71	0.64	
13	3.20	0.02	
14	2.68		
15	2.16		
16	1.64		
17	1.12		
18	0.61		
19	0.09		

3.2 MODEL INPUTS FOR THE 1976 REGION 1 PILOT PROJECT TRIALS

3.2.1 General

Region 1 of the Forest Service conducted a pilot project in the Helena National Forest, near Townsend, Montana, in early July 1976 to evaluate the effectiveness of Dylox and Orthene in controlling the western spruce-budworm. The spray program was carried out using a Bell 205 A-1 Turbojet helicopter with a spray system equipped with eight Model 350 Beecomist spray heads operating at 41 psig. The helicopter sprayed six spray plots during the program. Plot numbers 1, 2 and 7 were sprayed with Dylox (density of 1.07 grams per cubic centimeter) at an application rate of 1/2 gallon per acre. Plot numbers 3, 5 and 8 were sprayed with Orthene (density of 1.04 grams per cubic centimenter) at an application rate of 1 gallon per acre. Automate Red B and Rhodamine B dyes were respectively added to the Dylox and Orthene mixes to provide stains on Kromekote deposition sampling cards. The helicopter was nominally operated at a forward speed of 90 miles per hour with a swath width of 200 feet for all plots except plot number 3. One spray head became clogged during the first spray load delivered on Plot 3. This spray head was blocked during subsequent flights over Plot 3 and the helicopter flown at 79 miles per hour to maintain the proper application rate. The helicopter pilot attempted to maintain an altitude of 50 feet above the canopy while flying along terrain contours.

Terrain contours and helicopter flight paths for Plot 1 (Jimmy Creek) are shown in Figure 3-3. The pilot flew the spray lines shown near the ridges during the first part of each spray period and the lines near the valley floor during the last part of each spray period, to take advantage of the general change of wind direction from downslope to upslope that occurs during early morning hours. The filled circles numbered from 1 through 24 shown in Figure 3-3 represent the location

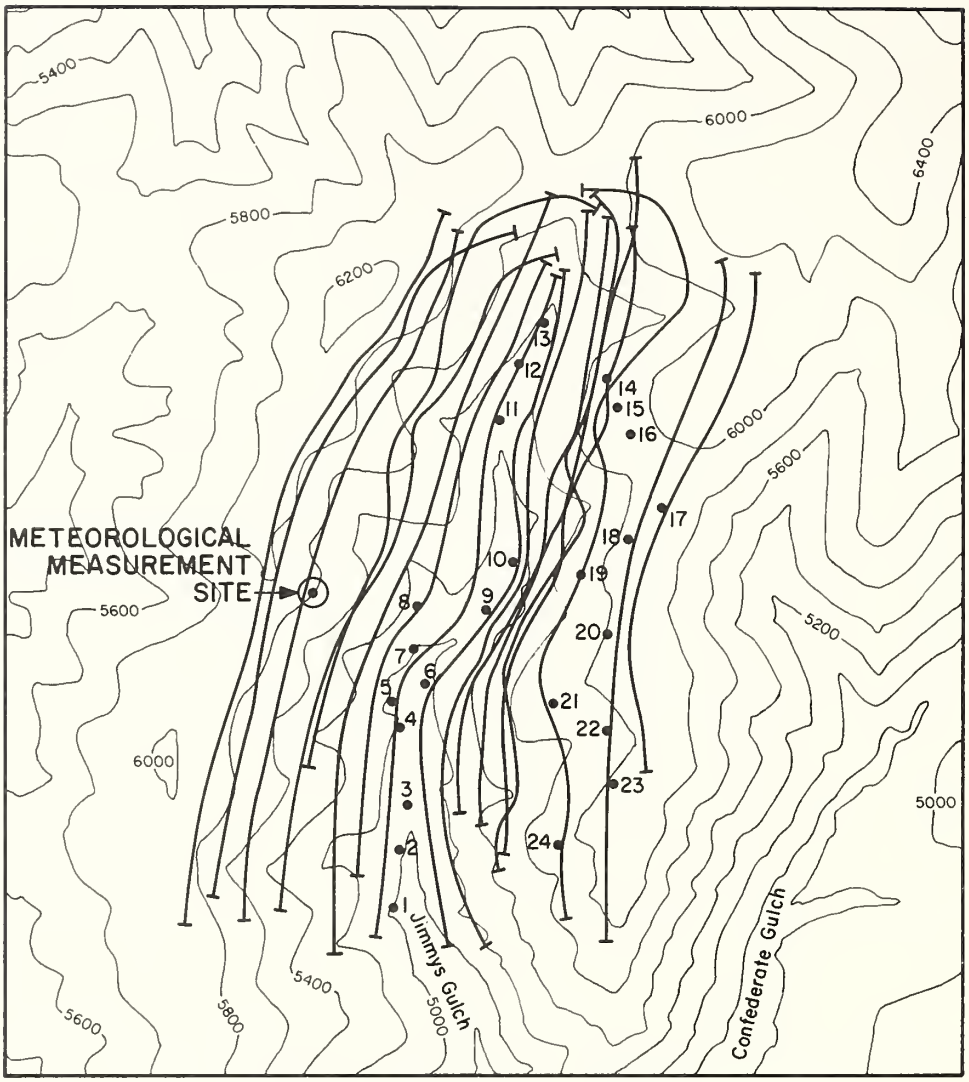

FIGURE 3-3. Terrain contours and aircraft flight paths for Block 1, 1976 Region 1 Pilot Project.

of tree clusters, consisting of three trees, where deposition measurements were made by placing four Kromkote cards at 90 degrees to one another beneath the drip line of each tree in the cluster. The location of the meteorological measurement site for Plot 1 is also shown in the figure. Measurements of wind speed and direction at a height of 2 meters were made in an open area at this location. A spherical Mylar balloon was also used to lift a hot-film anemometer for measuring wind speed at 50 feet above the canopy. Temperature profiles were measured to a height of 320 feet above the station using a Contel Metro-Sonde, which is raised and lowered by a tethered kite-balloon. These meteorological measurements were made at some location within the plots during all spray periods, and another 2-meter mast was used to measure wind speed and direction at an additional location on all plots except Plot 1. Ekblad, Miller and Flavell (1977) have described the meteorological measurements made by the Forest Service during the 1976 Region 1 Pilot Project, and also present topographic maps of the spray plots and maps of the helicopter flight paths numbered by the sequence in which they were flown.

Deposition, drift and meteorological measurements were also made downwind from the spray plots by the Agricultural Engineering Department of the University of California at Davis, California. Deposition and drift measurements were made to a distance of 4 miles from the down-canyon edge of the spray plots. Deposition measurements were made using Mylar sheets and Kromekote sampling cards at ground-level. Hi-Vol Staplex samplers were used to collect airborne drift (dosage) samples and several types of cascade impactors were employed to obtain mass distribution fractions. A 64-foot tower was erected at some point downwind from the spray plot for each trial to measure the size distributuion of particles in the vertical using Millipore air filters. Temperature differences between 8 and 32 feet were measured on the tower and wind velocities were measured at heights of 4, 8, 16, 32 and 64 feet. Wind direction was measured at a height of 16 feet on the tower.

Additionally, measurements of air temperature and drift were made by instruments on a DeHavilland Beaver aircraft. A full description of the measurement equipment used by the University of California and the results of the measurement program is given by Akesson, Yates and Carroll (1977).

Because of time and funding limitations under the contract, and because an appreciable portion of the time and funds were expended in developing the computer programs, model calculations of deposition and drift for comparison with measurements were made only for Plots 1, 2 and 3.

3.2.2 Source Inputs

Table 3-7 gives the characteristics of the Bell 205A-1 Turbo-jet helicopter required to calculate the sink rate ω of the wake vortices and the emission rate of Dylox and Orthene in units of grams per meter along the flight path. As shown in Figure 3-3, the helicopter flew 17 swaths over Plot 1. The approximate location of each flight path was noted on a topographic chart by an observer flying in a monitor aircraft. Since the computer program requires the line sources to be straight lines, the 17 swaths for Plot 1 were divided into 91 line sources to simulate the flight pattern. Coordinates of the tree clusters and line-source segments, expressed in the Universal Transverse Mercator (UTM) system, were determined for use in the deposition and drift models. Similarly, 112 line segments and 176 line segments were respectively used to simulate the flight patterns for Plots 2 and 3.

The source characteristics σ_o, x_R, τ and H' calculated from the expressions describing wake vortex effects in Section 2.3 and the aircraft release height above the forest canopy are presented in Table 3-8.

TABLE 3-7

BELL 205A-1 TURBO-JET HELICOPTER CHARACTERISTICS

Parameter	Value	
	Plots 1, 2	Plot 3
Rotor Diameter b (m)	14.63	14.63
Weight W_a (kg)	3917	3917
Air Speed V_a (m sec^{-1})	40.2	35.3
Source Emission Rate Q/L (g m^{-1})	30.7 (Dylox)	59.1 (Orthene)

TABLE 3-8

SOURCE INPUTS FOR PLOTS 1, 2 AND 3 OF THE
1976 REGION 1 PILOT PROJECT

Plot Number	σ_o (m)	x_R (m)	τ (sec)	H (m)	H' (m)	$\bar{V}_j$ (m sec^{-1})
1	3.69	11.9	7.3	15.2	9.8	0.338
2	3.69	8.1	7.3	15.2	9.8	0.338
3	3.69	7.5	6.1	15.2	12.9	1.24

*Both H and H' are measured above the top of the canopy.

The settling velocity $\bar{V}_j$ given in Table 3-8 as well as the mass distribution and settling velocities in Tables 3-9 and 3-10 for Dylox and Orthene are based on detailed measurements of spray deposits made during the extensive aircraft characterization trials held at Townsend, Montana, immediately prior to the Pilot Project. Details of the meteorological and deposition measurements made during these trials are contained in a report by Dumbauld and Rafferty (1977). The procedures described in Section 3.12 above for calculating V_j, γ_j and E_j for the Rennic Creek Trials were also used for calculating the values shown in Tables 3-9 and 3-10 for the 1976 Region 1 Pilot Project.

3.2.3 Meteorological Inputs

Meteorological model inputs required by the drift, deposition and canopy penetration models, except for wind direction, are presented in Table 3-11. Wind direction as well as wind speed vary greatly, both spatially and temporally, over the complex terrain sprayed in the Pilot Project and during the early morning changeover from downslope to upslope winds. A general indication of the time periods when downslope and upslope winds prevailed and the order in which swaths were flown is presented by Ekblad, Miller and Flavell (1977). We used this information and the topographic charts to establish a wind direction for use in predicting deposition at each tree cluster. As might be expected, downslope winds prevailed during the early morning hours and upslope winds prevailed during the late morning hours. A down-valley wind direction was used for model calculations of drift and deposition beyond the spray-plot, and only those line segments thought to be flown prior to the time winds became upslope and contributing to the drift and dosage measurements made by the University of California were used in the calculations. Wind speeds shown in Table 3-11 were obtained by averaging over the spray period the 2-meter measurements made at the single site within the spray block for Plot 1 and the measurements made at both sites within the spray block for Plots 2 and 3. Because of the

TABLE 3-9

MASS DISTRIBUTION, SETTLING VELOCITIES, REFLECTION COEFFICIENTS, AND IMPACTION EFFICIENCIES FOR PLOTS 1 AND 2 OF THE 1976 REGION PILOT PROJECT

Drop-Size Category j	Mean Drop Diameter (μm)	Fraction of Mass f_j	Settling Velocity V_j ($m\ sec^{-1}$)	Reflection Coefficient γ_j	Impaction Efficiency E_j	
					Plot 1	Plot 2
1	18.8	1×10^{-3}	1.17×10^{-2}	0.77	9.30×10^{-3}	6.30×10^{-3}
2	28.0	9×10^{-3}	2.59×10^{-2}	0.69	2.07×10^{-2}	1.39×10^{-2}
3	39.7	2×10^{-2}	5.20×10^{-2}	0.62	4.17×10^{-2}	2.79×10^{-2}
4	50.0	3×10^{-2}	8.24×10^{-2}	0.54	6.61×10^{-2}	4.42×10^{-2}
5	59.5	4×10^{-2}	1.17×10^{-1}	0.45	9.36×10^{-2}	6.26×10^{-2}
6	72.5	1×10^{-1}	1.73×10^{-1}	0.31	1.39×10^{-1}	9.30×10^{-2}
7	87.5	1×10^{-1}	2.35×10^{-1}	0.16	2.02×10^{-1}	1.35×10^{-1}
8	101	1×10^{-1}	2.76×10^{-1}	0.06	2.70×10^{-1}	1.81×10^{-1}
9	118	2×10^{-1}	3.38×10^{-1}	0	3.68×10^{-1}	2.46×10^{-1}
10	136	1×10^{-1}	4.28×10^{-1}	0	4.89×10^{-1}	3.27×10^{-1}
11	150	1×10^{-1}	5.00×10^{-1}	0	4.95×10^{-1}	3.98×10^{-1}
12	168	1×10^{-1}	5.89×10^{-1}	0	7.46×10^{-1}	4.99×10^{-1}
13	184	4×10^{-2}	6.77×10^{-1}	0	8.95×10^{-1}	5.99×10^{-1}
14	196	3×10^{-2}	7.46×10^{-1}	0	1	6.80×10^{-1}
15	212	2×10^{-2}	8.37×10^{-1}	0	1	7.95×10^{-1}
16	234	1×10^{-2}	9.29×10^{-1}	0	1	9.69×10^{-1}

TABLE 3-10

MASS DISTRIBUTION, SETTLING VELOCITIES, REFLECTION COEFFICIENTS AND IMPACTION EFFICIENCIES FOR PLOT 3 OF THE 1976 REGION 1 PILOT PROJECT

Drop-Size Category j	Mean Drop Diameter (μm)	Fraction of Mass f_j	Settling Velocity V_j ($m\ sec^{-1}$)	Reflection Coefficient γ_j	Impaction Efficiency E_j
1	62.0	1×10^{-3}	1.23×10^{-1}	0.43	1.04×10^{-1}
2	78.8	9×10^{-3}	1.99×10^{-1}	0.25	1.68×10^{-1}
3	94.7	2×10^{-2}	2.56×10^{-1}	0.11	2.43×10^{-1}
4	109	3×10^{-2}	3.01×10^{-1}	0	3.22×10^{-1}
5	121	4×10^{-2}	3.46×10^{-1}	0	3.97×10^{-1}
6	135	1×10^{-1}	4.15×10^{-1}	0	4.95×10^{-1}
7	168	1×10^{-1}	5.82×10^{-1}	0	7.65×10^{-1}
8	201	1×10^{-1}	7.65×10^{-1}	0	1
9	231	2×10^{-1}	9.15×10^{-1}	0	1
10	257	1×10^{-1}	1.02	0	1
11	274	1×10^{-1}	1.09	0	1
12	293	1×10^{-1}	1.18	0	1
13	312	4×10^{-2}	1.26	0	1
14	328	3×10^{-2}	1.35	0	1
15	353	2×10^{-2}	1.48	0	1
16	390	1×10^{-2}	1.68	0	1

TABLE 3-11

METEOROLOGICAL MODEL INPUTS FOR THE 1976 REGION 1
PILOT PROJECT PLOTS 1, 2 AND 3

Plot Number	Local Time	Wind Speed At 2 Meters ($m\ sec^{-1}$)	p	$\sigma_A = \sigma_E$ (degrees)	Air Density ($g\ cm^{-3}$)
1	0554-0820	1.21	0.20	4.14	1063
2	0545-0745	0.89	0.15	4.14	1063
3	0555-0858	1.24	0.15	4.14	1063

limited measurements of wind speed made above the canopy, the wind-profile exponents p in Table 3-11 are estimates based on experience. Because σ_A and σ_E were not measured during the Pilot Project, the values shown in the table are estimates. Air pressure was not measured at the spray sites and the estimates of air density in the table are for a standard pressure at the elevation of the spray plots.

3.2.4 Forest Description

A description of the tree clusters was not made during the 1976 Region 1 Pilot Project. However, during the early spring of 1977, a crew under the direction of Scott Tunnock, U. S. Forest Service, Missoula, Montana, returned to the site and obtained descriptions of the stand density, average tree height, and average crown width. The foliage density was classified according to the four types shown in Figure 2-4 for each tree cluster as well as for the entire spray plot. The results of this survey are shown in Tables 3-12, 3-13 and 3-14 for Plots 1, 2 and 3, respectively. The average forest description data used in the drift calculations for each plot appearing in the tables was obtained by averaging data supplied by the Forest Service for quarter-plots. Only data from those quarter-plots from which drift entered the down-valley flow were used in the average. The values of the probability of penetration (PRPEN) in the tables were assigned by reference to values suggested by Grim and Barry (1975), (i.e., 0.13 for a Foliage Type IV tree and 0.38 for a Foliage Type III tree). Values of the tree widths at one-meter intervals required for the canopy penetration model were obtained using the procedure for the Rennic Creek Trials described in Section 3.1.4. The last column in each of the tables shows the wind direction used in the model for calculating deposition at the tree cluster.

TABLE 3-12

FOREST DESCRIPTION FOR PLOT 1, 1976 REGION 1 PILOT PROJECT

Cluster Number	Average Stand Density (stems/acre)	Average Tree Height (m)	Average Crown Height (m)	Average Crown Width (m)	PRPEN	Wind Direction (deg)
1	80	8.53	5	4.57	0.38	140
2	110	9.75	6	3.35	0.13	150
3	30	6.71	4	2.44	0.13	175
4	90	10.7	6	3.96	0.13	190
5	95	10.8	6	4.49	0.13	150
6	100	11.0	6	4.88	0.13	195
7	80	6.71	4	1.83	0.13	180
8	230	7.62	4	3.35	0.38	170
9	110	8.23	5	2.73	0.13	210
10	50	8.23	5	4.88	0.13	050
11	50	12.2	7	3.96	0.13	205
12	80	8.53	5	2.44	0.13	195
13	110	9.14	5	3.96	0.38	205
14	190	7.62	4	2.13	0.38	100
15	30	9.75	5	4.88	0.13	090
16	120	8.83	5	2.74	0.13	060
17	120	10.7	6	3.66	0.13	100
18	70	11.0	6	3.66	0.13	105
19	50	7.32	4	3.35	0.13	100
20	20	10.4	6	4.88	0.13	105
21	140	9.45	5	3.35	0.13	075
22	60	7.92	4	2.44	0.13	060
23	80	7.32	5	2.59	0.13	105
24	100	6.71	4	2.74	0.13	075
25	80	10.1	6	4.27	0.13	240
Average Used In Drift Calculations	24	14.6	8	4.34	0.13	360

TABLE 3-13

FOREST DESCRIPTION FOR PLOT 2, 1976 REGION 1 PILOT PROJECT

Cluster Number	Average Stand Density (stems/acre)	Average Tree Height (m)	Average Crown Height (m)	Average Crown Width (m)	PRPEN	Wind Direction (deg)
1	120	10.7	6	3.66	0.13	355
2	120	10.7	6	3.66	0.13	015
3	100	10.1	6	4.88	0.13	045
4	100	9.14	5	4.27	0.13	345
5	70	8.53	5	3.96	0.13	015
6	30	8.23	5	4.27	0.13	315
7	160	7.92	4	3.96	0.13	045
8	40	8.53	5	3.35	0.13	340
9	280	8.84	5	4.27	0.13	305
10	70	9.45	5	3.66	0.13	080
11	130	10.4	6	3.66	0.13	070
12	190	11.6	6	4.27	0.13	140
13	390	9.75	5	4.88	0.13	135
14	110	7.31	4	4.57	0.13	150
15	170	8.53	5	3.35	0.13	215
16	120	8.84	5	4.27	0.13	270
17	150	8.53	5	4.27	0.13	265
18	250	7.62	4	3.66	0.13	150
19	50	8.23	5	3.05	0.13	165
20	140	7.92	4	3.05	0.13	140
21	40	12.5	7	5.18	0.13	105
22	220	8.23	5	5.18	0.13	040
23	180	10.4	6	4.27	0.13	225
24	50	10.4	6	3.35	0.13	225
25	60	7.92	4	3.35	0.13	265
Average Used In Drift Calculations	225	11.4	6	4.72	0.13	090

TABLE 3-14

FOREST DESCRIPTION FOR PLOT 3, 1976 REGION 1 PILOT PROJECT

Cluster Number	Average Stand Density (stems/acre)	Average Tree Height (m)	Average Crown Height (m)	Average Crown Width (m)	PRPEN	Wind Direction (deg)
1	30	8.23	5	5.49	0.13	140
2	90	11.3	6	5.49	0.13	165
3	90	11.3	6	5.49	0.13	195
4	130	7.01	4	3.05	0.13	105
5	20	8.23	5	3.96	0.38	105
6	80	8.53	5	4.27	0.13	160
7	70	10.7	6	5.49	0.13	190
8	80	8.84	5	4.12	0.13	195
9	90	7.01	4	2.74	0.13	165
10	80	8.84	4	5.49	0.13	95
11	110	7.01	4	2.44	0.38	110
12	60	11.0	6	4.88	0.13	110
13	80	7.92	4	4.27	0.13	100
14	120	10.1	6	4.27	0.13	260
15	120	10.1	6	4.27	0.13	165
16	120	10.1	6	4.27	0.13	165
17	100	6.71	4	2.44	0.13	135
18	110	8.23	5	3.35	0.13	195
19	60	9.45	5	3.96	0.13	120
20	90	8.23	5	4.88	0.13	125
21	90	7.62	4	4.27	0.13	135
22	50	8.23	5	3.96	0.13	150
23	150	8.53	5	4.57	0.38	160
24	80	8.33	5	3.05	0.13	210
25	190	7.93	4	3.05	0.38	210
Average Used In Drift Calculations	178	13.3	7	4.34	0.13	013

SECTION 4

COMPARISON OF MODEL CALCULATIONS WITH DEPOSITION AND DRIFT MEASUREMENTS

Model calculations of ground-level deposition are compared with deposition measurements made in the open and beneath the forest canopy during the Rennic Creek Trials in Section 4.1. Section 4.2 contains a comparison of calculated and measured deposition for the tree clusters sampled in Plots 1, 2 and 3 of the 1976 Region 1 Pilot Project as well as a comparison of calculated and measured deposition for sampler locations downwind from these plots.

4.1 COMPARISON OF CALCULATED AND MEASURED DEPOSITION FOR THE RENNIC CREEK TRIALS

The deposition model and the Grim-Barry canopy penetration model, respectively described in Section 2.1 and 2.2, were used in conjunction with the model inputs given in Section 3.1 to calculate profiles of ground-level deposition along the six sampling rows used in the Rennic Creek Trials. Figure 4-1 through 4-6 show calculated and measured profiles for Trial 2, which are typical of the results obtained for all five trials. Similar figures for all the trials are contained in Appendix A. In comparing the measured and calculated deposition densities, it should be noted that the "noise-level" of the measurements is probably between 0.1 and 1 mg m^{-2}. If all spray drops had diameters equal to the mass median diameter of 211 micrometers, a deposition density of 1 mg m^{-2} is equivalent to a density of about 240 drops per square meter, or less than 5 drops on a 17 x 11 cm sampling card. Also, as mentioned in Section 3.1, the position of the helicopter flight path with respect to the sampling grid was observed only as the aircraft passed over Row 3 of the grid. Since the model calculations of ground-level deposition are sensitive to aircraft position, especially with regard to the point where significant deposition begins to occur at

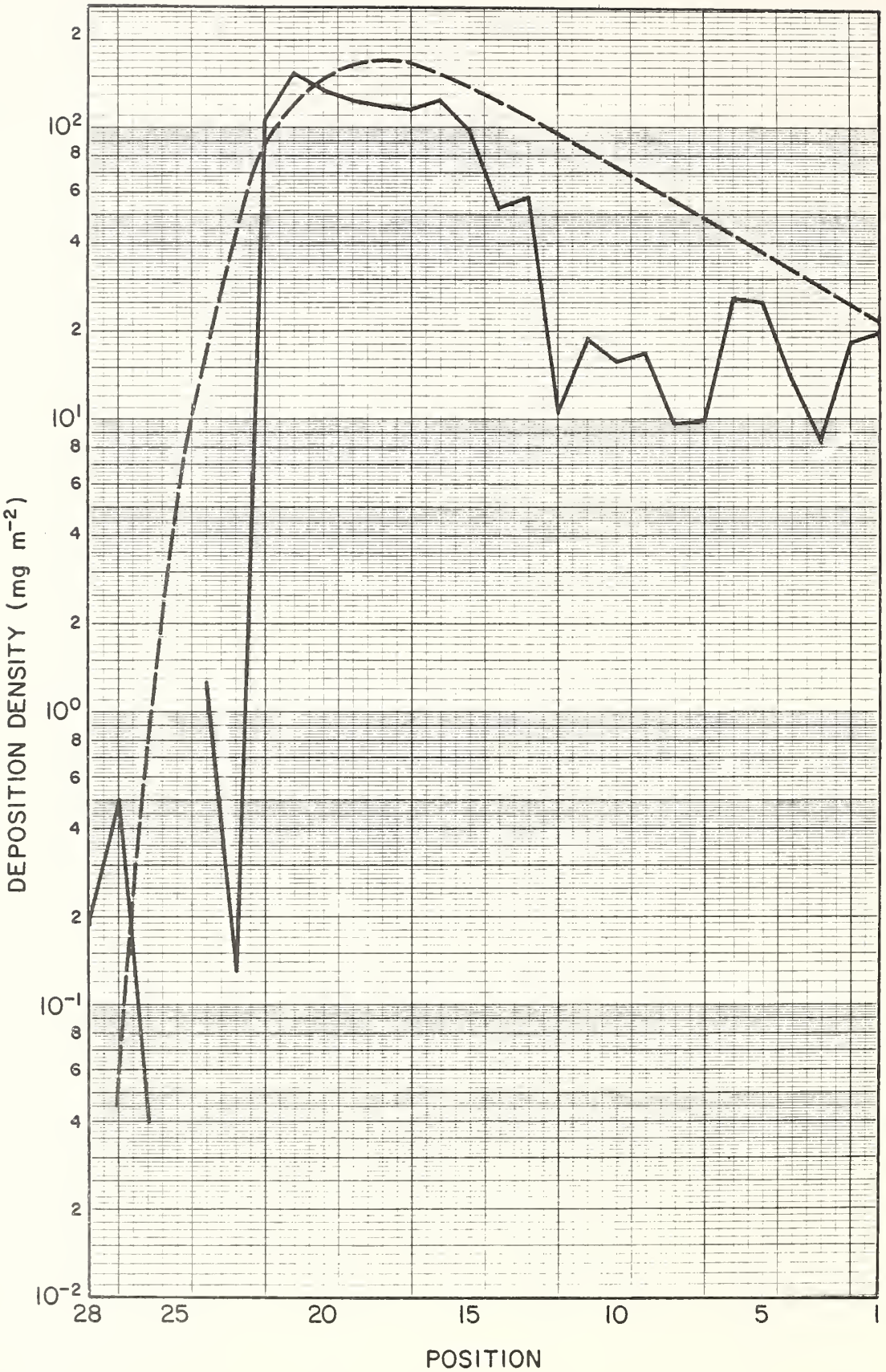

FIGURE 4-1. Predicted (dashed line) versus measured deposition densities for Row 1, Trial 2 of the Rennic Creek Trials.

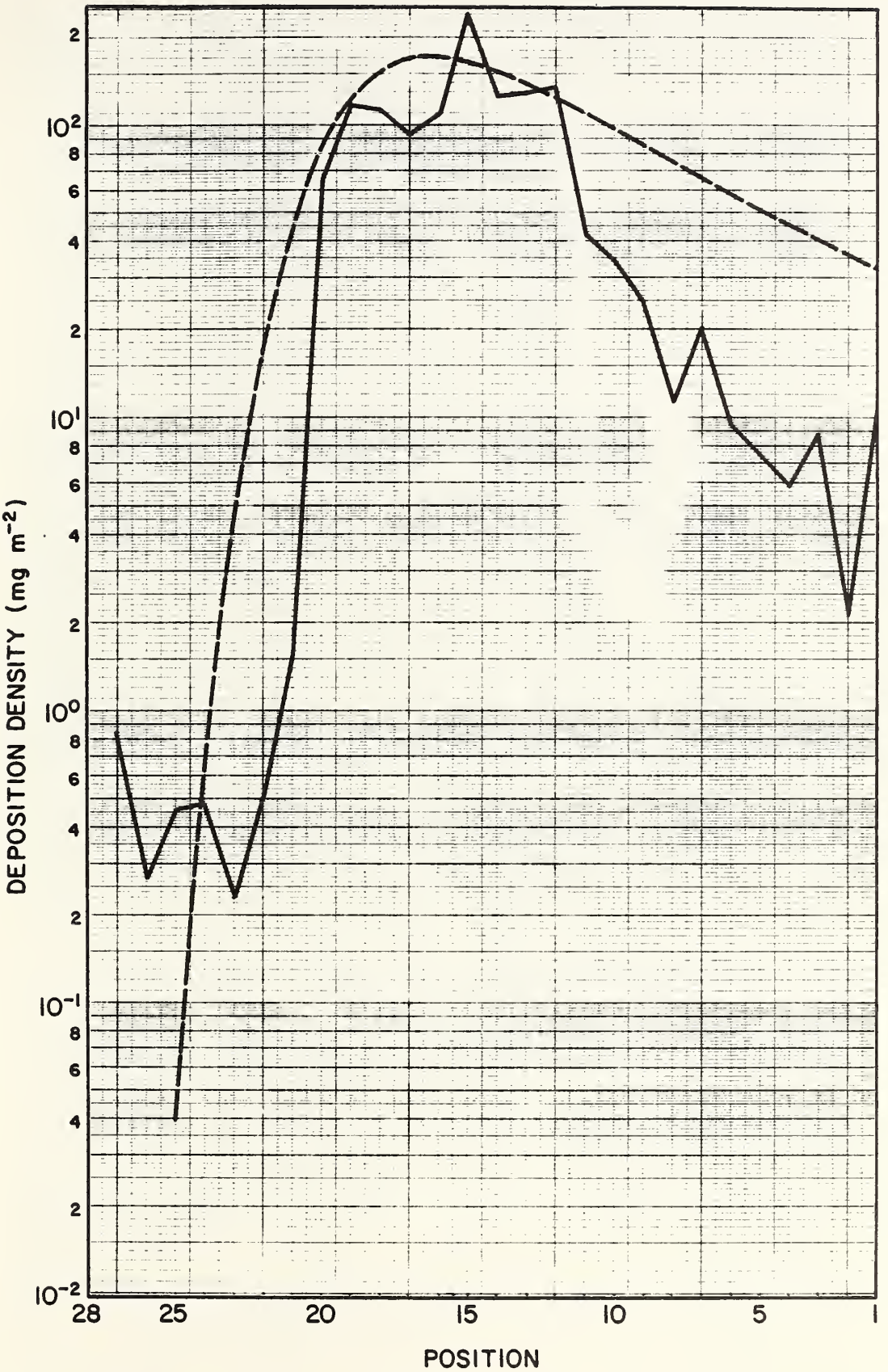

FIGURE 4-2. Predicted (dashed line) versus measured deposition densities for Row 2, Trial 2 of the Rennic Creek Trials.

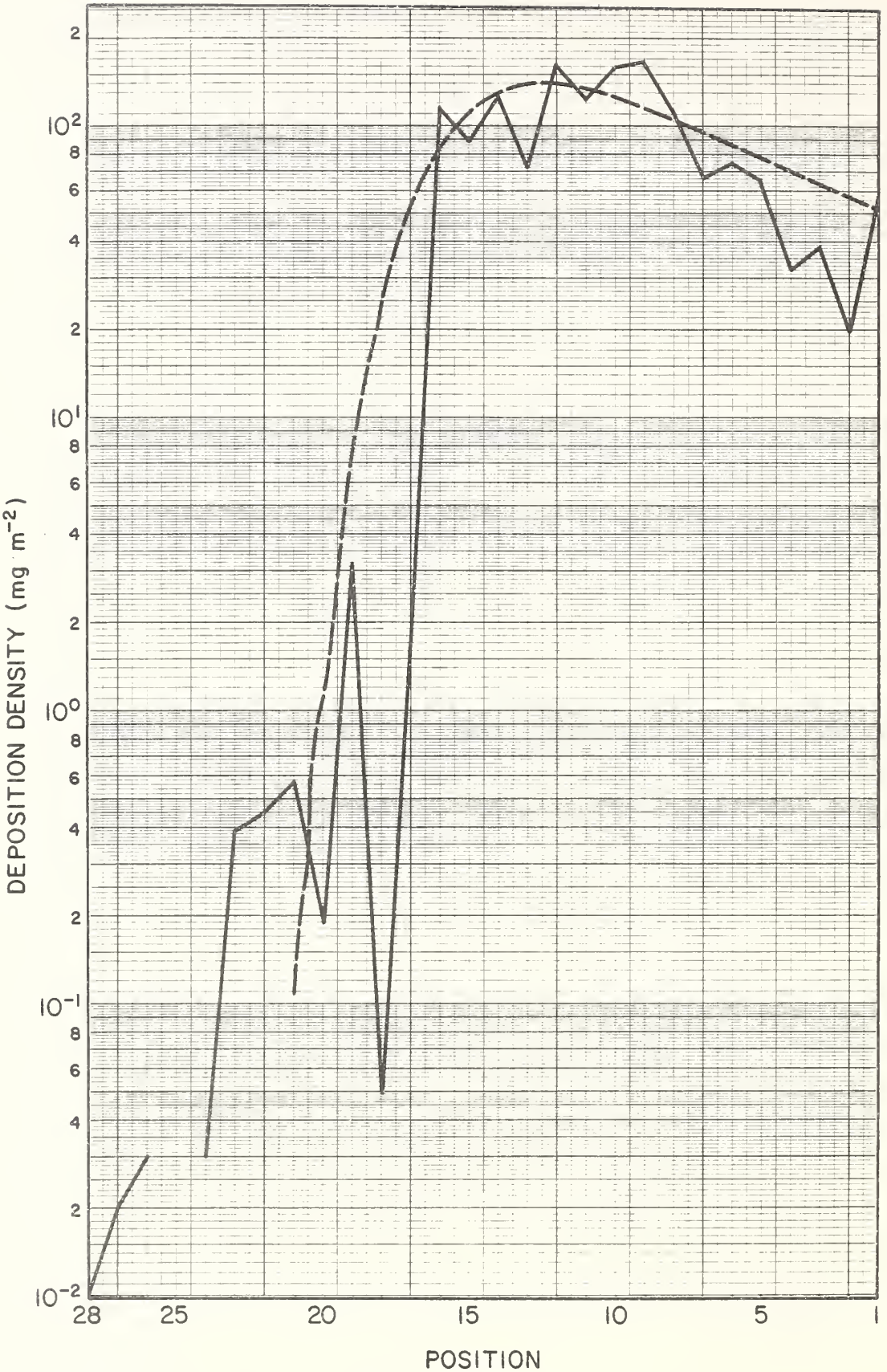

FIGURE 4-3. Predicted (dashed line) versus measured deposition densities for Row 3, Trial 2 of the Rennic Creek Trials.

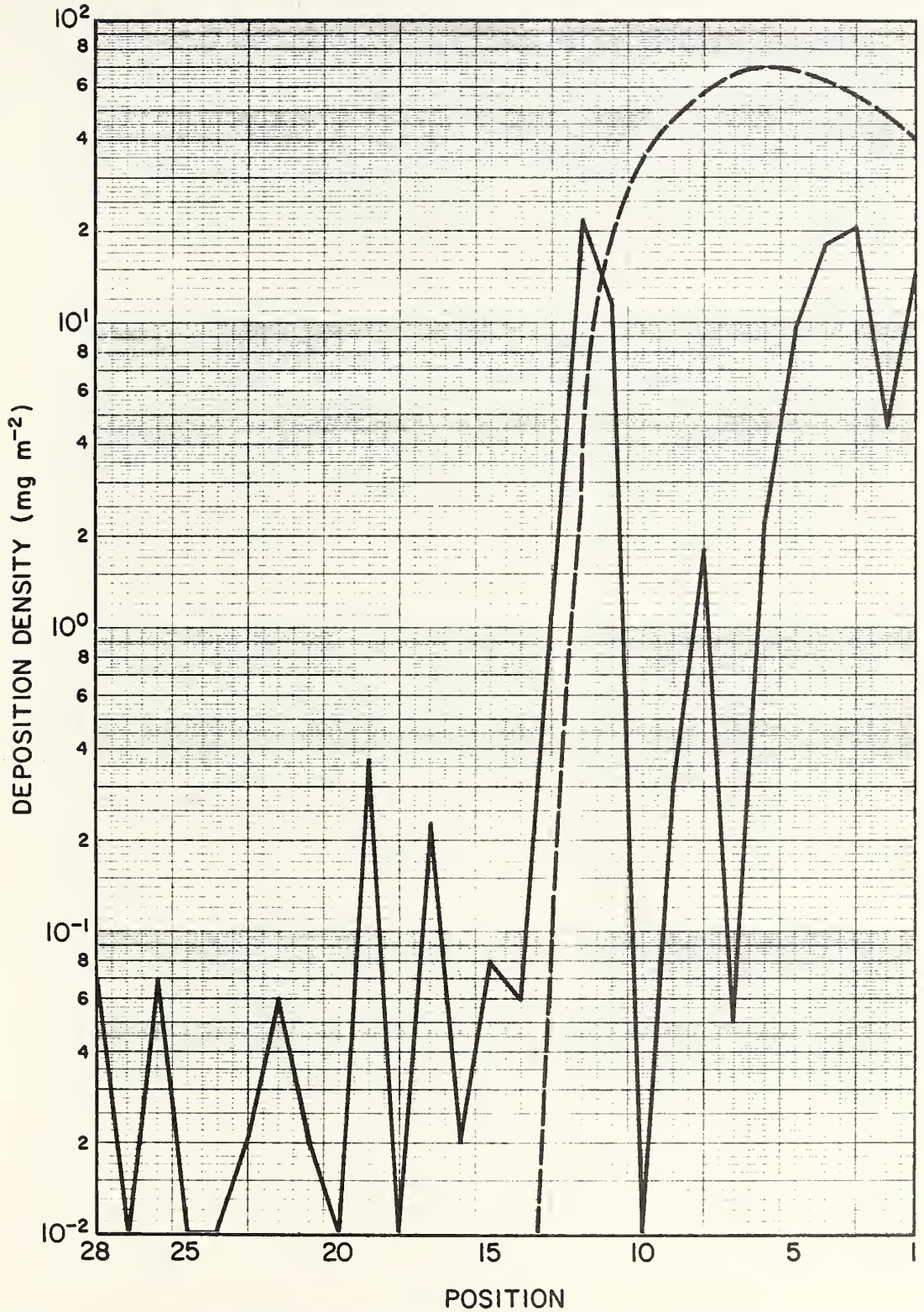

FIGURE 4-4. Predicted (dashed line) versus measured deposition densities for Row 4, Trial 2 of the Rennic Creek Trials.

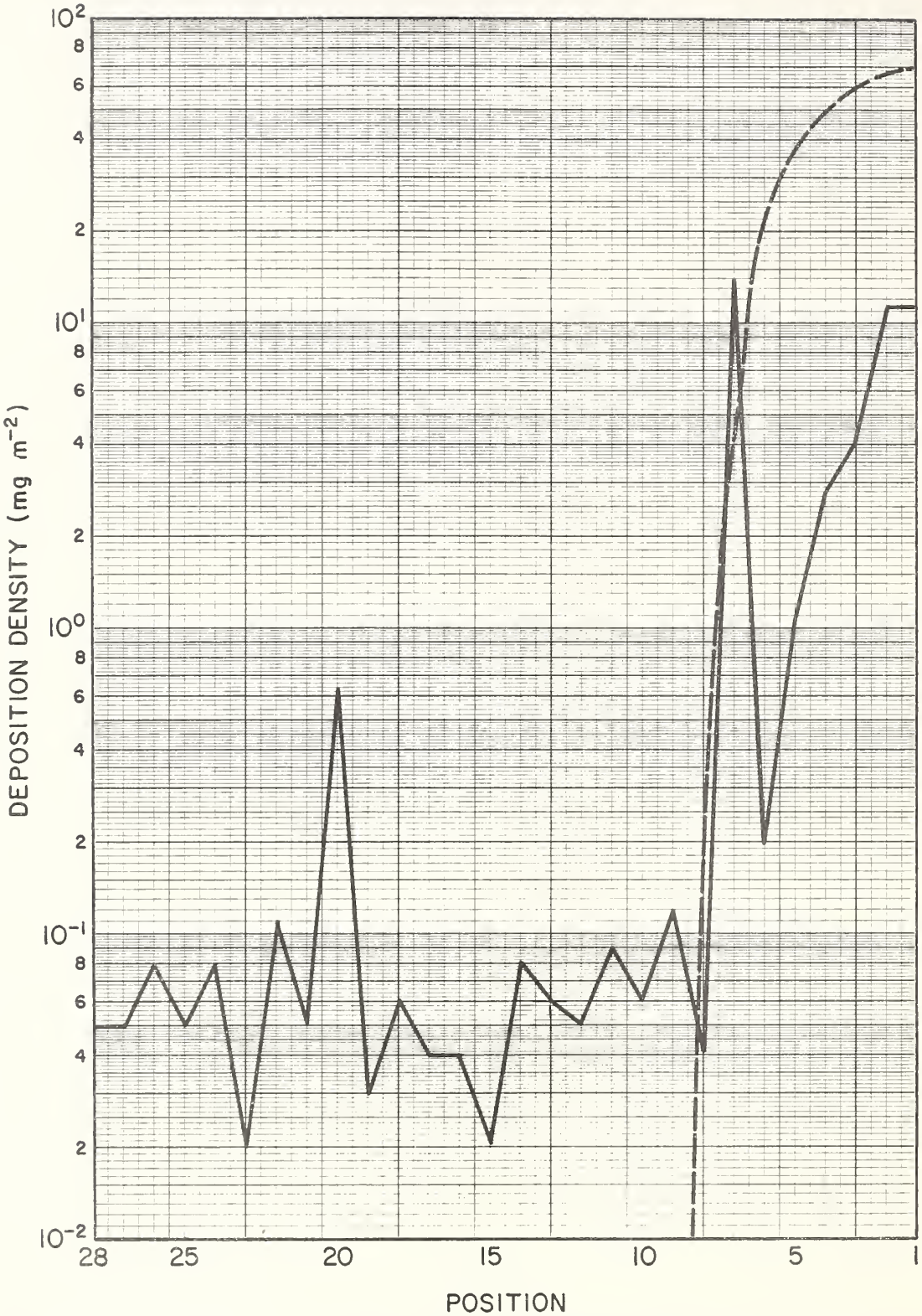

FIGURE 4-5. Predicted (dashed line) versus measured deposition densities for Row 5, Trial 2 of the Rennic Creek Trials.

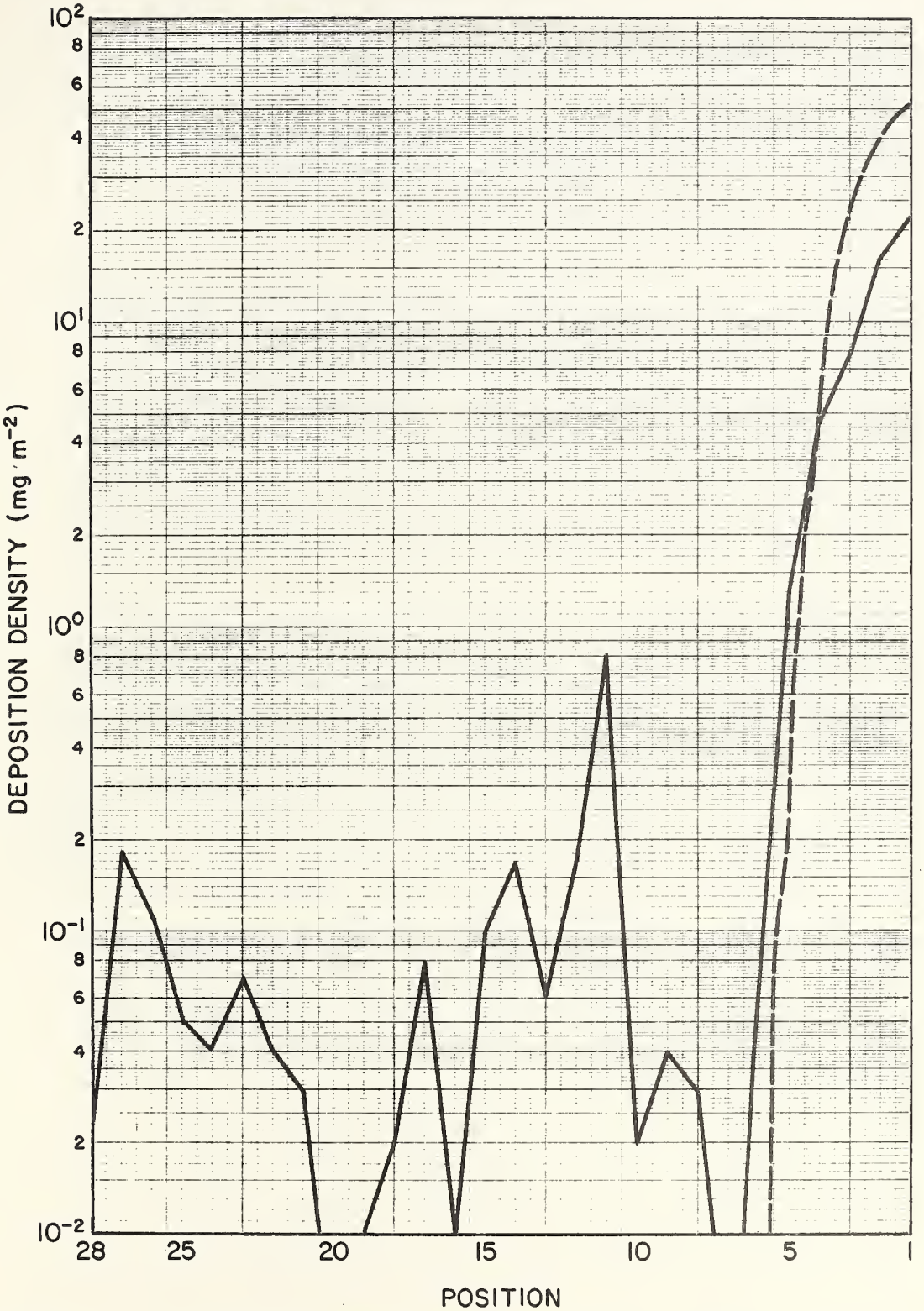

FIGURE 4-6. Predicted (dashed line) versus measured deposition densities for Row 6, Trial 2 of the Rennic Creek Trials.

the upwind boundary of the profile, the position of the flight path was adjusted to obtain the best fit between the location of the observed and model calculated peak deposition. In no case was the position of the helicopter flight path over Row 3 noted by the observers changed by more than the separation distance between samplers.

The results of the calculations shown in Figures 4-1 through 4-6 for Trial 2 and in the figures for the remaining trials presented in Appendix A indicate that the model performed well in predicting the general shape and magnitude of the measured deposition density profiles. This is very significant considering the number of variables which must be estimated or generalized for use in the model equations, the inherent uncertainty in the measurements and the use of indirect analysis procedures (counting and sizing of drop stains) to establish deposition densities.

For direct comparison of model predictions with measurements, we formed ratios of the average measured deposition density to the average calculated density along the sampling rows. The average measured deposition density was obtained by using only those continguous measured densities equal to or greater than 1 milligram per cubic meter and the average calculated density was obtained by using the model estimates for the same sampling positions along the rows. In many cases, the deposition profiles were not contained by the sampling rows, with significant deposition levels likely occurring beyond the downwind limit of the sampling array (for example, see Figure 4-6). Therefore, the ratios may not be representative of model performance over the entire deposition swath. These ratios of average measured and calculated deposition density for each trial and sampling row are presented in Table 4-1. Inspection of Table 4-1 shows that in most cases the model overestimates the measured average deposition density. The model calculations are more accurate for Row 3 where the position of the flight path was best known. Table 4-2 summarizes the measured and calculated

TABLE 4-1

RATIOS OF AVERAGE MEASURED AND PREDICTED DEPOSITION DENSITY FOR INDIVIDUAL SAMPLING ROWS OF THE RENNIC CREEK TRIALS

Trial Number	Sampling Row					
	1	2	3	4	5	6
1	0.48	0.13	1.01	1.05	1.48	1.05
2	0.63	0.66	0.83	0.19	0.15	0.43
3	0.41	0.25	0.39	1.21	0.12	0.23
4	0.29	0.25	0.72	0.36	0.53	0.57
5	0.32	0.20	0.61	0.45	0.21	0.50
Average Ratio (All Trials)	0.43	0.27	0.69	0.62	0.35	0.58

TABLE 4-2

MEASURED AND CALCULATED AVERAGE DEPOSITION DENSITIES ($mg\ m^{-2}$) FOR THE OPEN AND FORESTED AREAS OF THE RENNIC CREEK TRIALS

Trial Number	Rows In Open Area			Rows In Trees		
	Measured	Calculated	$\frac{\text{Measured}}{\text{Calculated}}$	Measured	Calculated	$\frac{\text{Measured}}{\text{Calculated}}$
1	43.3	83.9	0.52	33.0	29.7	1.11
2	62.3	88.9	0.70	8.2	40.1	0.20
3	30.4	86.1	0.35	32.5	51.1	0.63
4	34.2	83.7	0.41	23.0	49.8	0.46
5	39.1	103.4	0.38	22.7	51.5	0.44
Average (All Trials)	41.9	88.8	0.47	24.2	45.0	0.54

average deposition densities in the open and forested areas of the Rennic Creek Trials. The ratios of measured and calculated deposition density shown in Table 4-2 indicate the models tend to overestimate average deposition densities in both areas by about a factor of two. The model overestimation of average deposition densities may be in part due to evaporation losses of material during transport. The drop-size distribution used in the model is assummed to reflect the effects of evaporation, but the model formulation described in Section 2 does not expressly consider evaporation.

4.2 COMPARISON OF MODEL ESTIMATES WITH MEASURED DEPOSITION AND DRIFT FOR THE 1976 REGION 1 PILOT PROJECT

The deposition and drift models described in Section 2.1 and the Grim-Barry canopy penetration model in Section 2.2 were used in conjunction with the model inputs given in Section 3.2 to obtain model estimates for comparison with deposition measurements made at tree clusters and deposition and drift measurements made down-valley from the spray plots.

As noted in Section 3.2, ground-level deposition beneath a tree cluster was measured at four locations beneath each of the three trees comprising the cluster. Since the models predict the average deposition in the vicinity of each cluster, the deposition measurements from all twelve cards in a cluster were averaged to obtain a single estimate for comparison with the model value. The average measured and calculated deposition densities, and the ratios of measured and calculated deposition, for each tree cluster in Plots 1, 2 and 3 are respectively presented in Tables 4-3, 4-4 and 4-5. Inspection of the three tables shows that the ratios of measured and calculated deposition densities are highly variable. Although we do not know with certainty the causes for the large variability exhibited by the ratios, the following factors

significantly affect the accuracy of modeling deposition beneath tree clusters:

(1) As experience in modeling the deposition profiles for Rennic Creek has shown, knowledge of the specific location of the spray aircraft with relation to the sampler is an extremely important factor for obtaining correspondence between measured and observed deposition densities. Aircraft spray paths for the 1976 Region 1 Pilot Project Trials were drawn on a 1 to 24,000 scale topographic map (see Ekblad, Miller and Flavell, 1977) by an observer in another aircraft monitoring the spray project. We used these sketches to position the aircraft for the model calculations.

(2) The canopy penetration model assumes that trees used in the model are randomly distributed within their assigned area according to their estimated stem density; also, the card samplers used to measure deposition density are assumed to be randomly distributed beneath trees and in open spaces. The card samplers in the 1976 Region 1 Pilot Project, following the practice for measuring deposition densities in tree clusters, were placed beneath the drip-line of trees within the cluster. Heavier drops with relatively large settling velocities would therefore have to penetrate the trees before impacting on cards and thus the model might be expected to overpredict deposition even for clusters in the immediate vicinity of the spray swath.

(3) Meteorological measurements of wind speed and direction were made at only a few locations within the spray plot. However, Ekblad, Miller and Flavell (1977) have indicated the time periods when winds were generally downslope, in transition to upslope and upslope during each spray period in their Tables 1

through 8. We used this information, the slope direction from a topographic map of the plot area and the times spraying took place in the general vicinity of each tree cluster to assign a single wind direction for use in calculations for the tree cluster. This assigned wind direction was used to calculate the contribution of every line segment in the spray plot to the deposition at the tree cluster. Relatively large errors could be introduced into the calculations if the values assigned to the wind direction and speed are in error.

(4) The median tree densities for spray Plots 1, 2 and 3 are respectively about 80, 120 and 90 stems per acre, as compared to 285 stems per acre for the Rennic Creek Trials. Model inputs, such as the wake-induced stabilization height of the spray cloud above the canopy, which were valid for the relatively denser forest at Rennic Creek, may not be valid for the tree clusters in the spray plots for the 1976 Region 1 Pilot Project.

The median ratios of measured and calculated deposition density beneath tree clusters are 0.40, 0.19 and 0.40 for spray Plots 1, 2 and 3. The corresponding median ratios for Plots 1 and 3 are only slightly less than the average ratios of measured and calculated deposition densities for sampling rows in the open (0.49) and in the trees (0.54) for the Rennic Creek Trials; the median ratio for Plot 2 of the 1976 Region 1 Pilot Project is about half as large (0.20). The tree cluster samples for Plots 1 and 3 were taken in a major valley or near the ridge lines on either side of the major valley. Tree cluster deposition sampling for Plot 2 was accomplished in three separate smaller valleys as well as along ridge lines in the vicinity of the valleys. The fact that the terrain for Plot 2 was more complex than for Plots 1 and 3 may account for the smaller median ratio for Plot 2 because spray material

released in one valley may not have been transported by the winds to the tree clusters in the other valleys, as assumed in the model calculations.

Figures 4-7, 4-8 and 4-9 respectively show profiles of calculated dosages and dosages measured by the University of California down-valley from Plots 1, 2 and 3. Similar profiles of calculated and measured deposition are shown in Figures 4-10 through 4-12. Inspection of Figures 4-7 through 4-9 indicates that the model consistently overpredicts measured dosages in most cases by more than an order of magnitude. Also, the measured dosages for Plots 1 and 2 decrease with distance at a faster rate than the model calculations. However, the slope of the calculated profile for Plot 3 shown in Figure 4-9 is consistent with the slope of the measured dosages. It should be noted that Plot 3 was sprayed with Orthene and Plots 1 and 2 were sprayed with Dylox. Since the drop-size distribution for Orthene produced by the spray aircraft is comprised of larger drops than the drop-size distribution for Dylox, the dosage should decrease more rapidly with distance downwind from Plot 3. While the calculated profiles reflect this property, the slopes of the measured dosage profiles are nearly the same for all three plots. The slopes of the deposition profiles shown in Figures 4-10 through 4-12 should also reflect the effects of differences in drop-size distribution on the rate of decrease in deposition with distance. Inspection of these figures again shows that the slope of the calculated profiles agrees with the slope of the measured deposition profile for Plot 3, but the slopes of the calculated profiles for Plots 1 and 2 do not agree with the slopes of the measured profiles.

We are at present unable to explain the discrepancies between the calculated and measured dosage and deposition downwind from the spray plots. However, we believe that the simple wind field assumed in the drift calculations is a major cause of the discrepancies. The terrain of the three spray plots is sufficiently complex that it is practically impossible, with the limited wind data available, to describe accurately

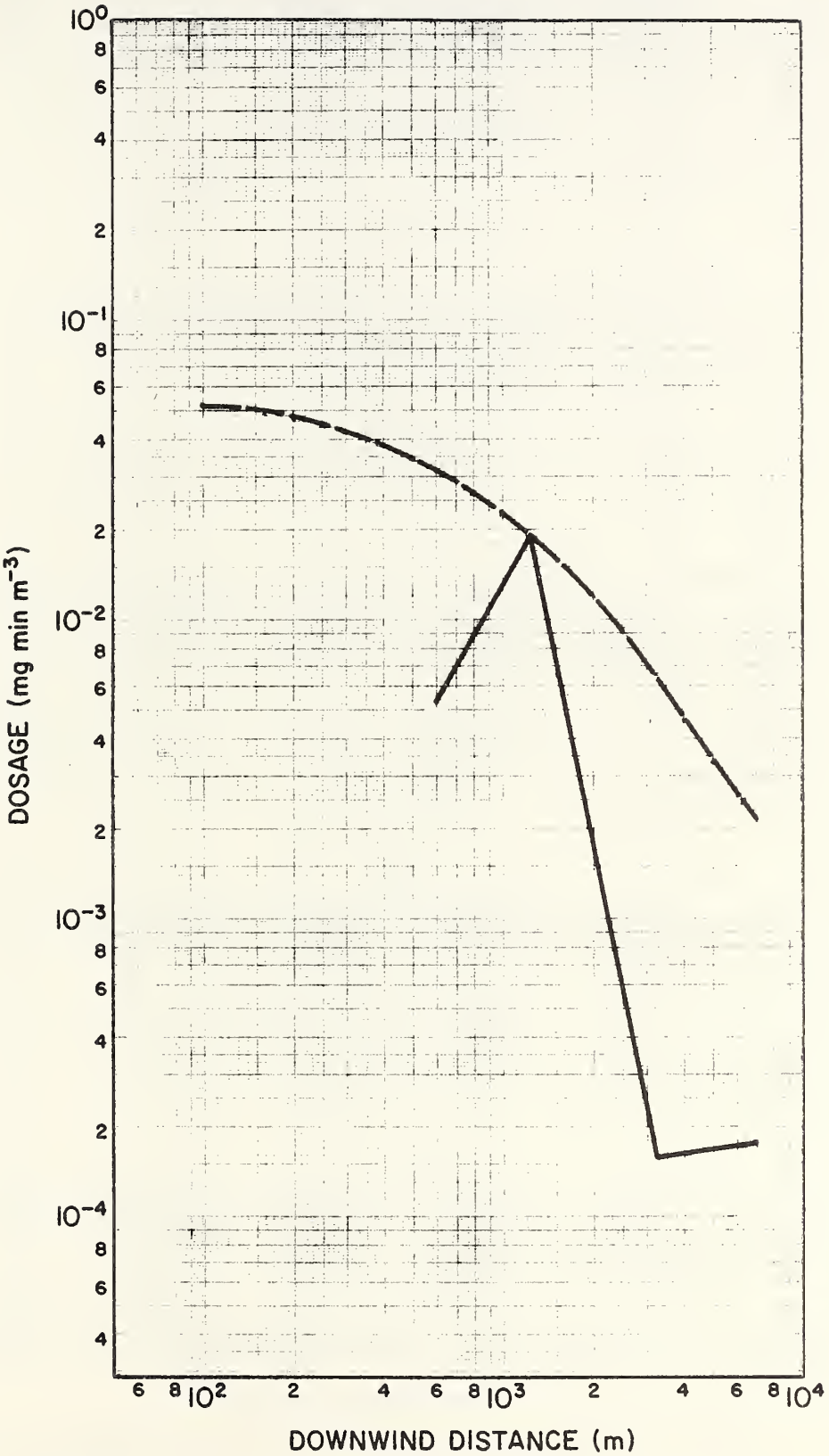

FIGURE 4-7. Predicted (dashed line) versus measured dosage profiles down-valley from Plot 1, 1976 Region 1 Pilot Project.

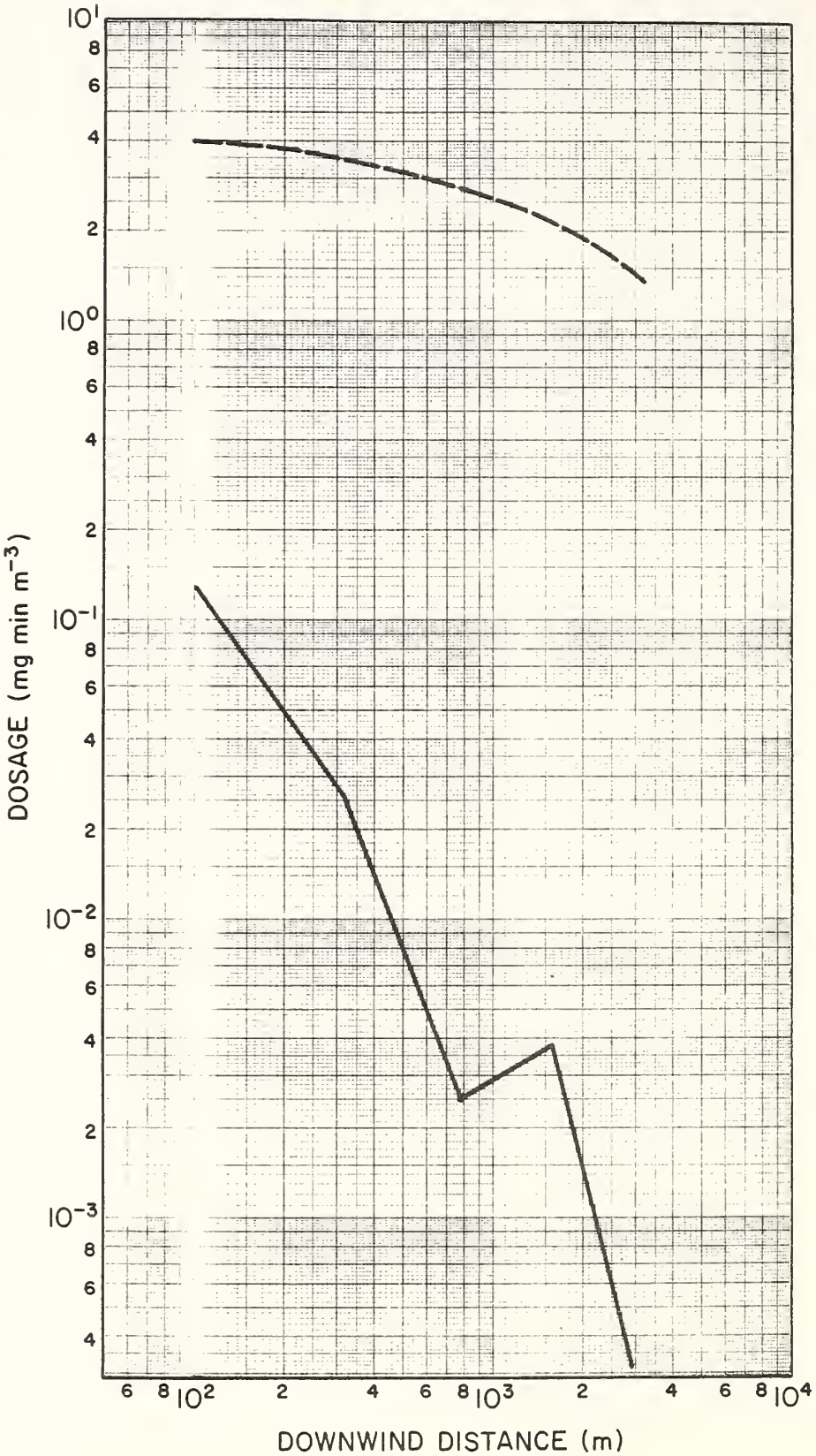

FIGURE 4-8. Predicted (dashed line) versus measured dosage profiles down-valley from Plot 2, 1976 Region 1 Pilot Project.

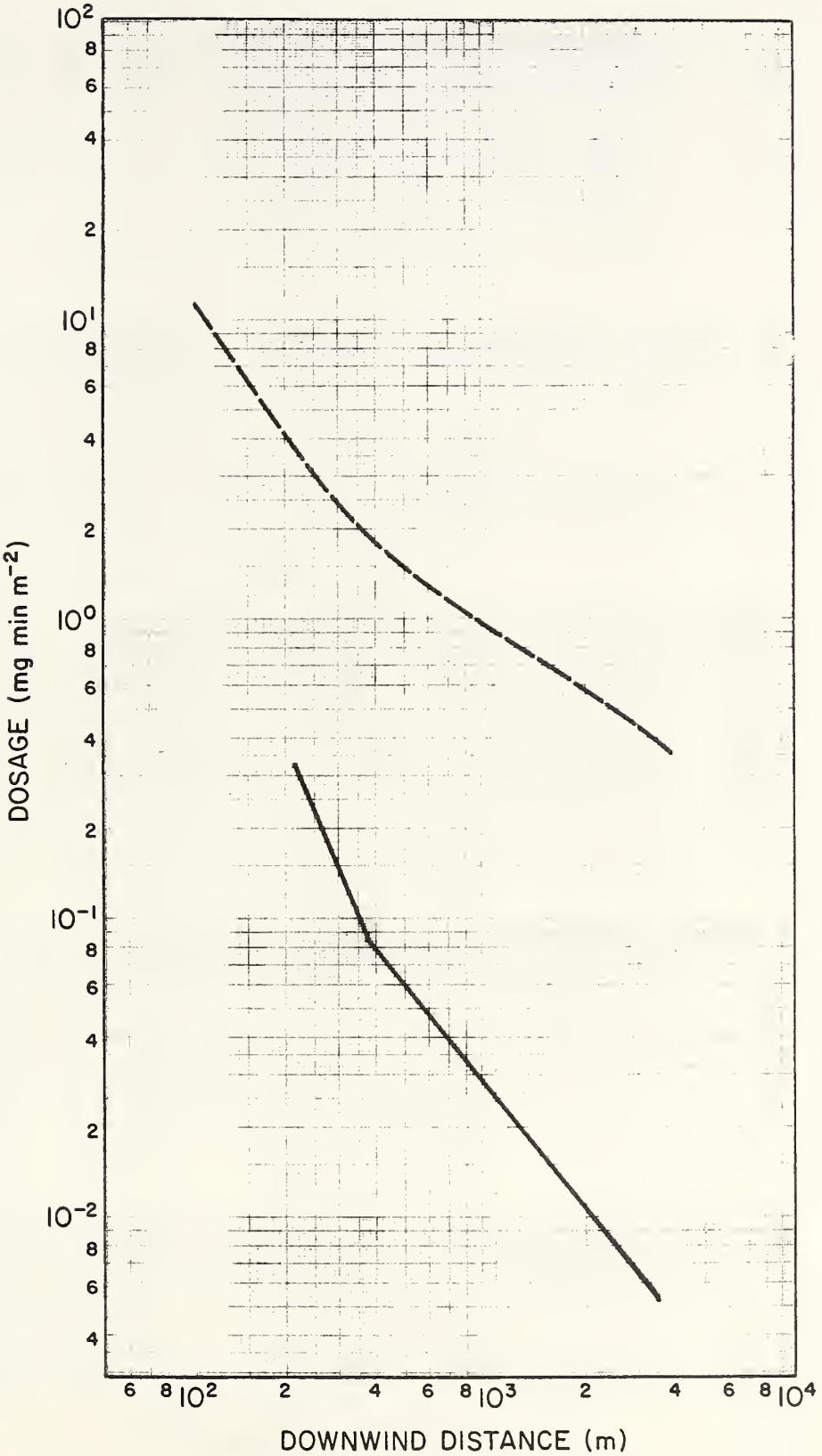

FIGURE 4-9. Predicted (dashed line) versus measured dosage profiles down-valley from Plot 3, 1976 Region 1 Pilot Project.

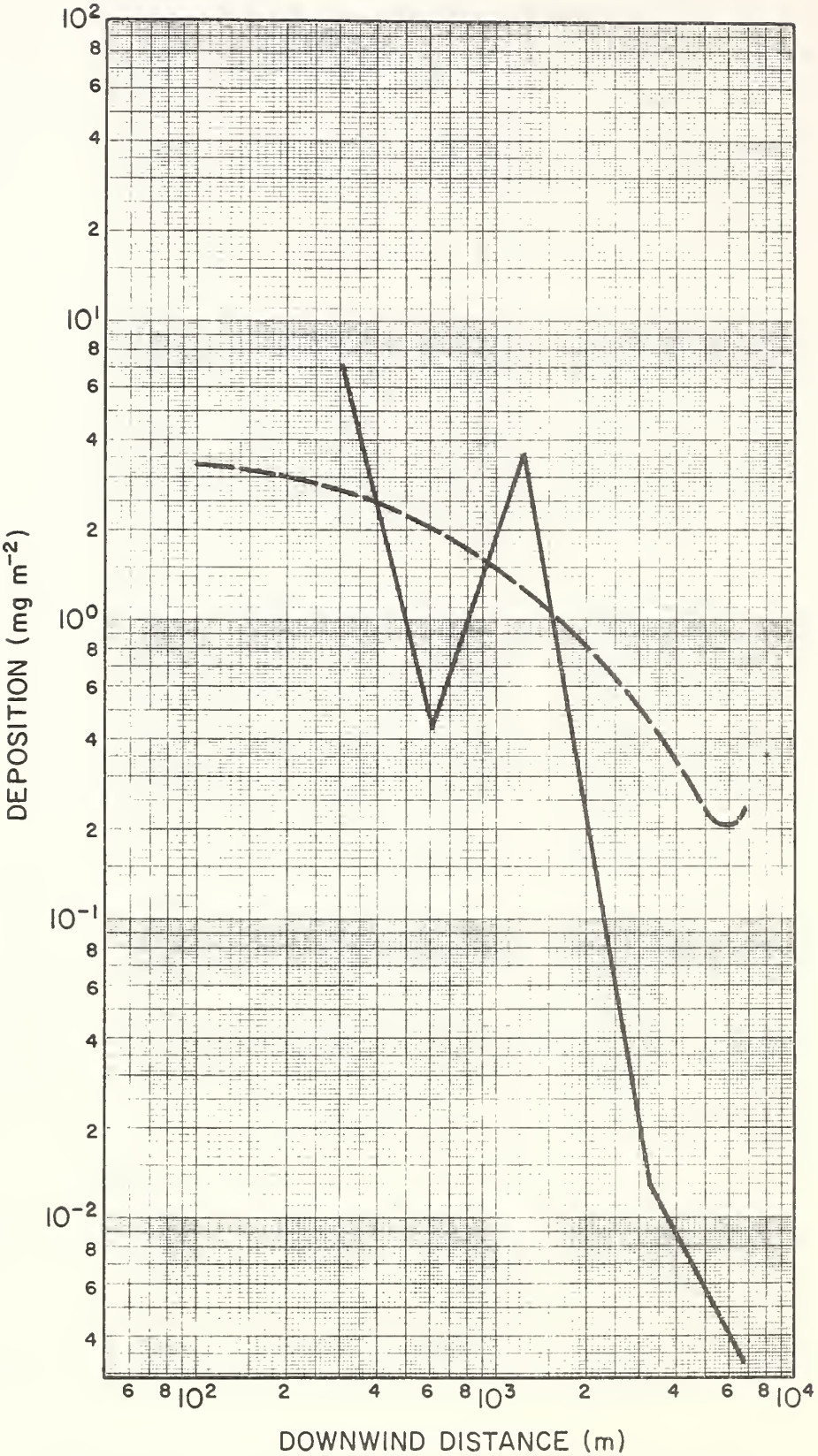

FIGURE 4-10. Predicted (dashed line) versus measured deposition profiles down-valley from Plot 1, 1976 Region 1 Pilot Project.

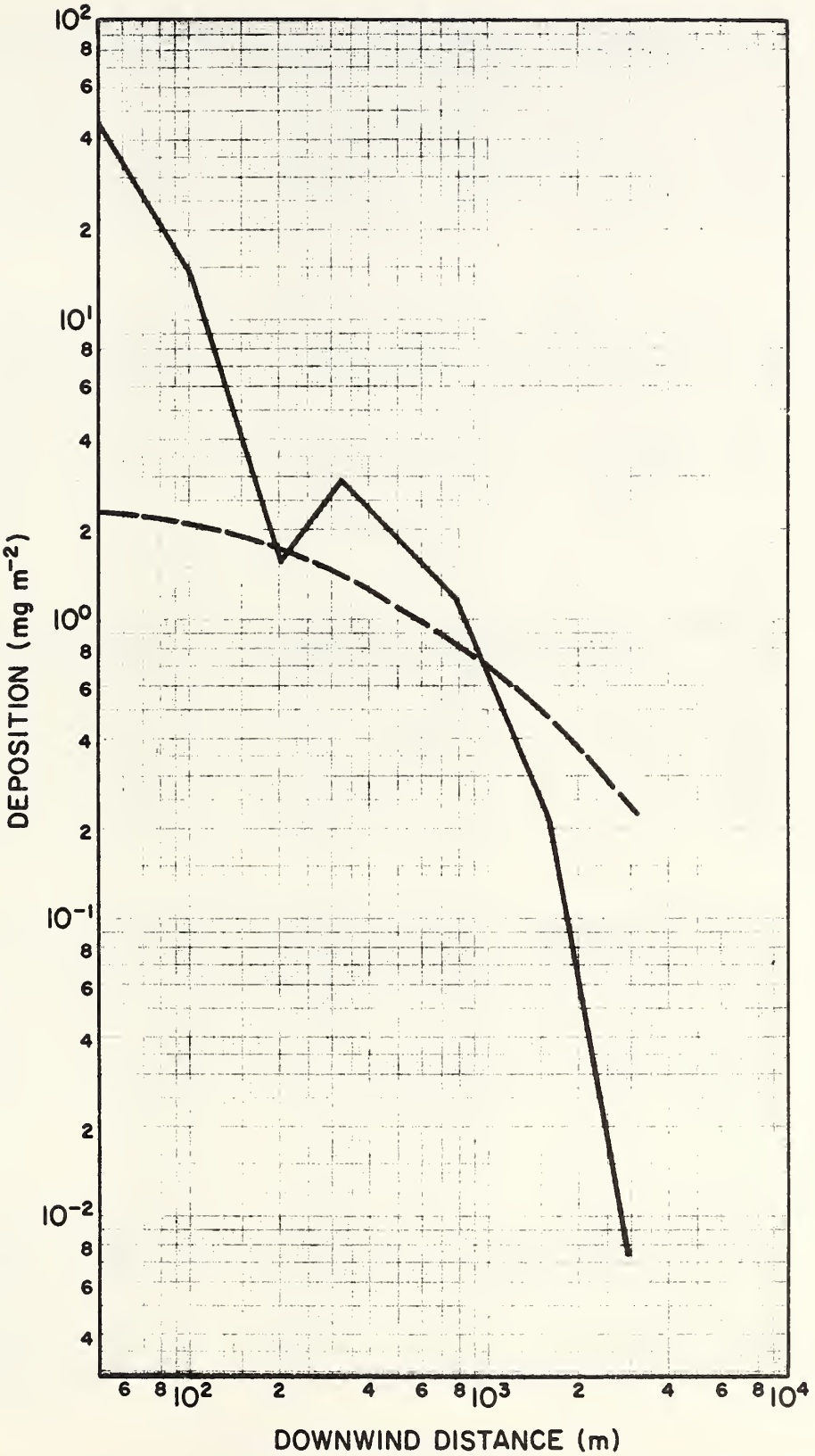

FIGURE 4-11. Predicted (dashed line) versus measured deposition profiles down-valley from Plot 2, 1976 Region 1 Pilot Project.

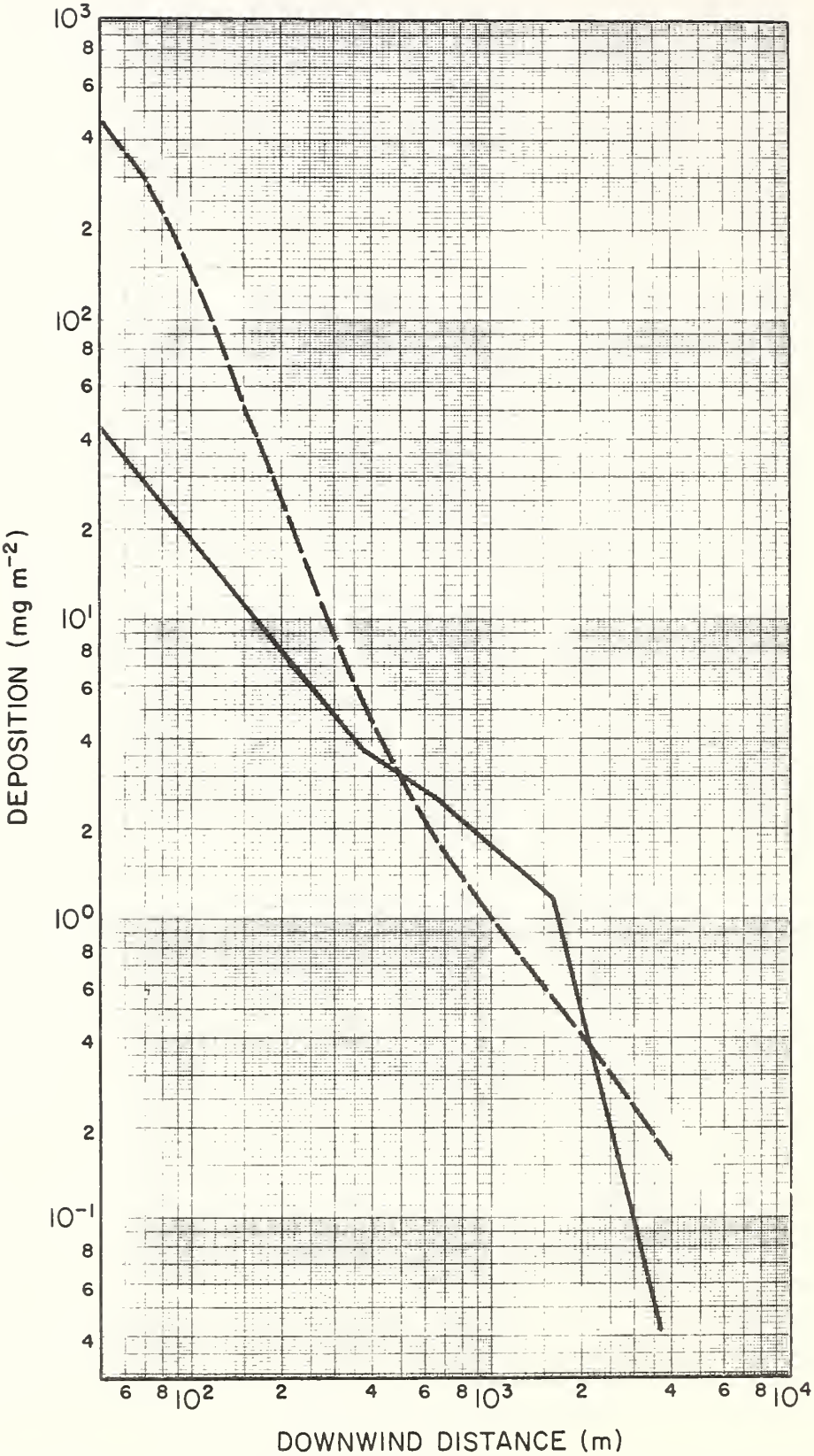

FIGURE 4-12. Predicted (dashed line) versus measured deposition profiles down-valley from Plot 3, 1976 Region 1 Pilot Project.

the trajectories of the spray plumes within the spray plot and to determine the contribution of the various spray lines to the composite spray cloud that is eventually transported downvalley to the points where the drift measurements were made.

SECTION 5
SUMMARY AND RECOMMENDATIONS

As noted in Section 1 of this technical report, the three major objectives of this study were to begin the construction of a data base of forest spray information, use the data base to refine and adapt models for predicting spray behavior, and to use the models to evaluate measurements made during the 1976 Region 1 Pilot Project and to demonstrate the potential usefulness of these modeling techniques. We believe we have met these objectives.

Much of the contract effort was spent in developing a new line-source model program for predicting deposition and dosage downwind from aerial spray releases and in improving the computer program for the Grim-Barry canopy penetration model prescribed for use in the study. The development of the new program for predicting dosage and deposition was necessary for economically performing calculations downwind from the many line sources flown in a typical spray project, most of which are not flown exactly perpendicular to the mean wind direction. The new models used in developing the program are unique in that analytical solutions have been obtained for expressing dispersion from line sources oriented at arbitrary angles to the mean wind direction which are based on the well-known Gaussian plume modeling approach. We believe the development of these computer codes to be a major accomplishment under the contract. Improvements were also made in the computer program for the Grim-Barry canopy penetration model to correct program coding errors discovered in the program supplied to the H. E. Cramer Company and to make the program output compatible with requirements of the deposition and dosage model codes.

The deposition and canopy penetration model programs were used to calculate deposition for comparison with measurements made along sampling rows beneath the forest canopy and in open areas for five trials

conducted at the Rennic Creek site in Montana. Comparison of the model calculations with the measurements made in both locations indicates that the models are capable of predicting the general shape of the deposition profiles measured along the rows. The model calculations on the average overestimated the measured ground-level deposition by about a factor of two, which we believe must be considered an excellent performance in view of the variability exhibited by the measurements and the many factors which must be accounted for in making the model calculations. Also, the models do not directly account for the evaporation of material during transport, which may contribute to the overestimation of deposition density.

The models were also used to calculate ground-level deposition beneath trees for comparison with deposition measurements made beneath tree clusters on Plots 1, 2 and 3 of the 1976 Region 1 Pilot Project. Ratios of measured and calculated deposition for the tree clusters were extremely variable, although the median ratios for the plots showed that calculated deposition exceeds the measured deposition by a factor of 2.5 to 5. Comparisons of dosage and deposition calculations with drift measurements made down-valley from the spray plots were disappointing, with the models overpredicting measured dosage in most cases by more than an order of magnitude and mixed results obtained for the deposition calculations. We are convinced that the differences between the model calculations and measured deposition and dosage for the 1976 Region 1 Pilot Project are not caused by basic deficiencies in the modeling techniques. We believe that the major difficulty in modeling dispersion within the spray plots and down-valley from the spray plots is the inability to describe accurately the wind field over the complex terrain in which the spraying was conducted and, thus, the inability to specify accurately the trajectories of the spray clouds.

In conclusion, we believe the results of this study demonstrate the potential usefulness of the deposition, dosage and canopy penetration

models in designing spray strategies including the definition of source strength requirements for achieving specified deposition levels, estimation of swath widths and the specification of the separation distance between flight paths. Until further verification of the models is accomplished, the results of this study indicate a more accurate representation of average measured deposition density can be achieved by dividing calculated deposition densities by a factor of two.

Further verification of the models described in this report is highly desirable and necessary to develop confidence in their use. Based on the results of this study, the following recommendations are made:

(1) The potential usefulness of models for predicting spray behavior could be best evaluated if the models were used to design spray strategies for pilot projects conducted by the USDA, Forest Service. The recommendation is made that the models described in this report be considered for active use in developing spray strategies for future pilot projects.

(2) Specific provision for verification of the models should be made in the design of sampling networks for selected future pilot projects where the models have been used to develop spray strategy. For example, sampling grid designs similar to that used in the Rennic Creek trials are better suited for purposes of model verification than the tree cluster sampling network used in the 1976 Region 1 Pilot Project. Careful consideration must also be given to the design of a meteorological sampling network suited for best representing the wind-field in complex terrain.

(3) The verification of model drift estimates is a particularly difficult problem in complex terrain. For this reason, we

recommend that careful consideration be given to the selection of spray plots in complex terrain and sampling designs which may be better suited for verification of model drift estimates. For example, a spray plot at the head of a long major valley may be better suited for model verification than a spray plot located on a ridge with a number of valleys leading from the ridge. Consideration should also be given to conducting some special spray projects in less complex terrain with open and forested areas to develop confidence in the application of the models.

(4) A major difficulty in predicting drift in complex terrain occurs because of the inability to describe the spray cloud trajectory. For this reason, we believe consideration should be given to the development of a mesoscale wind-field model for complex terrain that could be used in conjunction with the dispersion and canopy penetration models described in this report.

(5) Because of the time and funding limitation under this contract, it was not possible to make full utilization of the available data. Further model development and verification similar to the study described in this report could likely be performed with these data. Suggested data sources include the 1973 Pine Butterfly Project, additional spray plots in the 1976 Region 1 Pilot Project, and deposition data from the aircraft characterization trials held prior to the 1976 Region 1 Pilot Project.

(6) The recommendation is made that a study be conducted to determine the feasibility and effects of including techniques for estimating evaporation losses of material within the disperson model construct developed in this study.

REFERENCES

Akesson, N. B., W. E. Yates and J. J. Carroll, 1977: Airborne and fallout drift losses of pesticide sprays under a forest canopy. Final Report, DFTM Activity Number: 2-4 Agreement PSW-3, 21-395, Agricultural Engineering Department, University of California, Davis, California 95616.

Bell Helicopter Company, 1966: Helicopter Techniques for Aerial Application, Agricultural Helicopter Section, Bell Helicopter Company, Forth Worth, Texas.

Cramer, H. E., et al., 1972: Development of dosage models and concepts. Final Report under Contract DAAD09-67-C-0020(R) with the U. S. Army, Deseret Test Center Report DTC-TR-72-609, Fort Douglas, Utah.

Dumbauld, R. K., J. E. Rafferty and H. E. Cramer, 1976: Dispersion deposition from aerial spray releases. Paper presented at the Third Symposium on Atmospheric Turbulence, Diffusion and Air Quality, Raleigh, North Carolina. Reprint available from American Meteorological Society, Boston, Massachusetts.

Dumbauld, R. K. and J. E. Rafferty, 1977: Development of a field manual for the characterization of spray from small aircraft. Final Report under Contract No. 26-3694, Forest Service Equipment Development Center, Missoula, Montana.

Ekblad, R. B., G. Miller and T. H. Flavell, 1977: Meteorological data supplement, 1976 Spruce Budworm Pilot Test, Helena National Forest. ED&T 2425, Forest Service Equipment Development Center, Missoula, Montana.

Grim, B. S. and J. W. Barry, 1975: A canopy penetration model for aerially disseminated insecticide spray released above coniferous forests. Final Report under MEDC Project No. 2425, Forest Service Equipment Development Center, Missoula, Montana.

Jones, D. N., 1970: Introduction to jet-engine exhaust and trailing vortex wakes. Technical Report No. 226. U. S. Air Force, Air Weather Service (MAC).

McDonald, J. E., 1960: An aid to computation of terminal fall velocities of spheres. J. Met., 17, 463.

Pasquill, F., 1974: Atmospheric Diffusion (Second Edition. Ellis Horwood Limited, Sussex, England, 429.

Prandtl, L. and O. G. Tietjens, 1934: Fundamentals of Hydro- and Aeromechanics. Dover Publications, Inc., New York, New York.

Slade, D. H. (ed.), 1968: Meteorology and Atomic Energy. Prepared by Air Resources Laboratories, ESSA, for U. S. Atomic Energy Comission, 445.

APPENDIX A

This appendix contains figures showing predicted and measured deposition densities for each of the six sampling rows for Trials 1 through 5 of the Rennic Creek Trials.

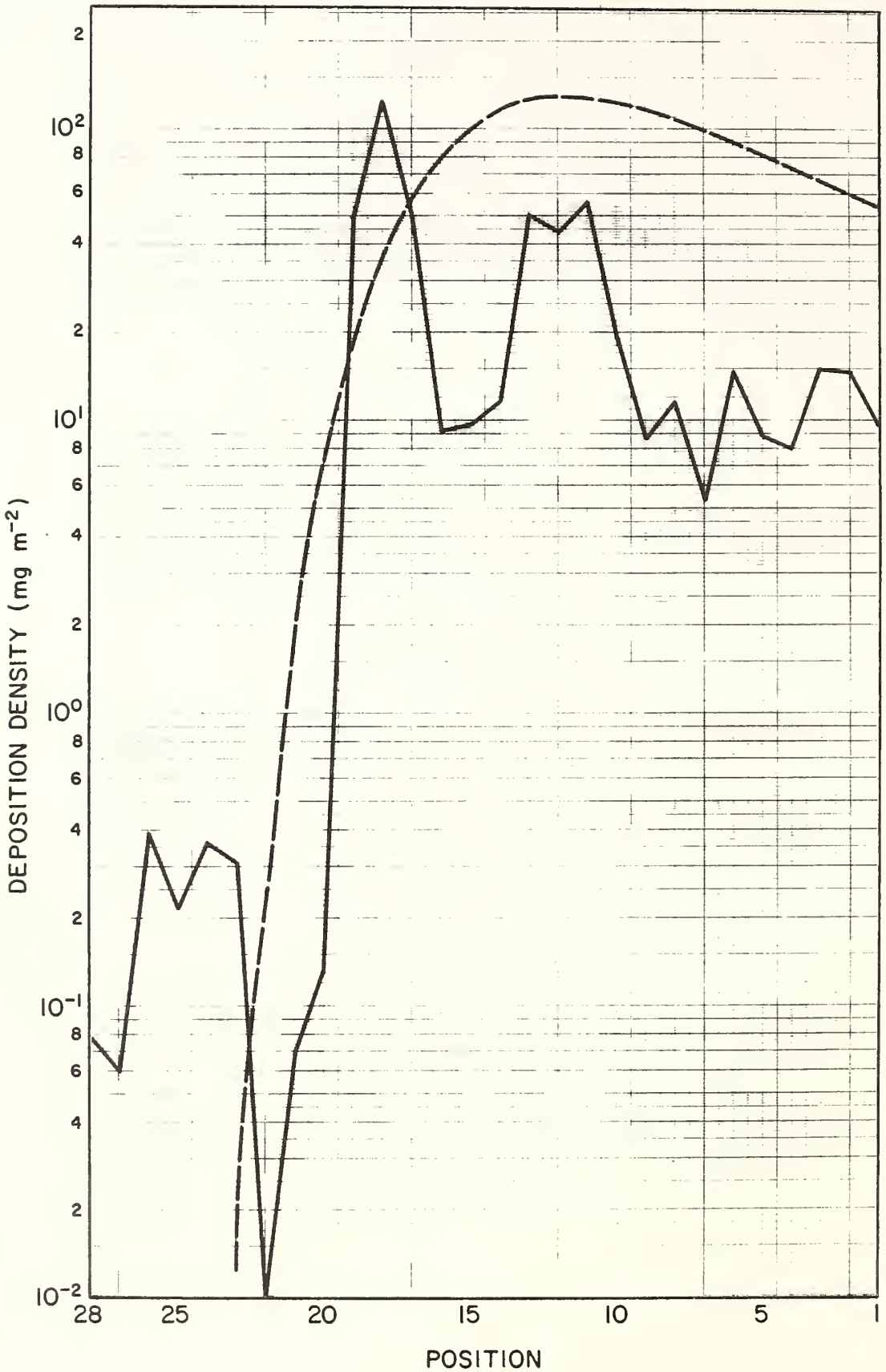

FIGURE A-1. Predicted (dashed line) versus measured deposition densities for Row 1, Trial 1 of the Rennic Creek Trials.

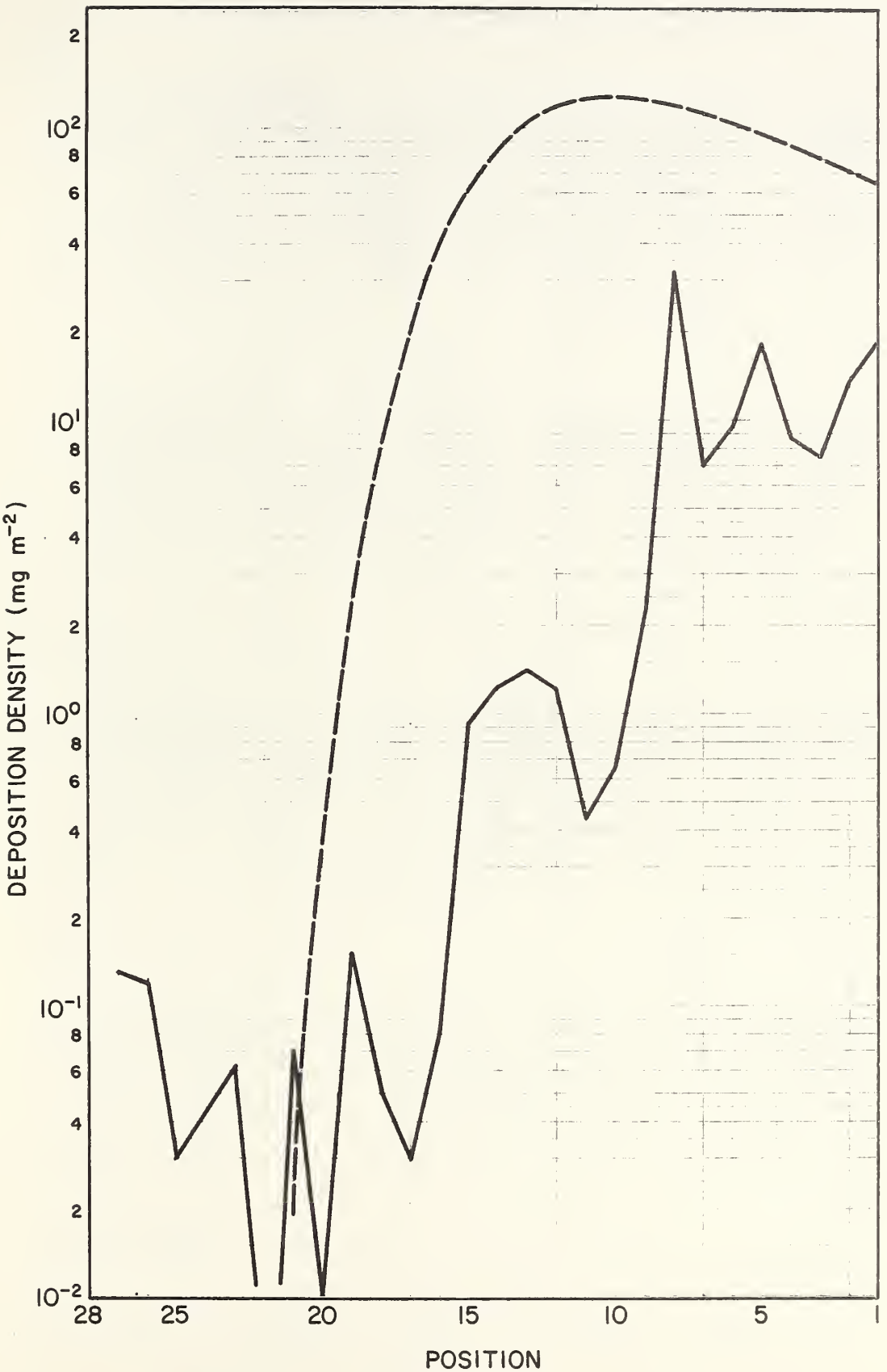

FIGURE A-2. Predicted (dashed line) versus measured deposition densities for Row 2, Trial 1 of the Rennic Creek Trials.

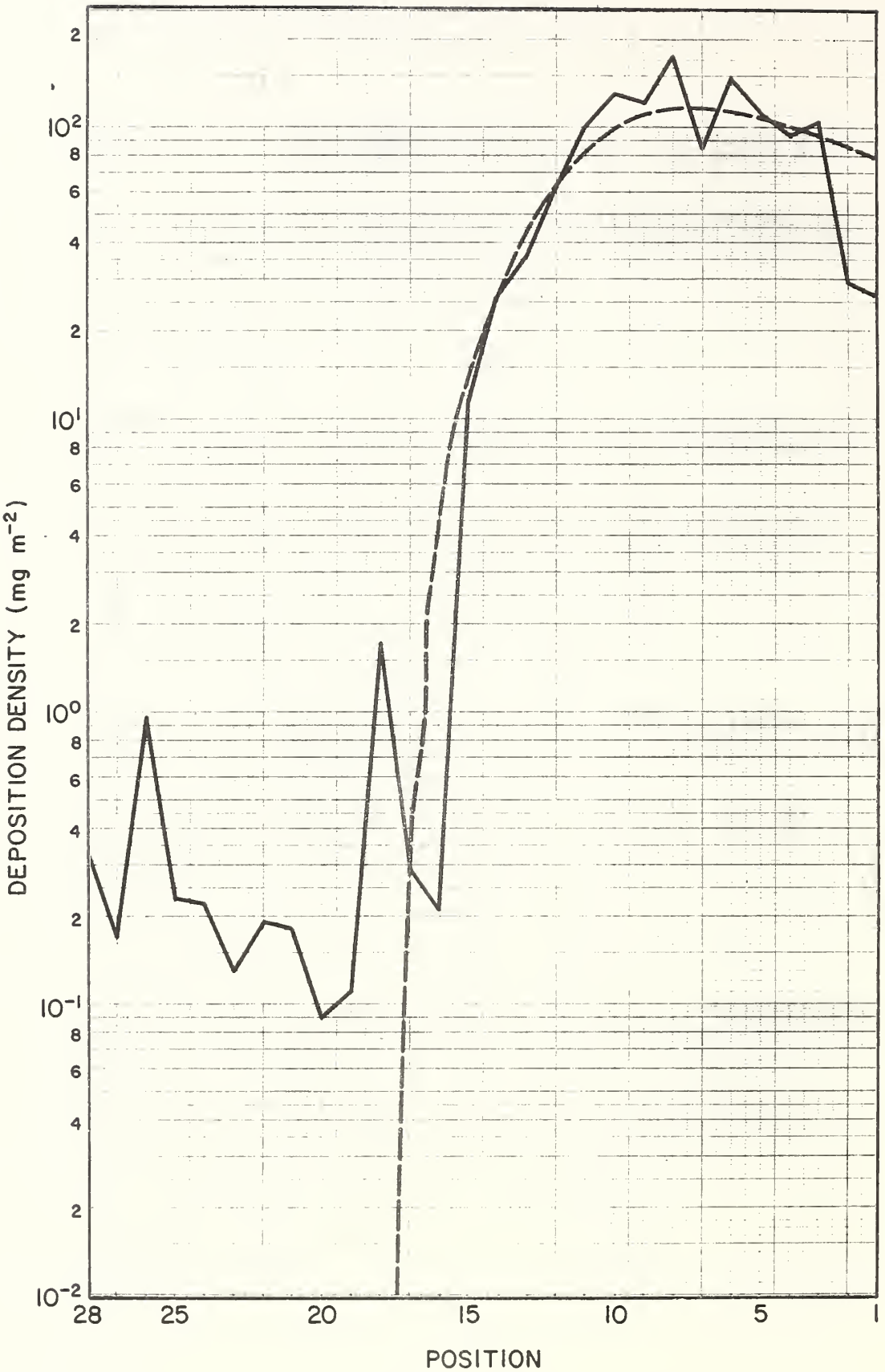

FIGURE A-3. Predicted (dashed line) versus measured deposition densities for Row 3, Trial 1 of the Rennic Creek Trials.

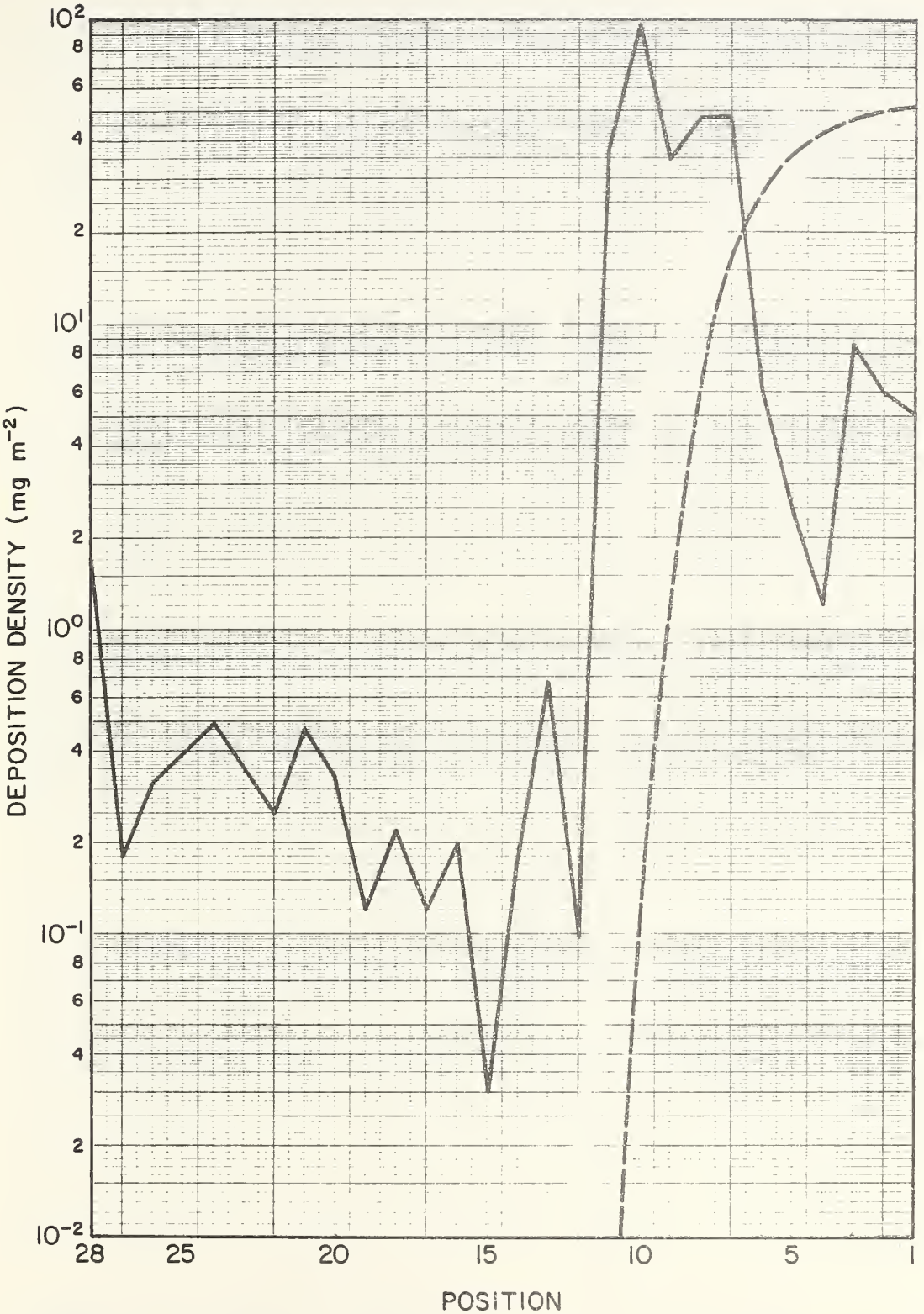

FIGURE A-4. Predicted (dashed line) versus measured deposition densities for Row 4, Trial 1 of the Rennic Creek Trials.

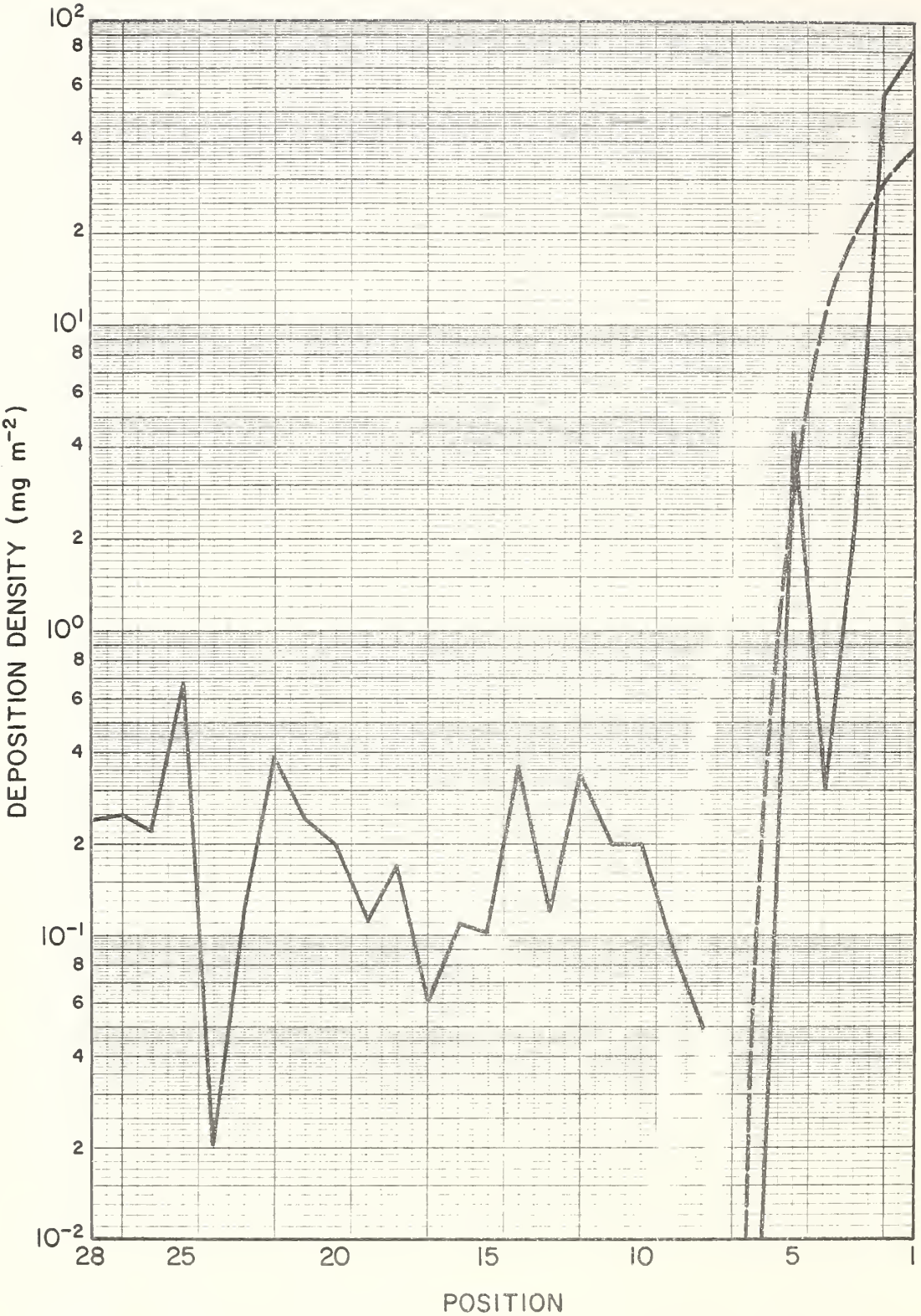

FIGURE A-5. Predicted (dashed line) versus measured deposition densities for Row 5, Trial 1 of the Rennic Creek Trials.

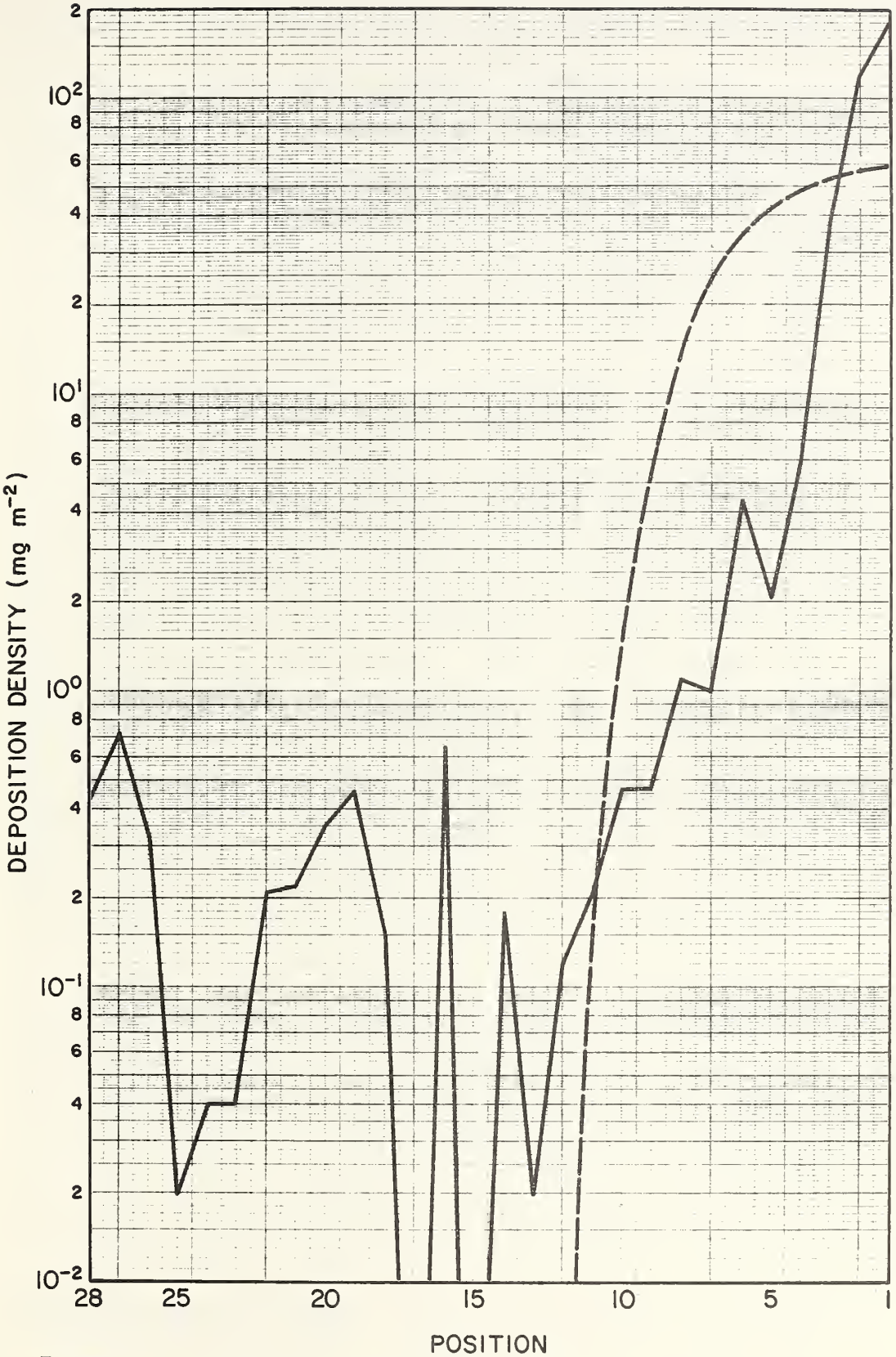

FIGURE A-6. Predicted (dashed line) versus measured deposition densities for Row 6, Trial 1 of the Rennic Creek Trials.

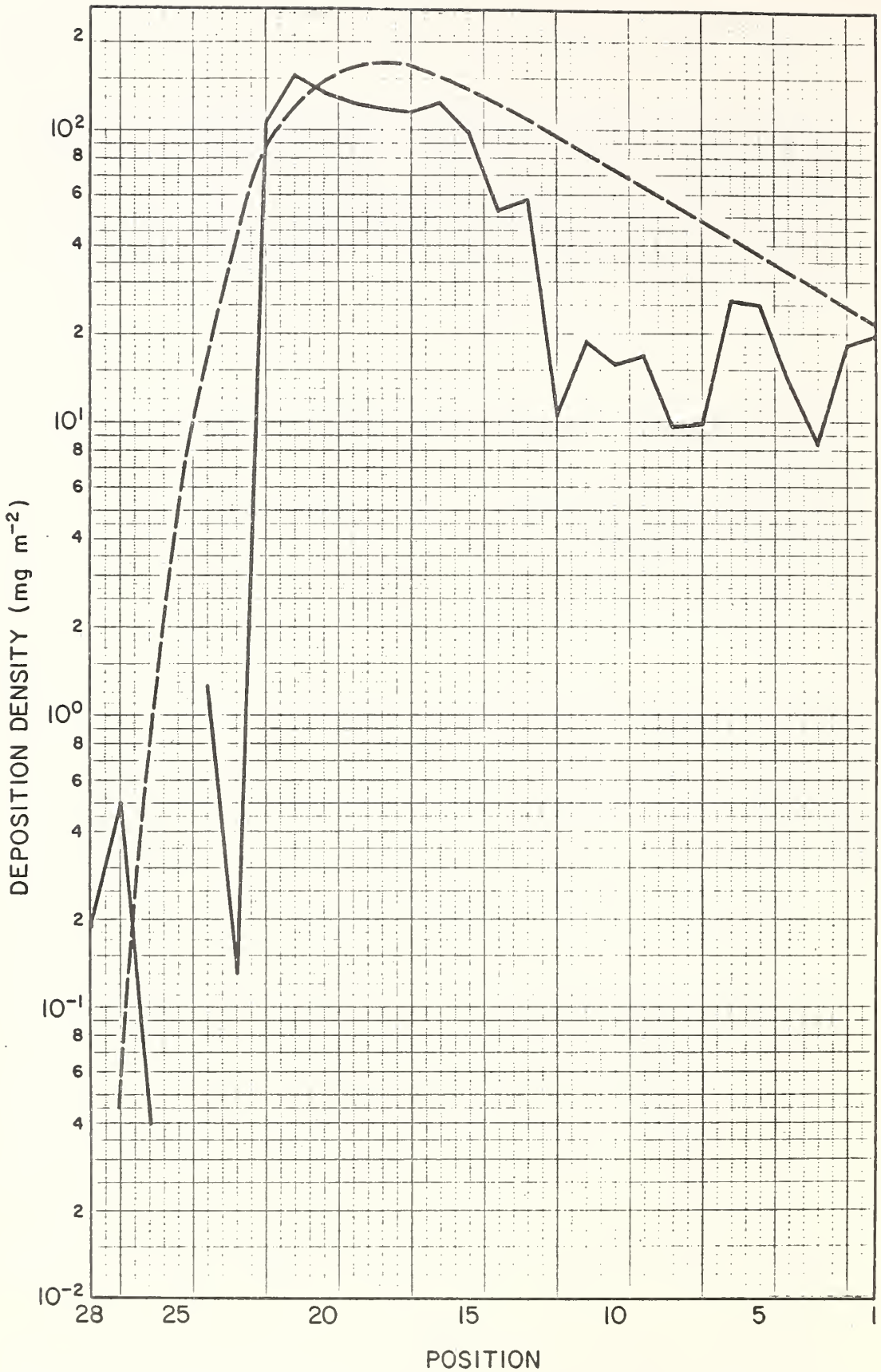

FIGURE A-7. Predicted (dashed line) versus measured deposition densities for Row 1, Trial 2 of the Rennic Creek Trials.

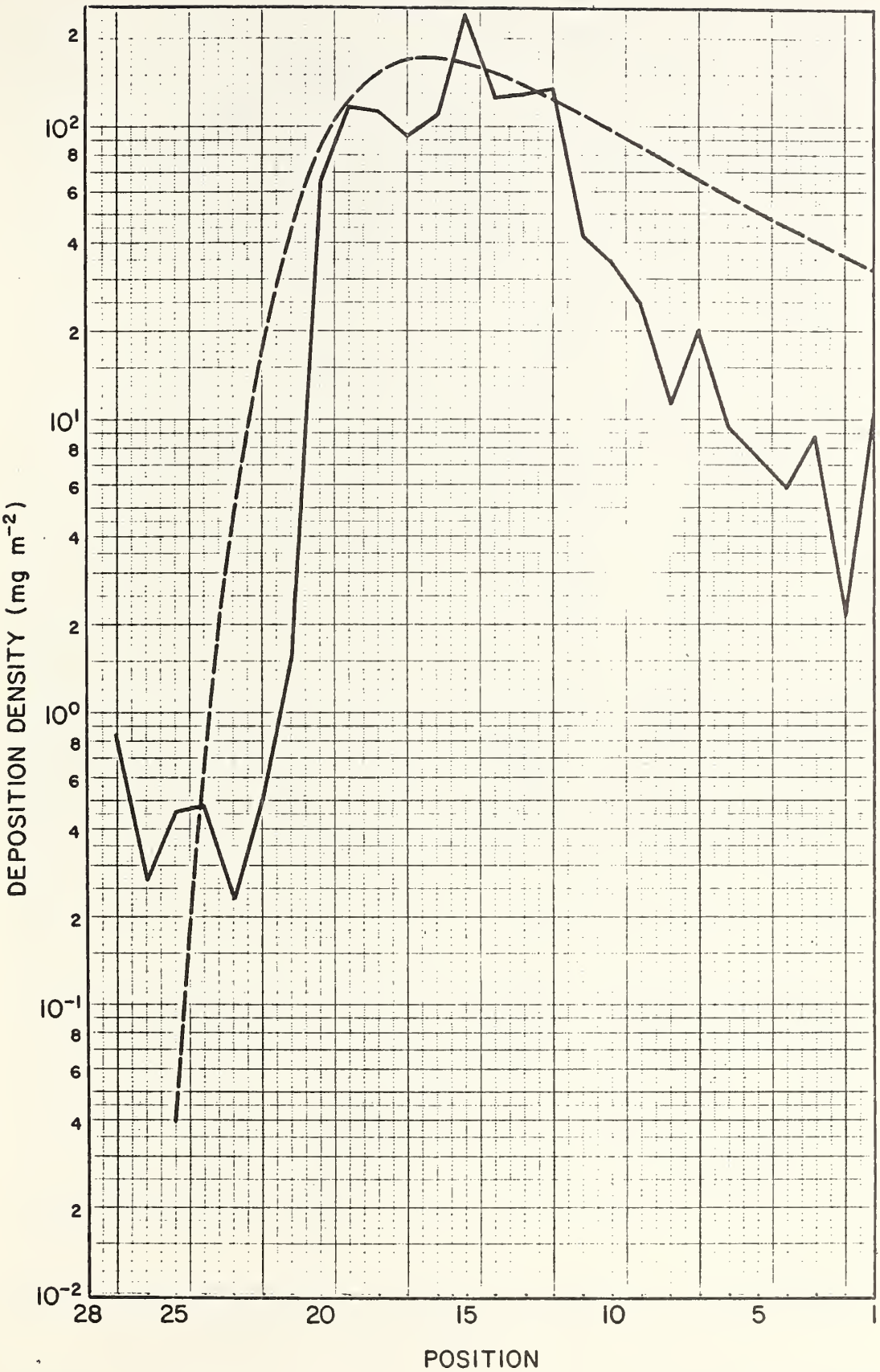

FIGURE A-8. Predicted (dashed line) versus measured deposition densities for Row 2, Trial 2 of the Rennic Creek Trials.

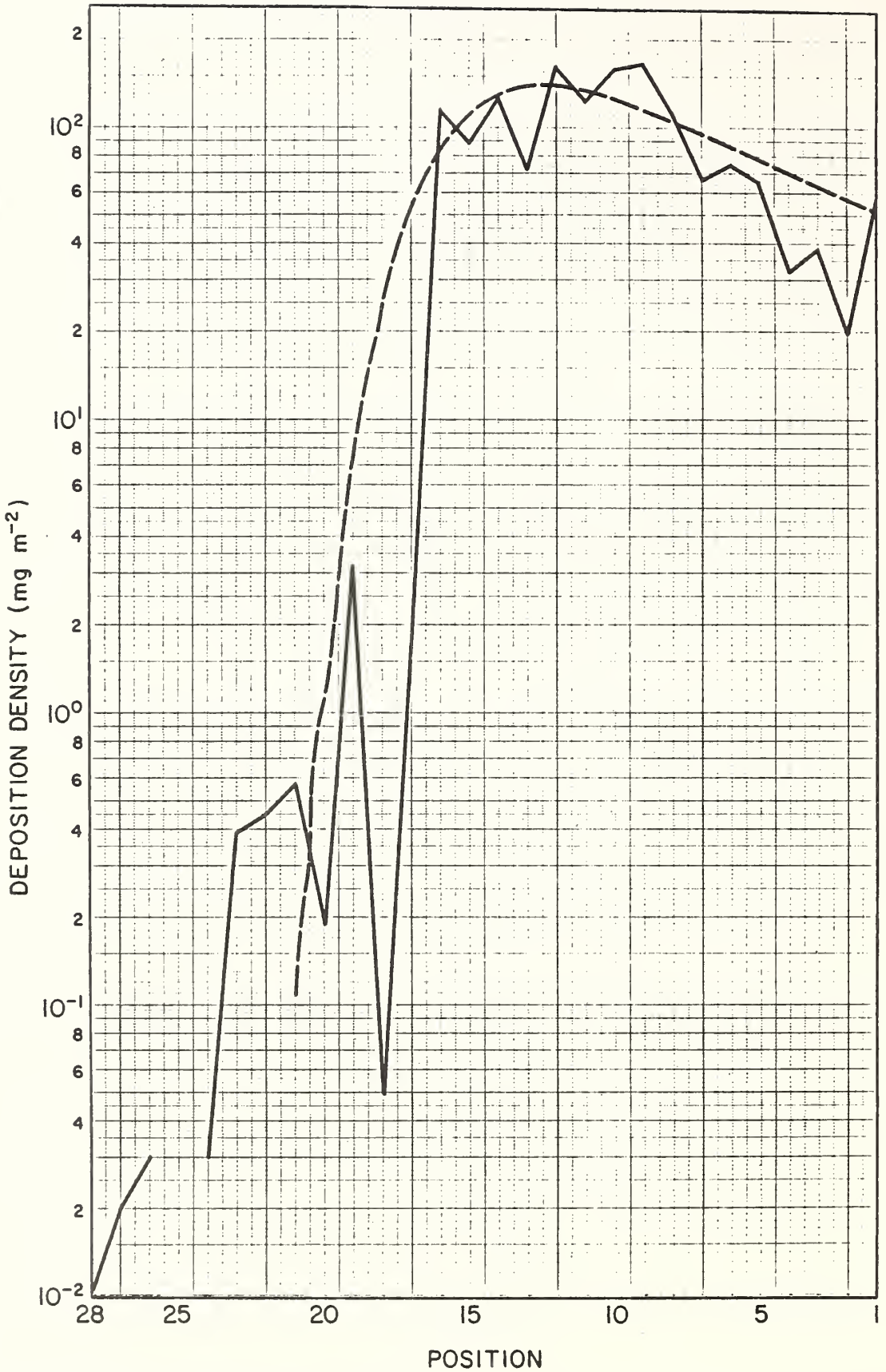

FIGURE A-9 Predicted (dashed line) versus measured deposition densities for Row 3, Trial 2 of the Rennic Creek Trials.

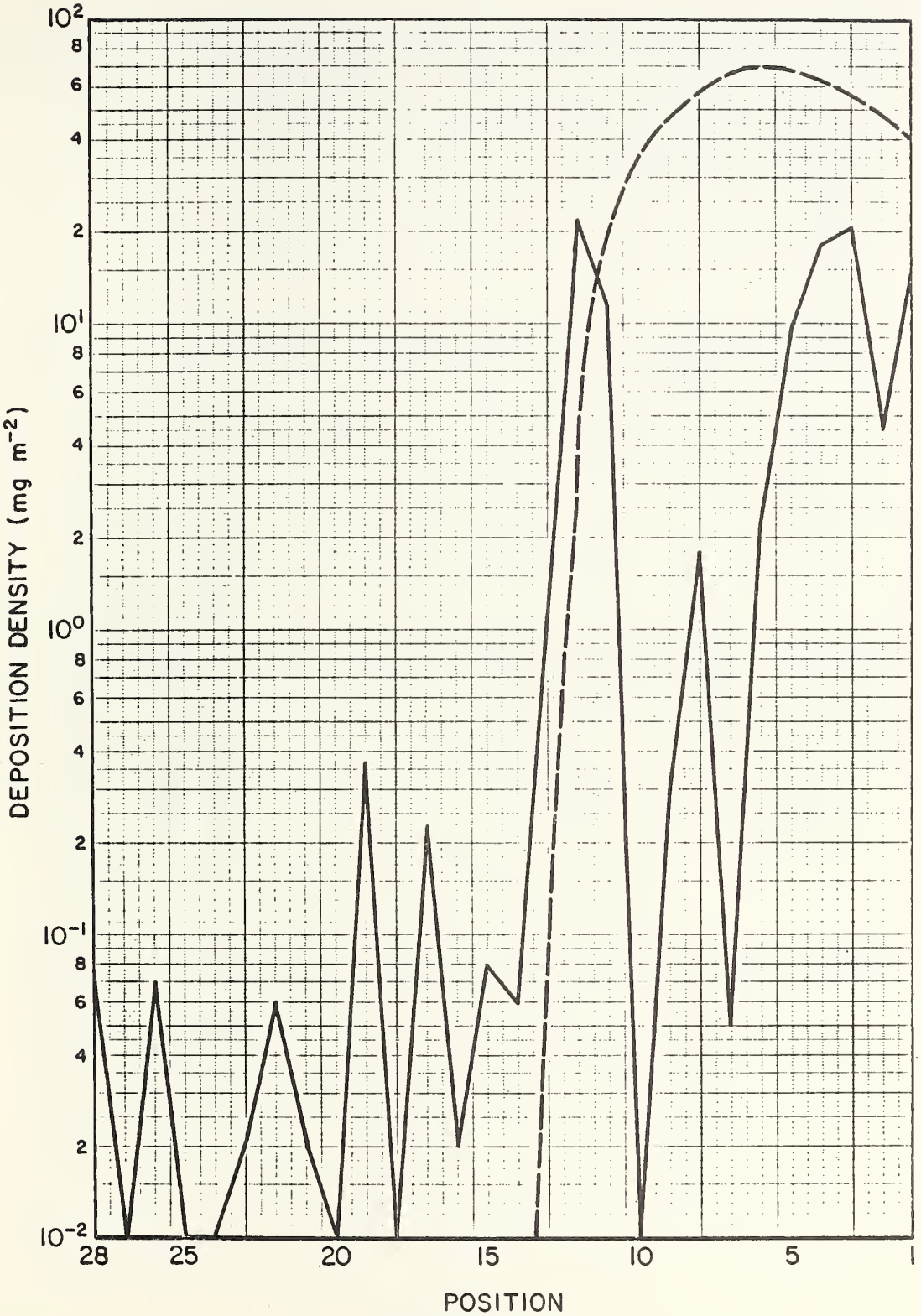

FIGURE A-10. Predicted (dashed line) versus measured deposition densities for Row 4, Trial 2 of the Rennic Creek Trials.

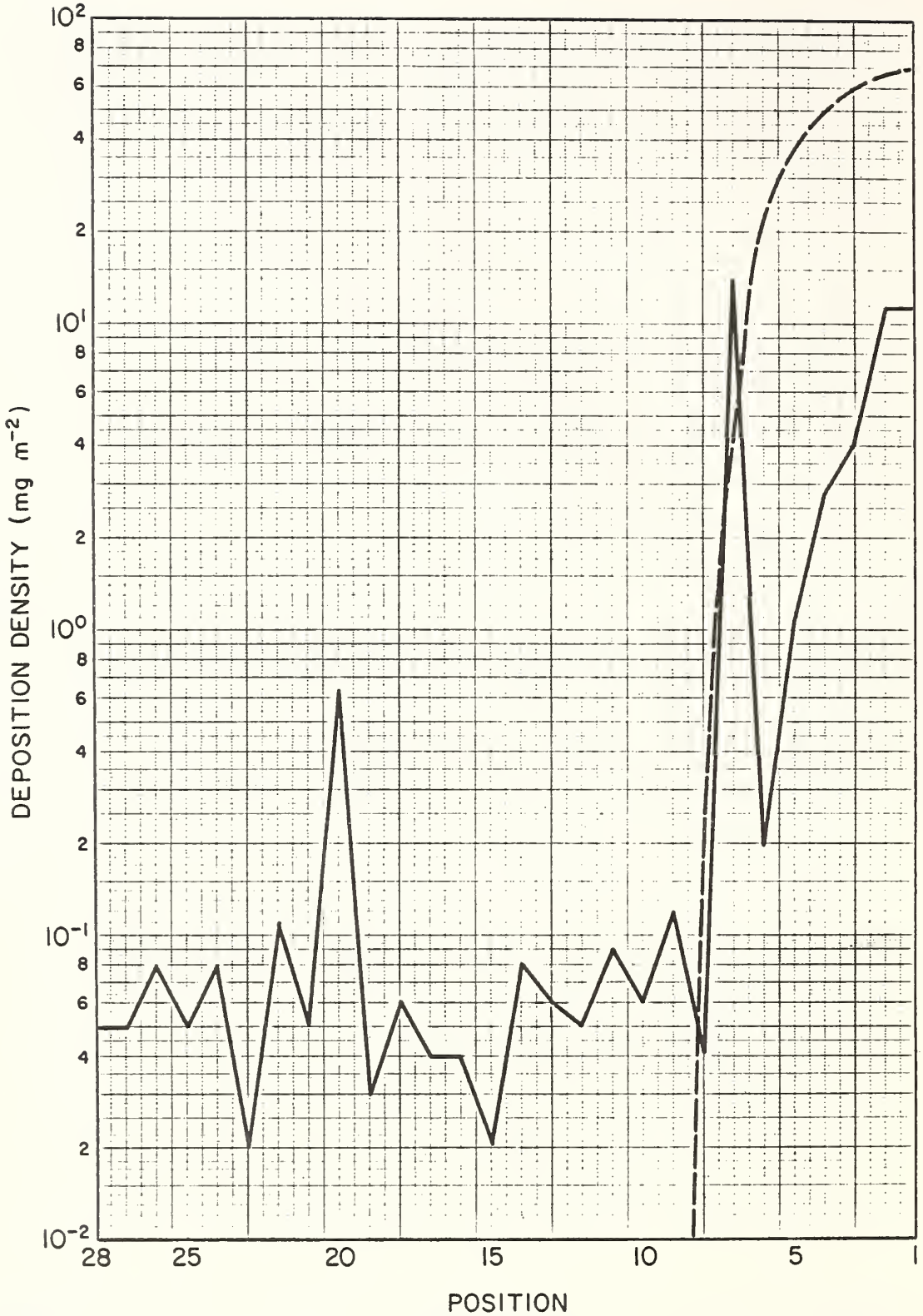

FIGURE A-11. Predicted (dashed line) versus measured deposition densities for Row 5, Trial 2 of the Rennic Creek Trials.

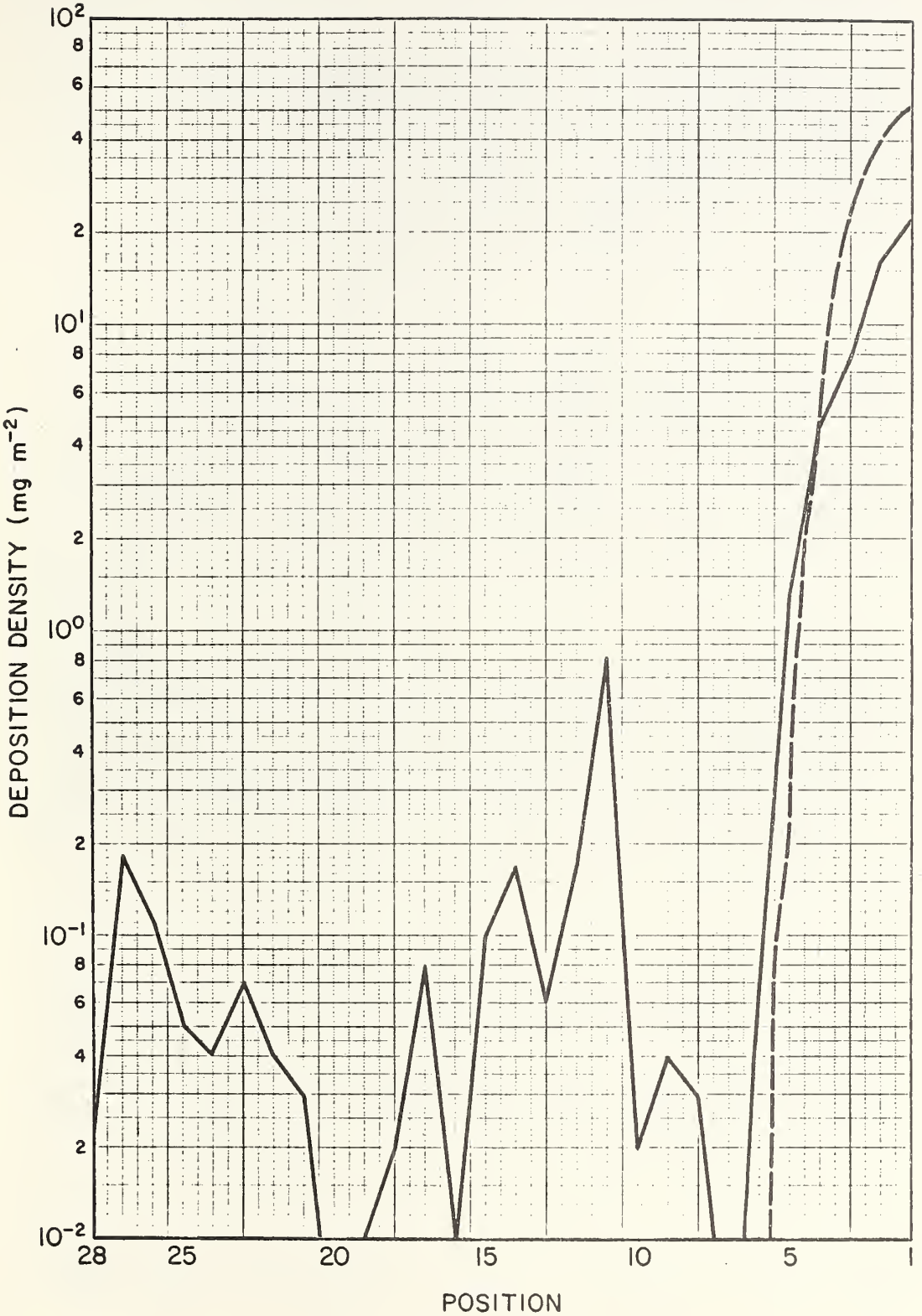

FIGURE A-12. Predicted (dashed line) versus measured deposition densities for Row 6, Trial 2 of the Rennic Creek Trials.

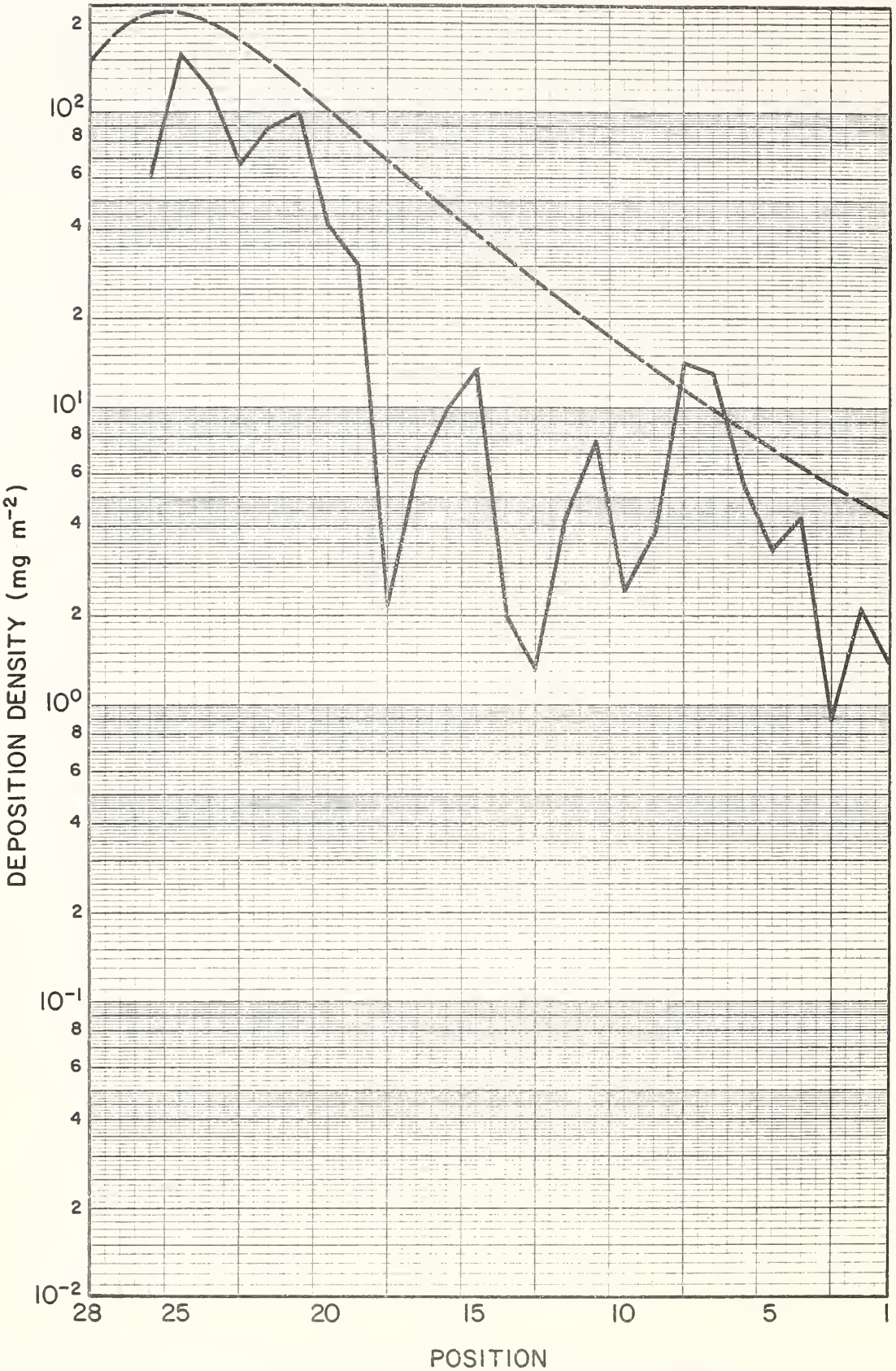

FIGURE A-13. Predicted (dashed line) versus measured deposition densities for Row 1, Trial 3 of the Rennic Creek Trials.

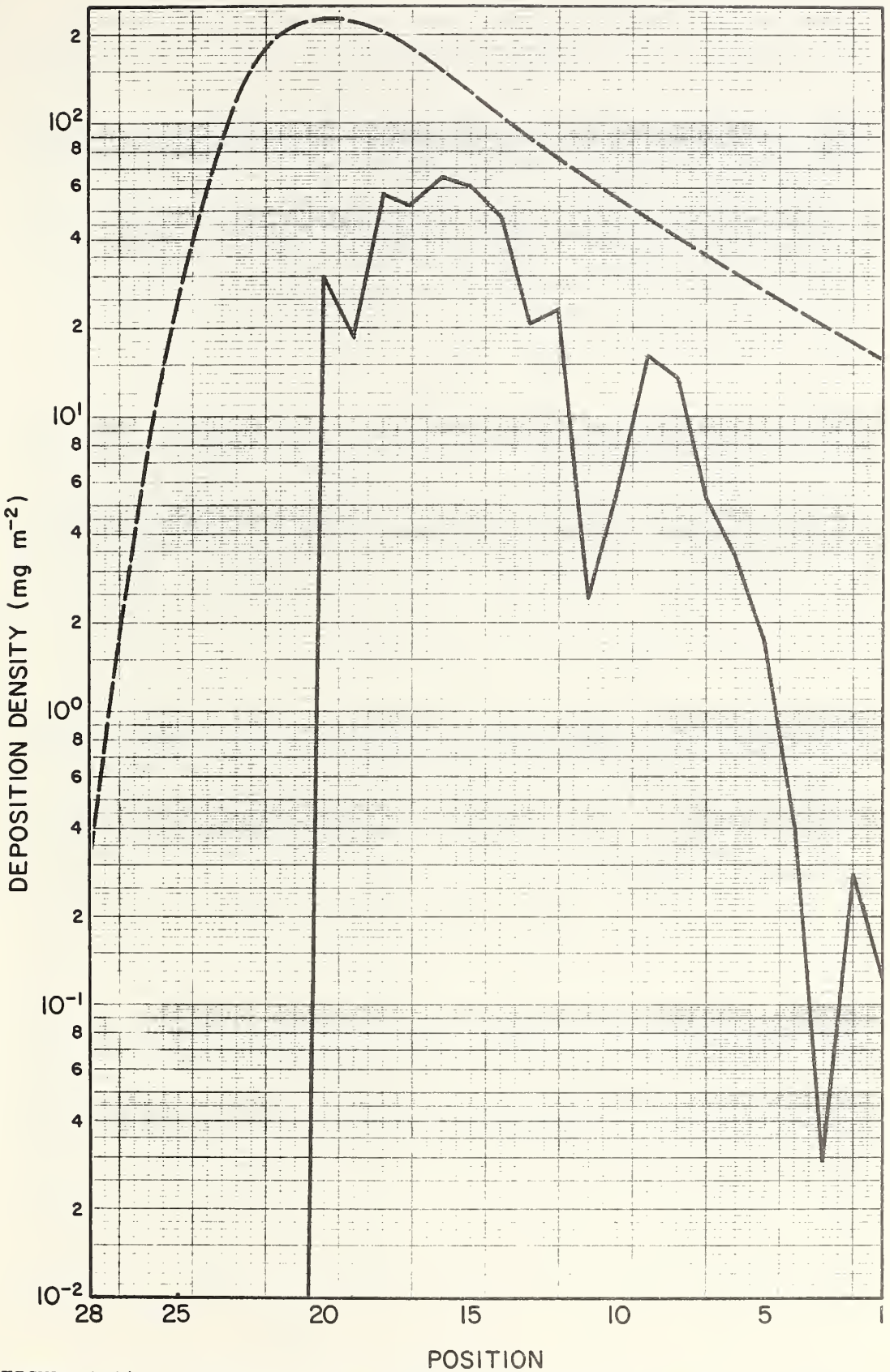

FIGURE A-14. Predicted (dashed line) versus measured deposition densities for Row 2, Trial 3 of the Rennic Creek Trials.

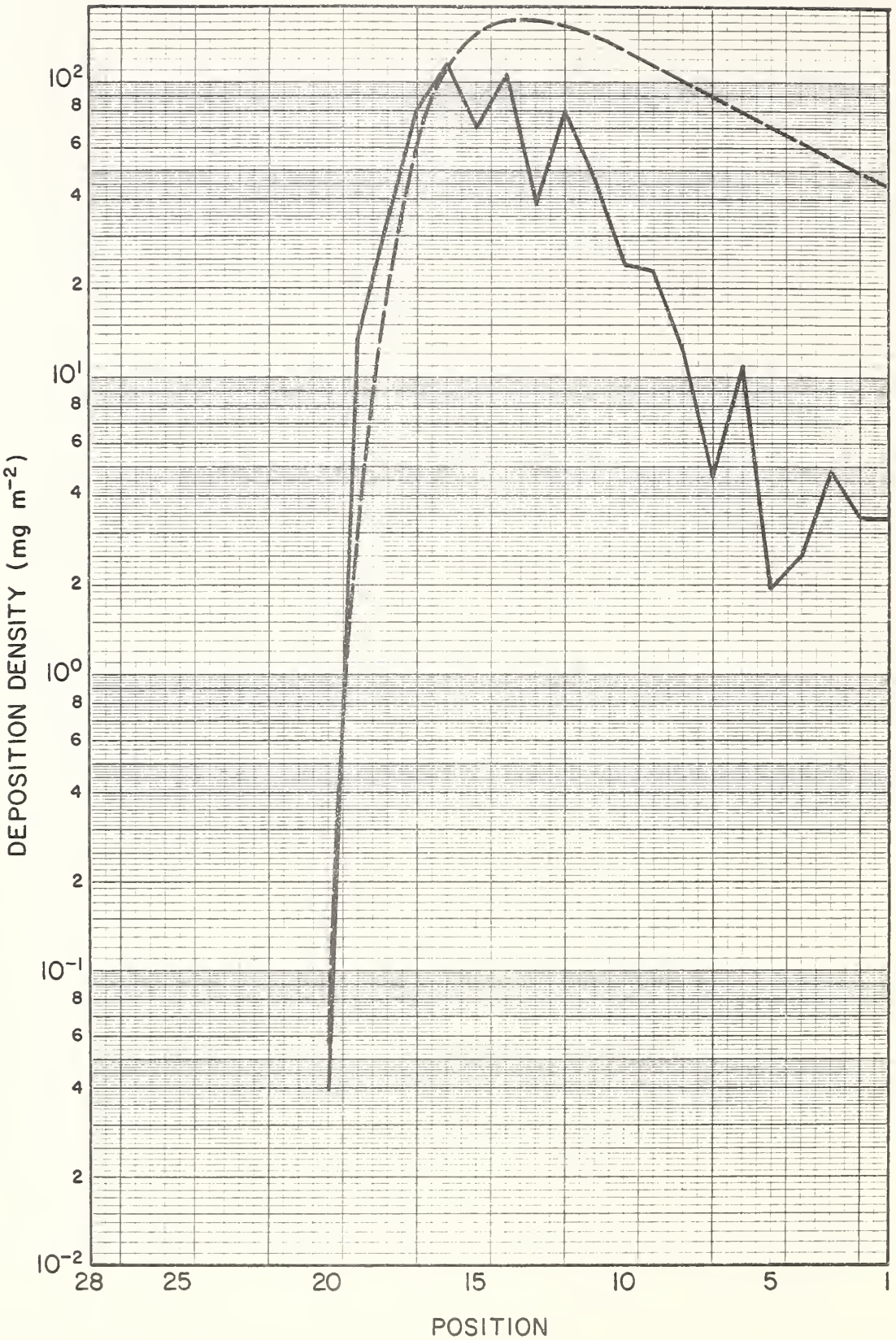

FIGURE A-15. Predicted (dashed line) versus measured deposition densities for Row 3, Trial 3 of the Rennic Creek Trials.

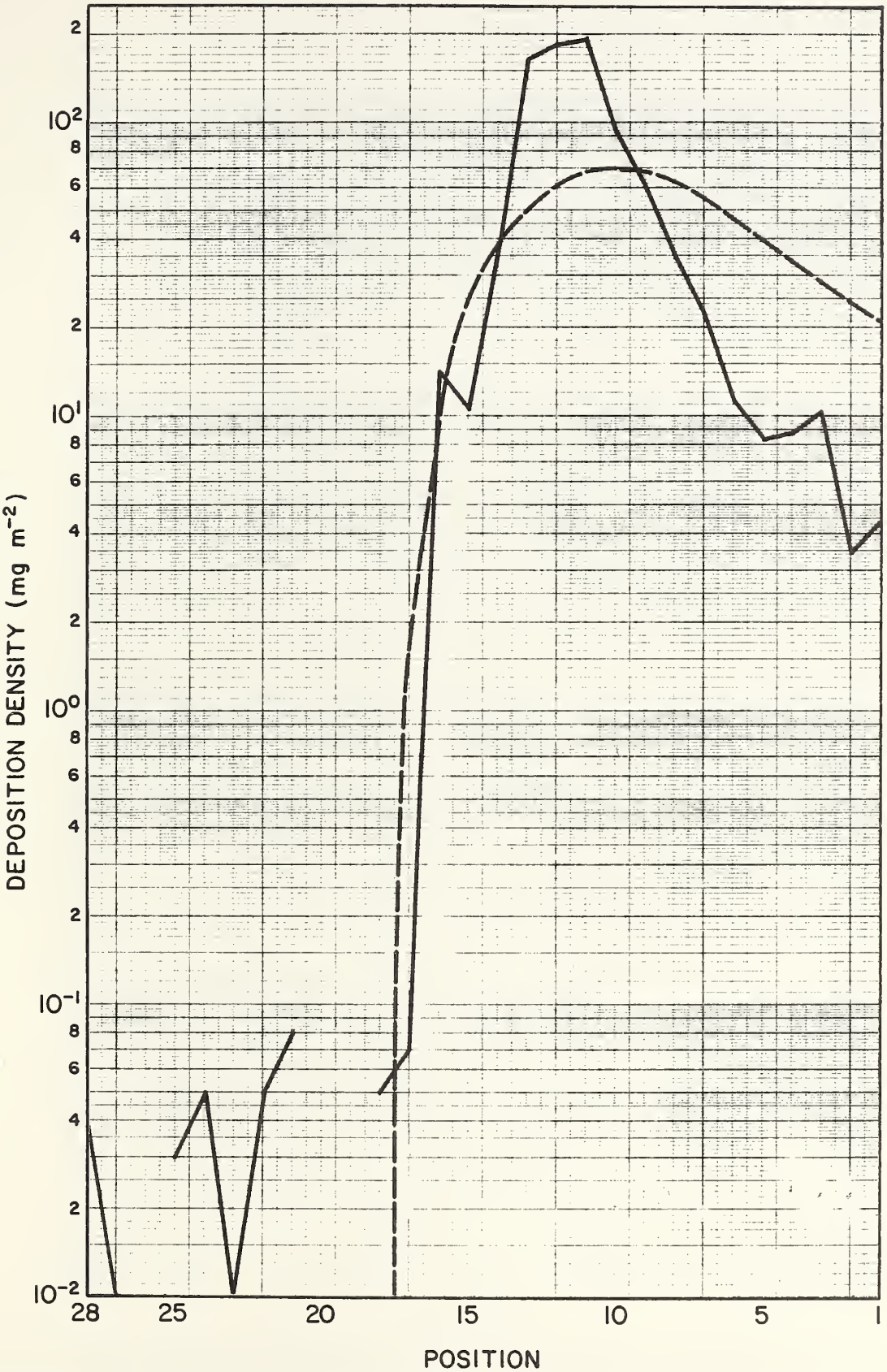

FIGURE A-16. Predicted (dashed line) versus measured deposition densities for Row 4, Trial 3 of the Rennic Creek Trials.

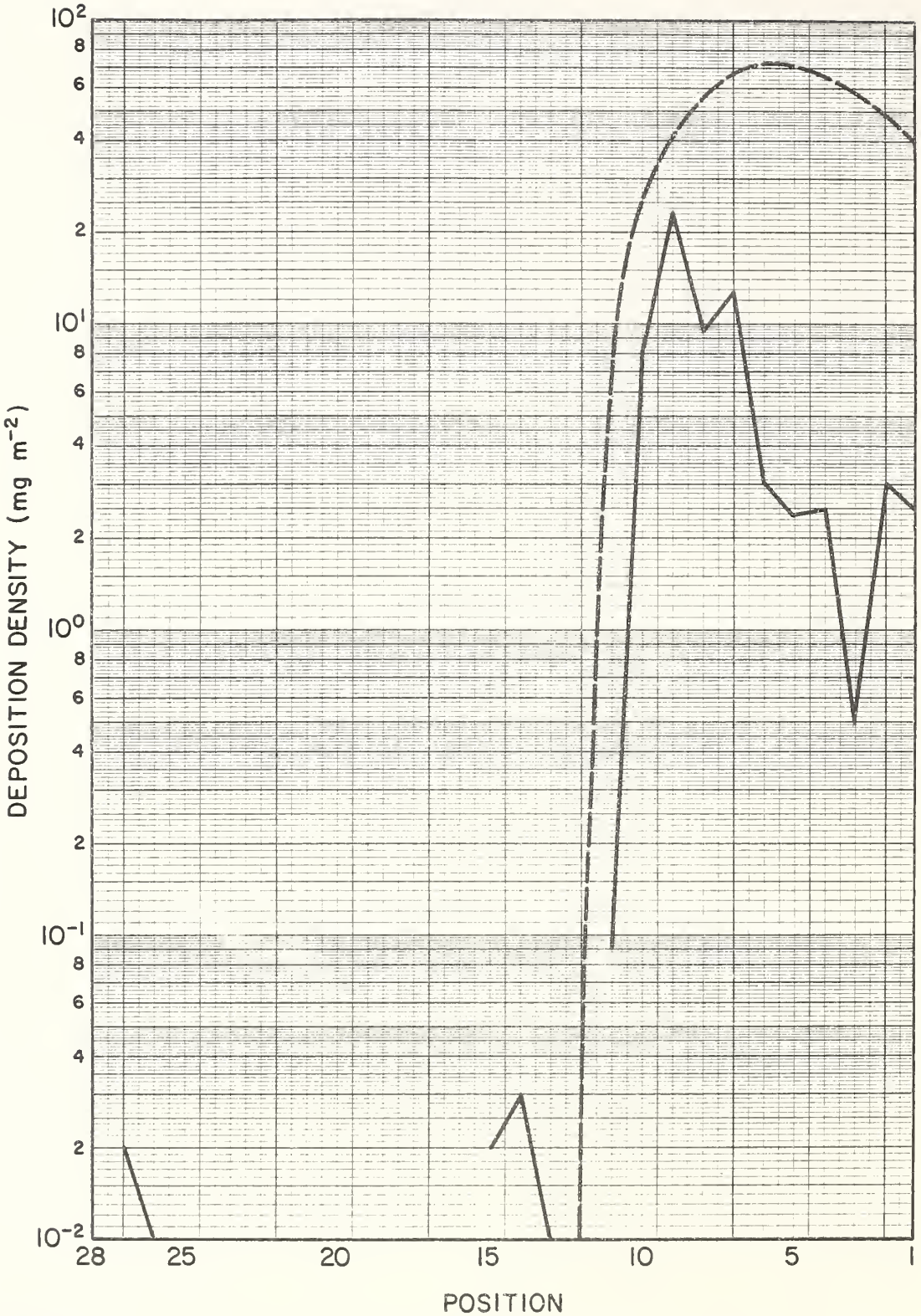

FIGURE A-17. Predicted (dashed line) versus measured deposition densities for Row 5, Trial 3 of the Rennic Creek Trials.

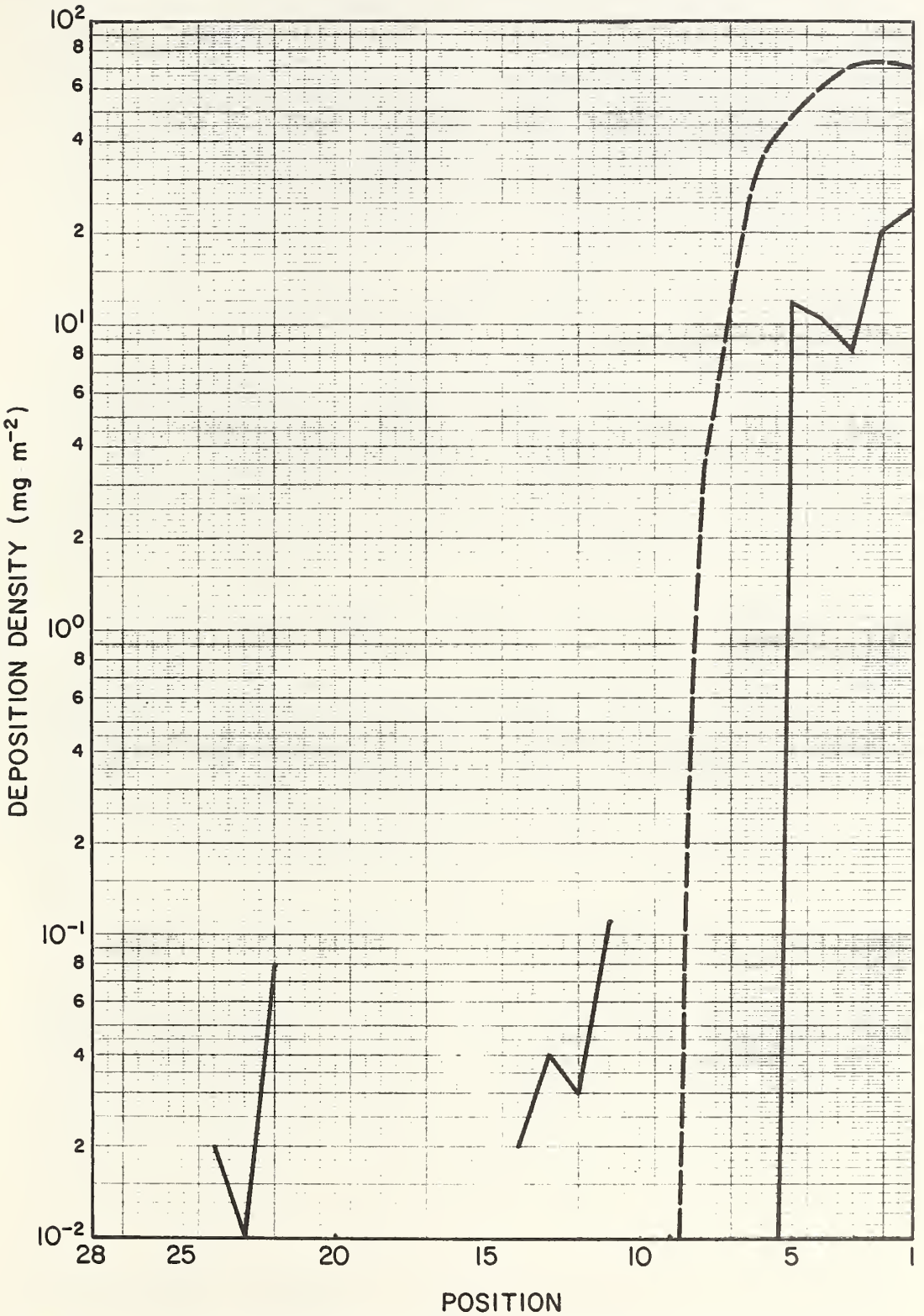

FIGURE A-18. Predicted (dashed line) versus measured deposition densities for Row 6, Trial 3 of the Rennic Creek Trials.

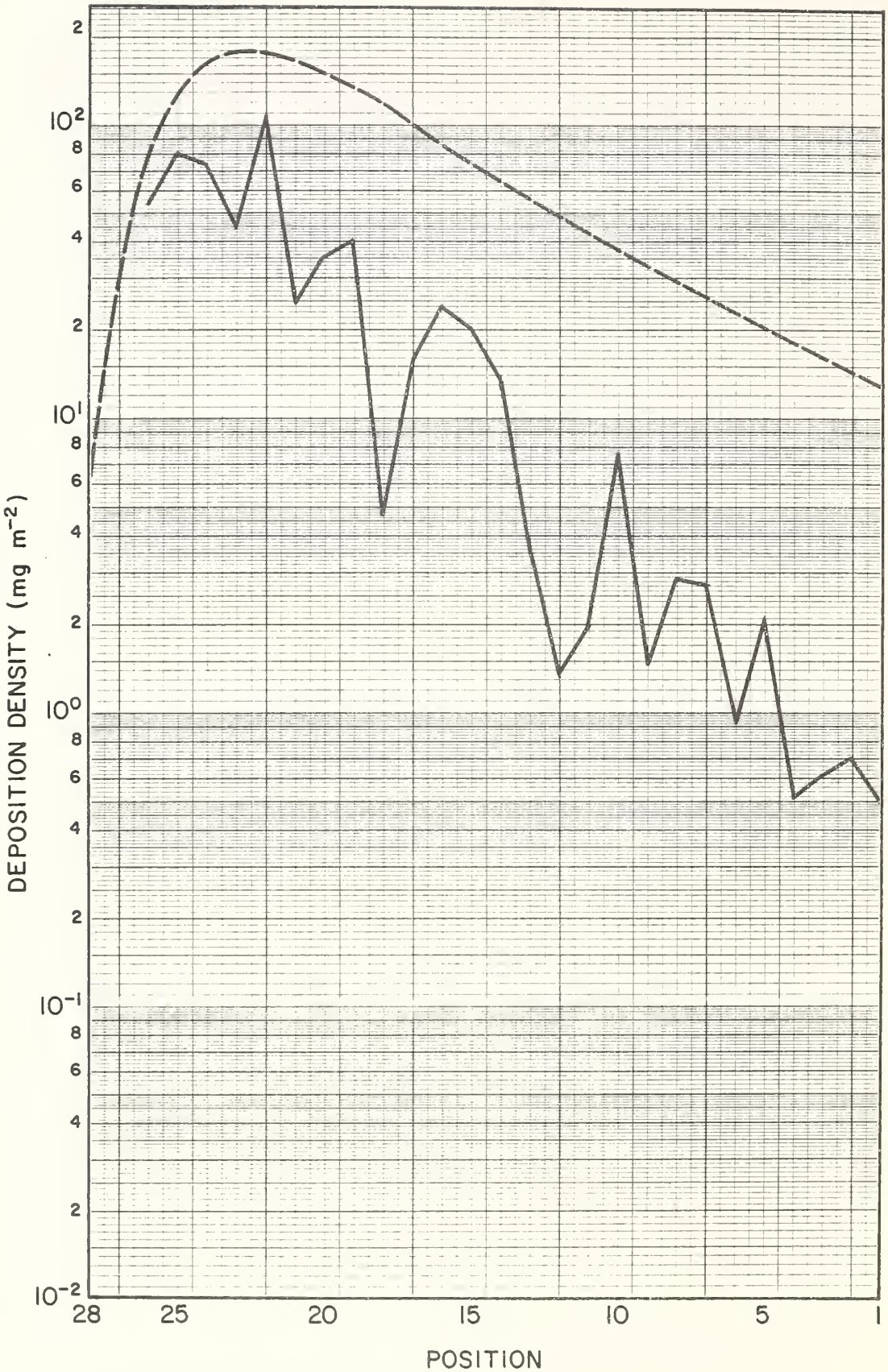

FIGURE A-19. Predicted (dashed line) versus measured deposition densities for Row 1, Trial 4 of the Rennic Creek Trials.

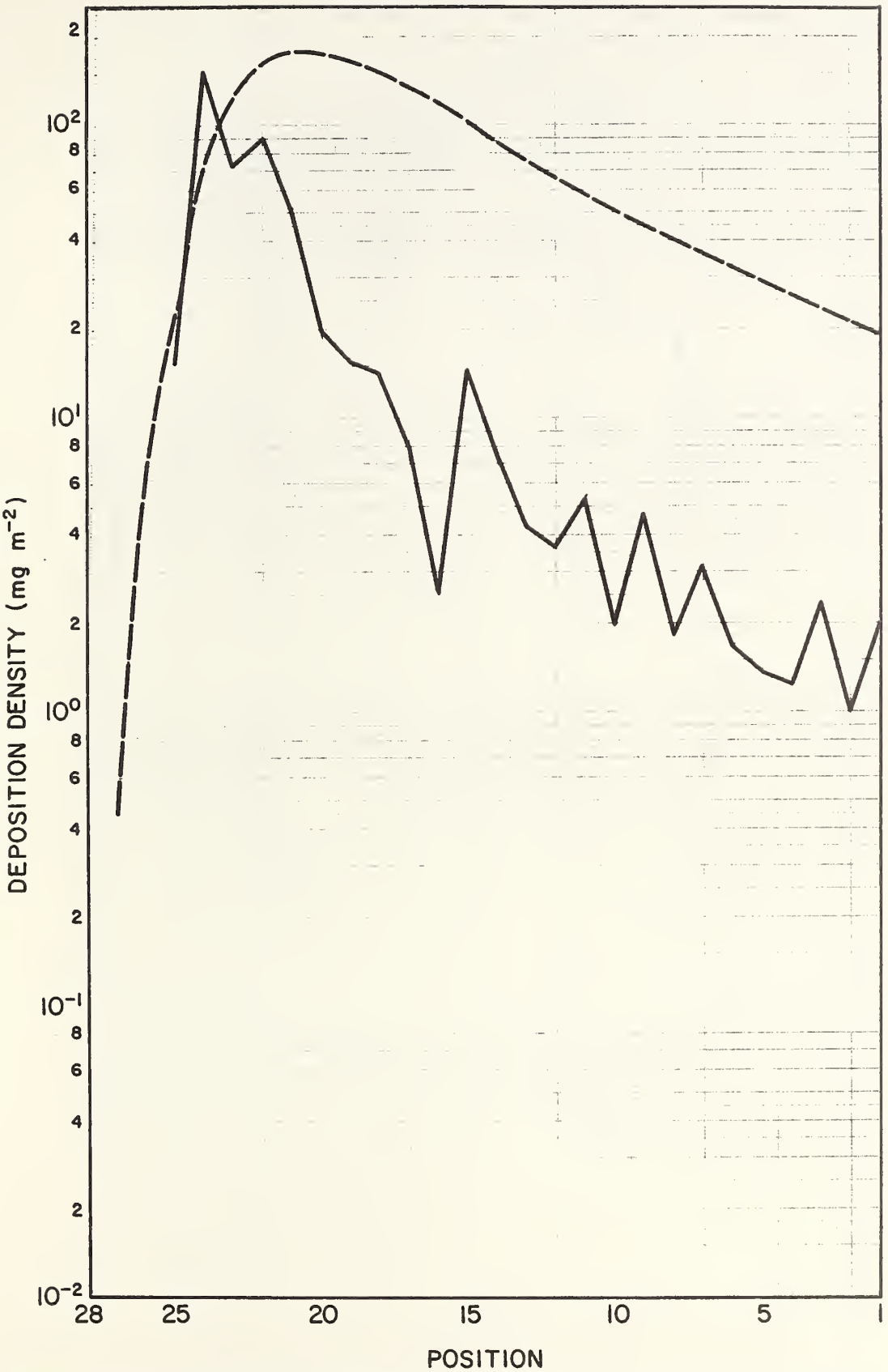

FIGURE A-20. Predicted (dashed line) versus measured deposition densities for Row 2, Trial 4 of the Rennic Creek Trials.

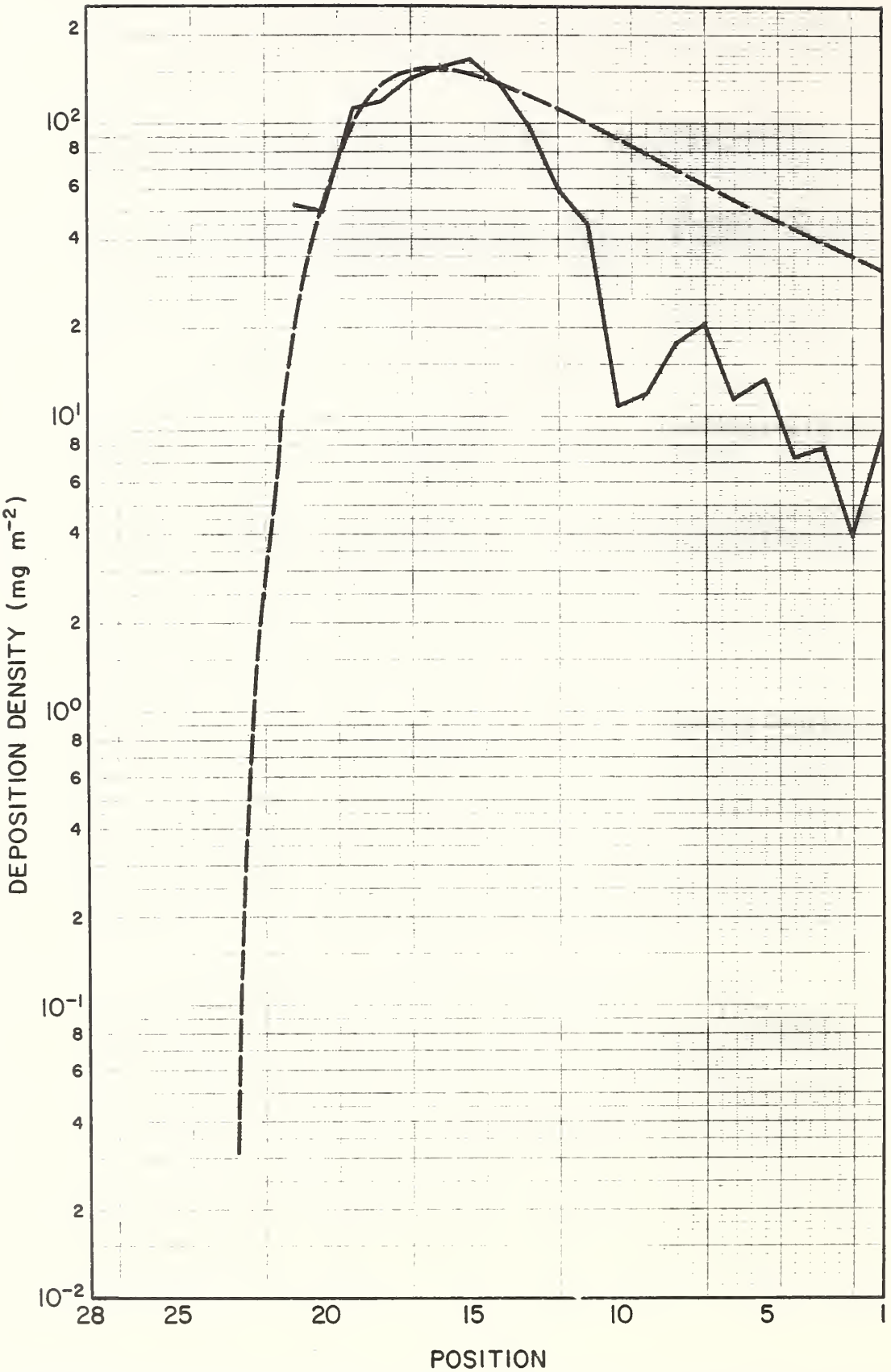

FIGURE A-21. Predicted (dashed line) versus measured deposition densities for Row 3, Trial 4 of the Rennic Creek Trials.

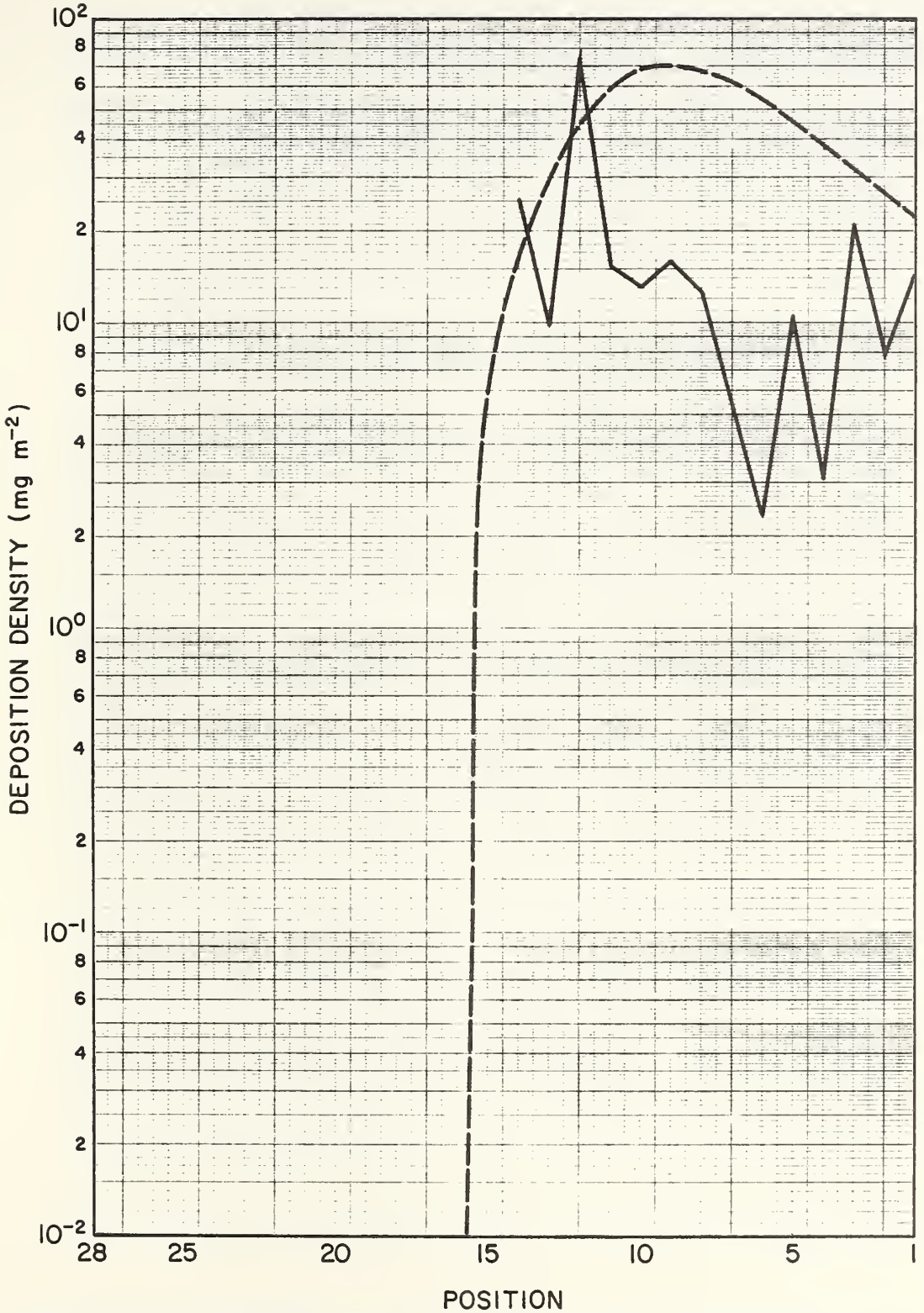

FIGURE A-22. Predicted (dashed line) versus measured deposition densities for Row 4, Trial 4 of the Rennic Creek Trials.

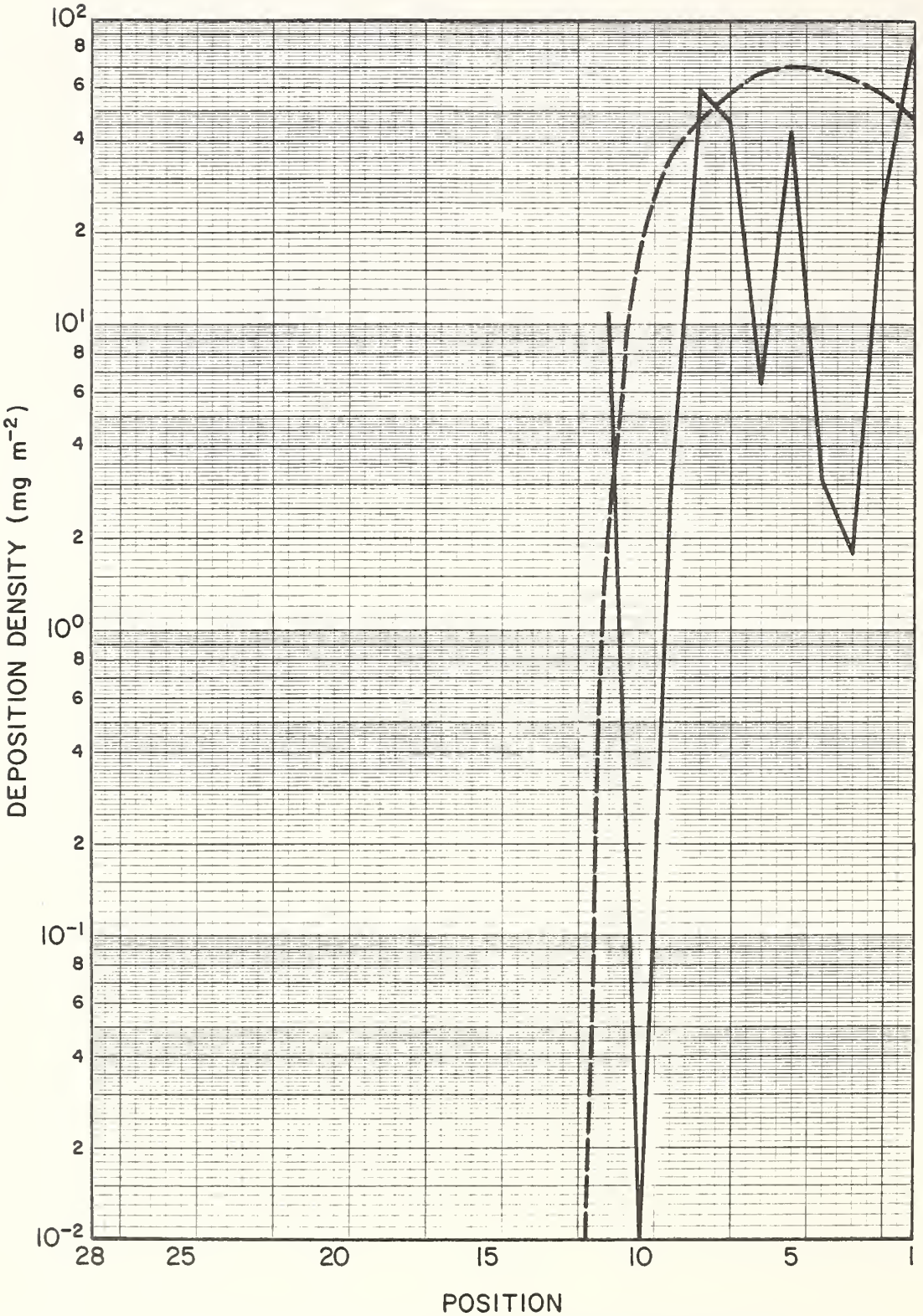

FIGURE A-23. Predicted (dashed line) versus measured deposition densities for Row 5, Trial 4 of the Rennic Creek Trials.

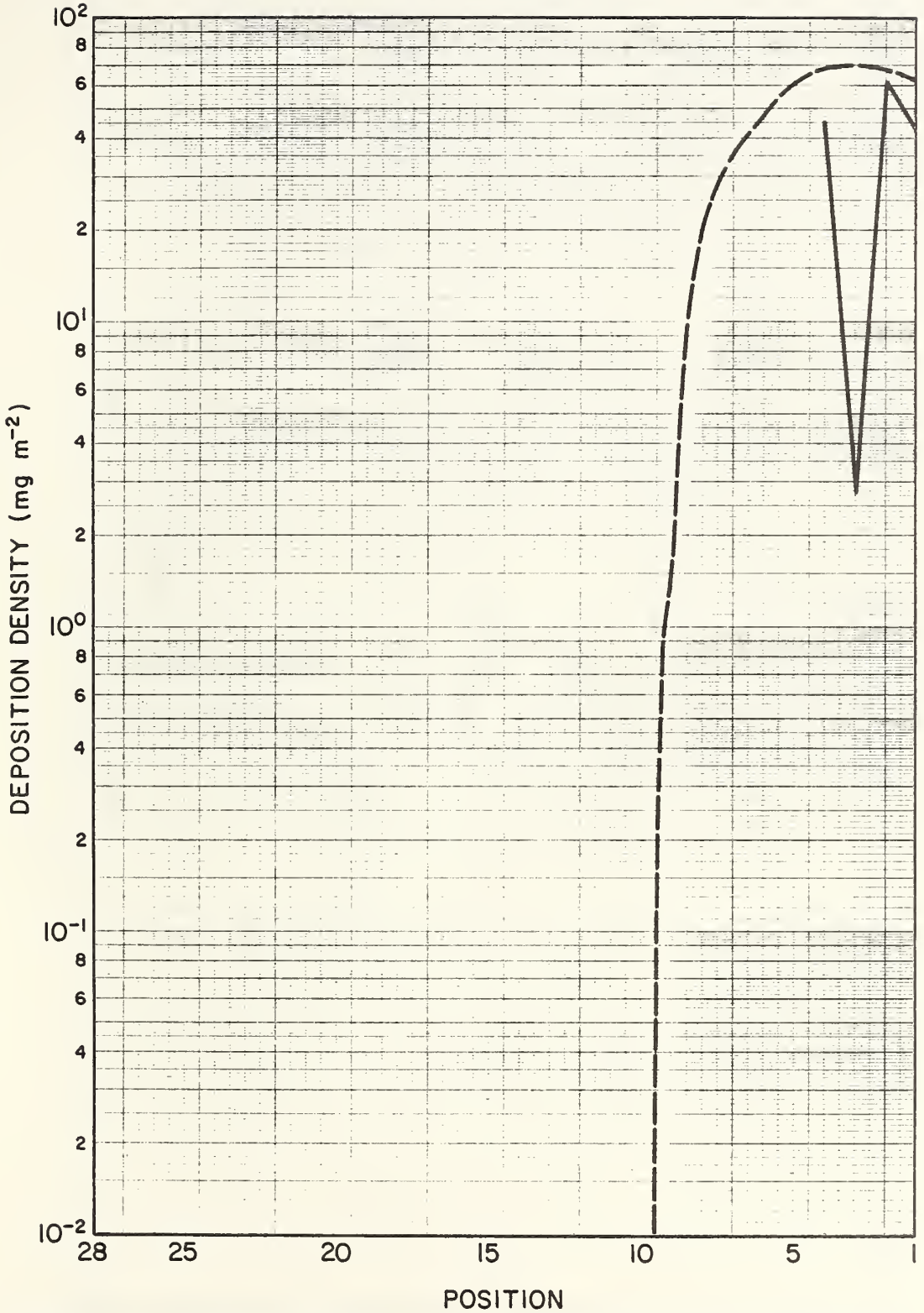

FIGURE A-24. Predicted (dashed line) versus measured deposition densities for Row 6, Trial 4 of the Rennic Creek Trials.

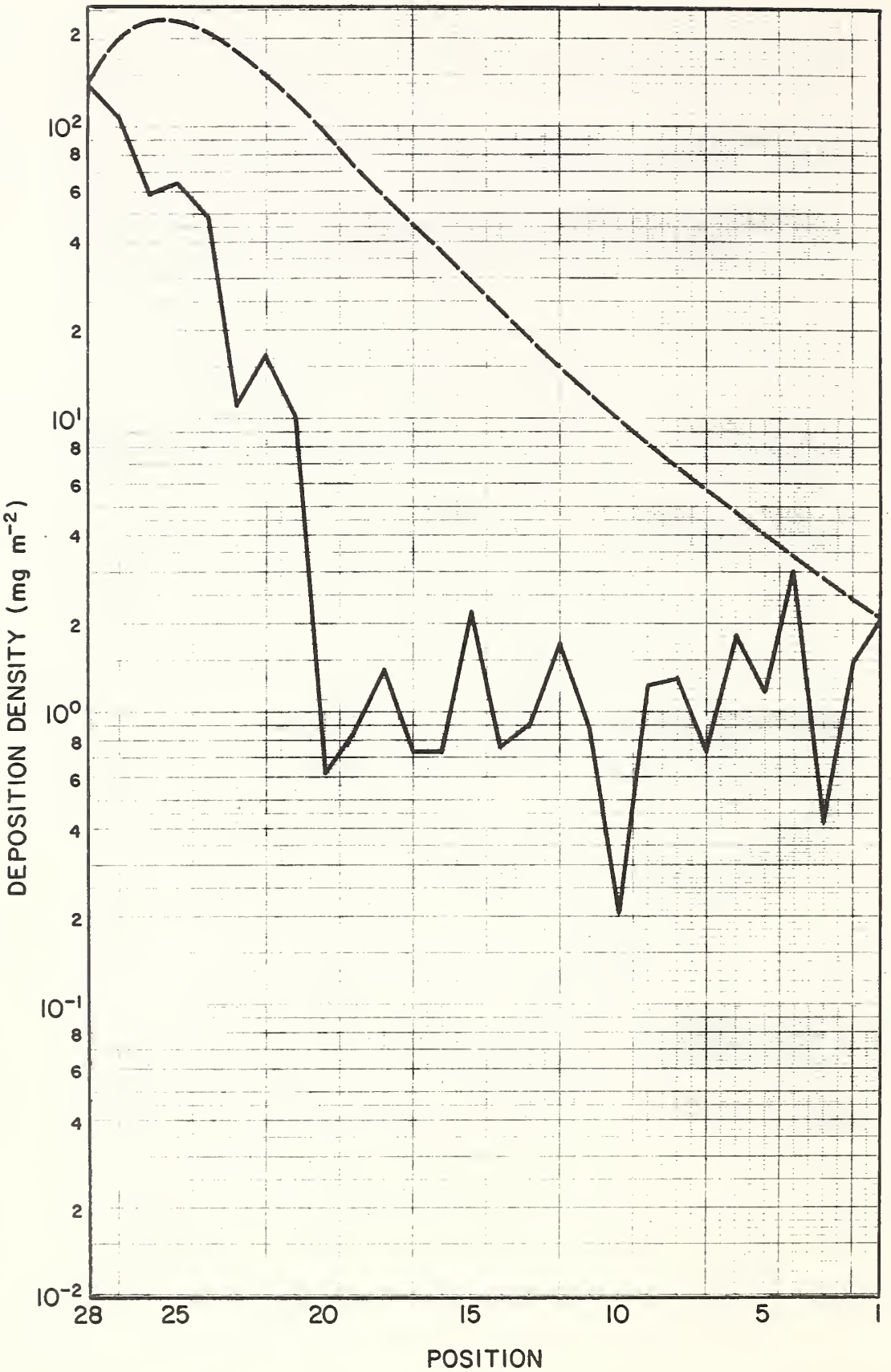

FIGURE A-25. Predicted (dashed line) versus measured deposition densities for Row 1, Trial 5 of the Rennic Creek Trials.

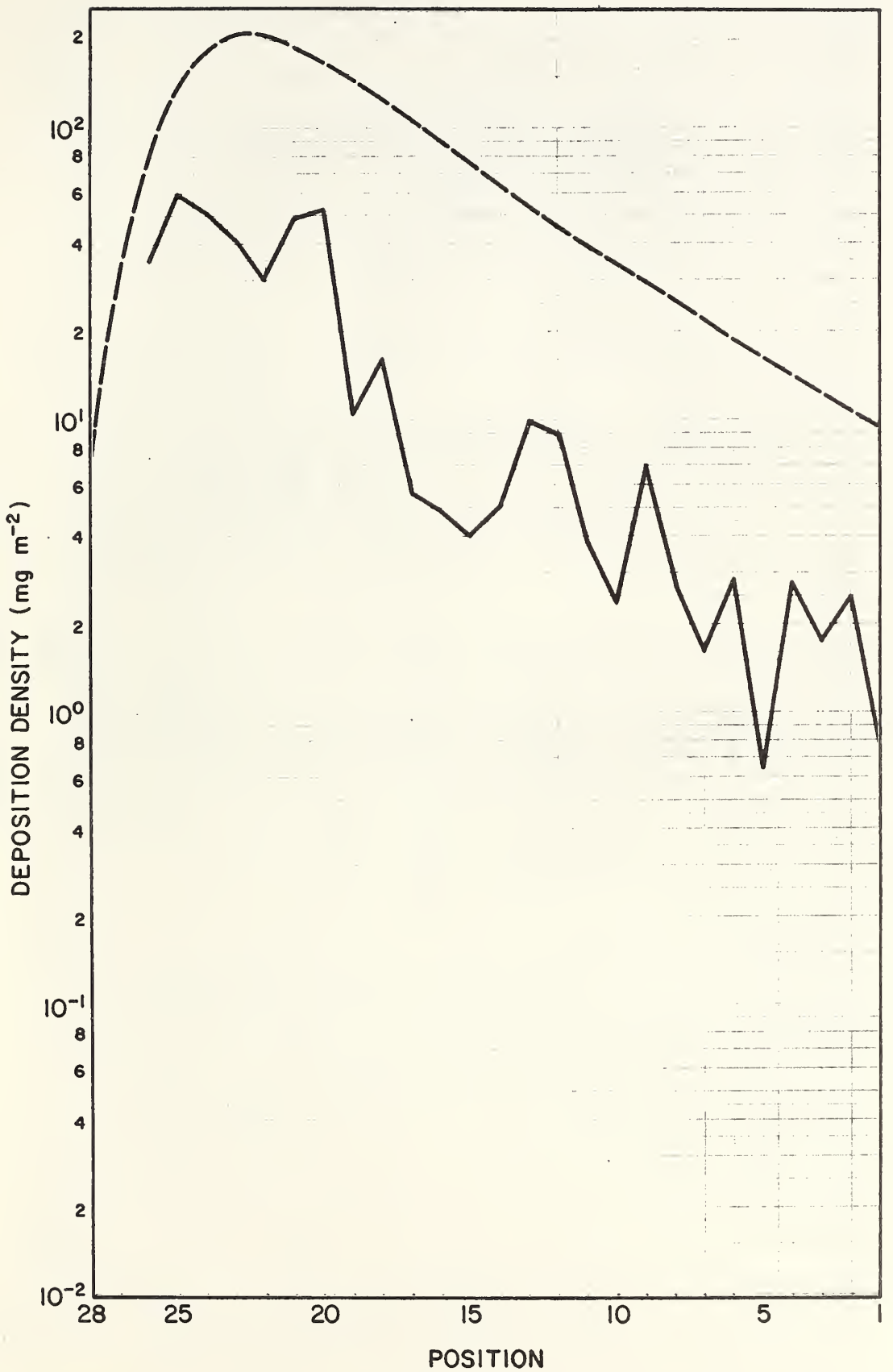

FIGURE A-26. Predicted (dashed line) versus measured deposition densities for Row 2, Trial 5 of the Rennic Creek Trials.

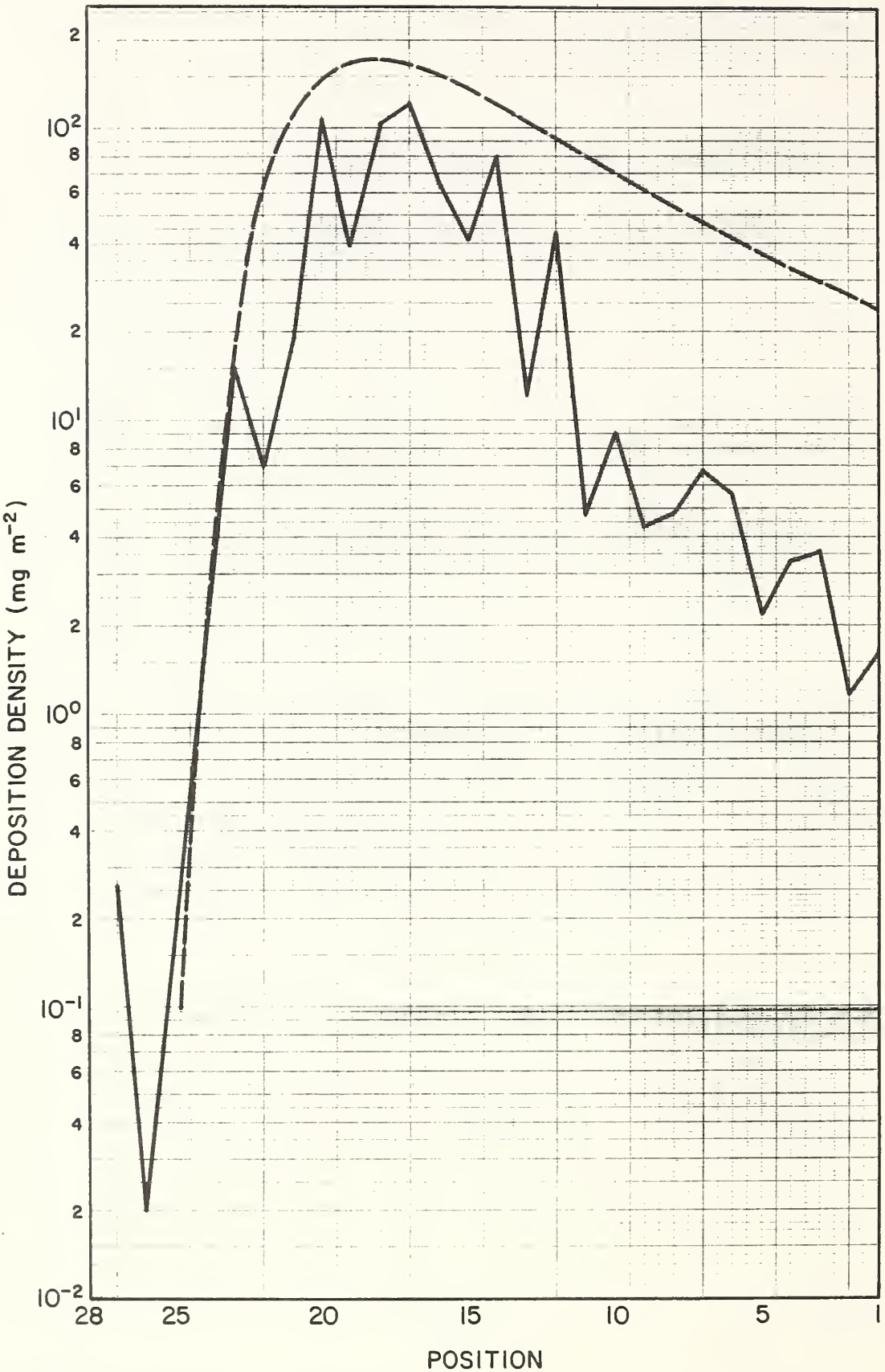

FIGURE A-27. Predicted (dashed line) versus measured deposition densities for Row 3, Trial 5 of the Rennic Creek Trials.

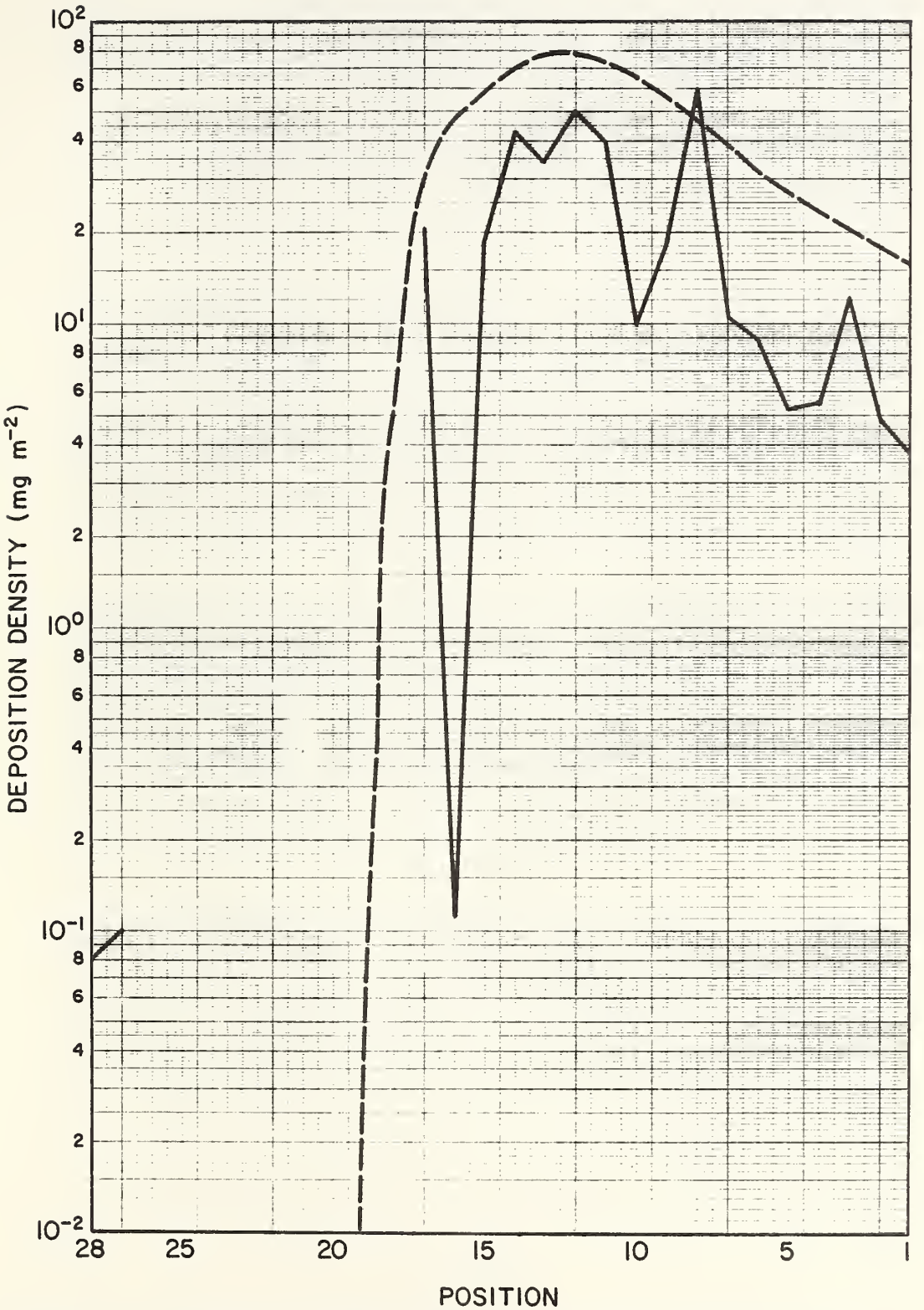

FIGURE A-28. Predicted (dashed line) versus measured deposition densities for Row 4, Trial 5 of the Rennic Creek Trials.

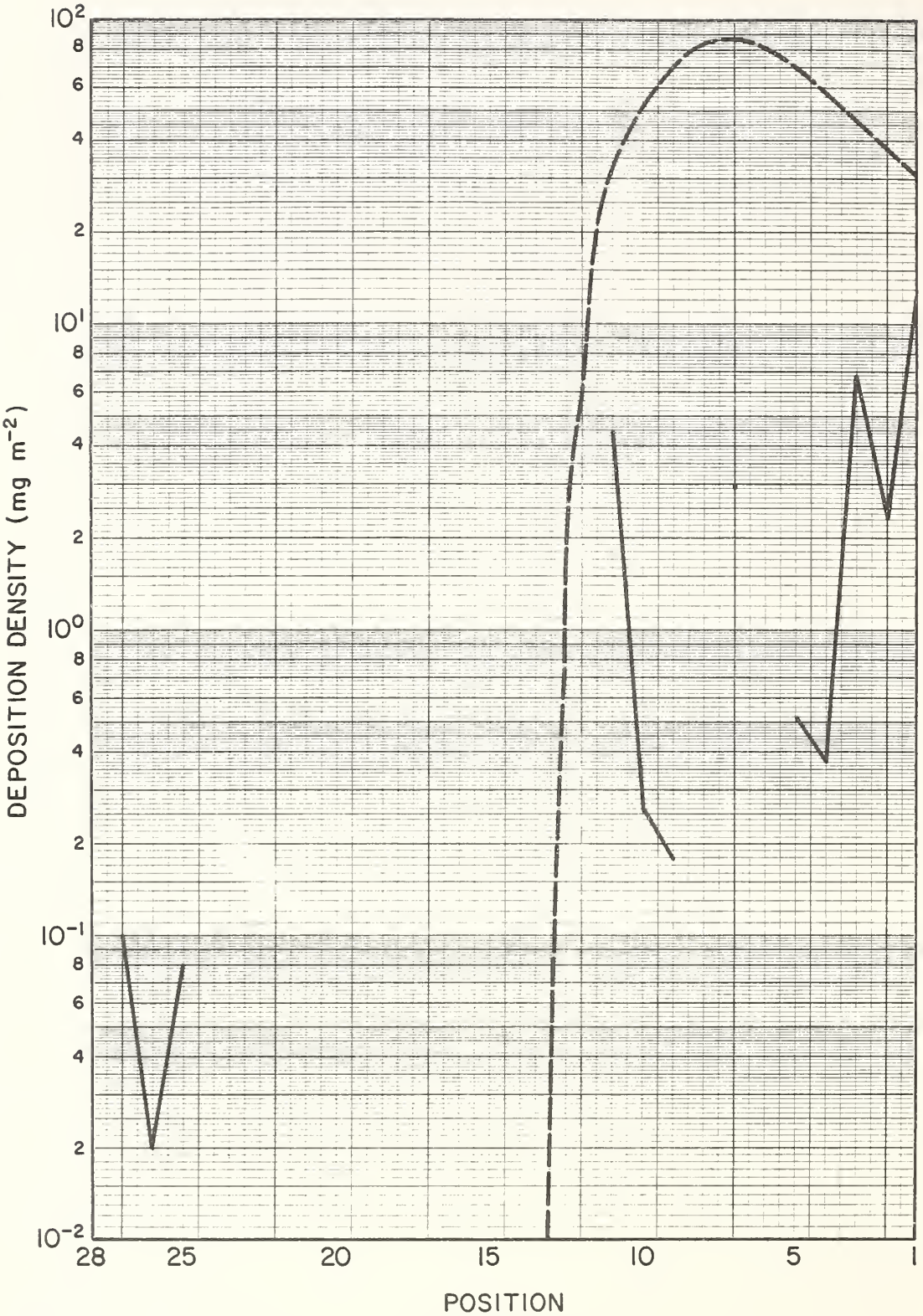

FIGURE A-29. Predicted (dashed line) versus measured deposition densities for Row 5, Trial 5 of the Rennic Creek Trials.

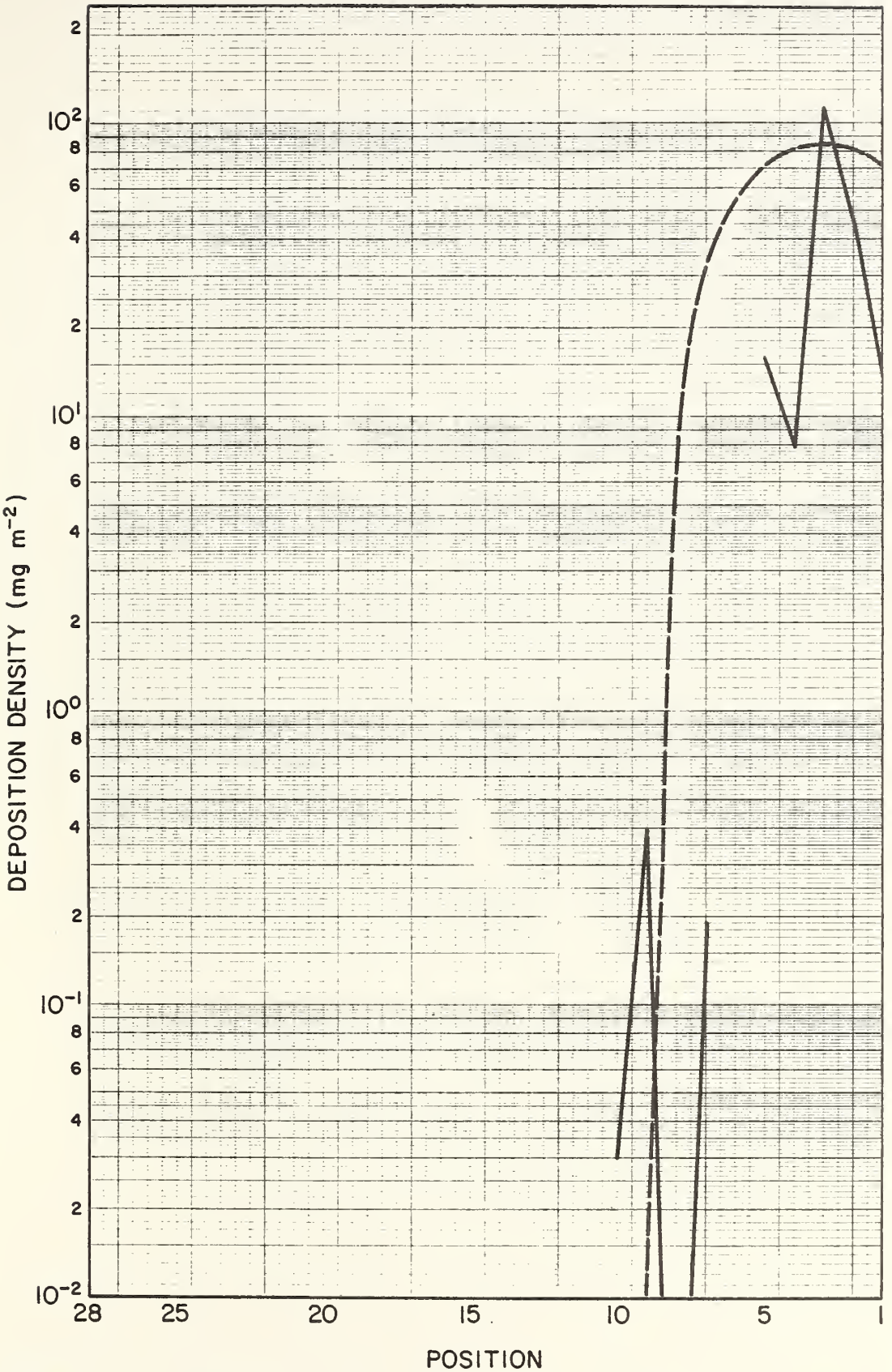

FIGURE A-30. Predicted (dashed line) versus measured deposition densities for Row 6, Trial 5 of the Rennic Creek Trials.

APPENDIX B

MATHEMATICAL BASIS OF THE DRIFT AND DEPOSITION MODELS

The drift and deposition models for aerial spray releases respectively given by Equations (2-1) and (2-24) in the main body of the text are derived from the Gaussian dosage formula for an instantaneous volume source with a modified vertical term to account for gravitational settling as well as reflection of the spray drops at the earth's surface and at the base of an elevated inversion. To account for gravitational settling, the alongwind axis of the spray cloud is assumed to intersect the ground or the top of the forest canopy at a distance proportional to the product of the release height H' and mean cloud transport speed $\bar{u}$ divided by the settling velocity V_j for the j^{th} drop-size category (see Pasquill 1974, p. 146). Spray drops that come in contact with the base of an elevated inversion are assumed to be completely reflected (see Slade 1968, p. 346) while the spray drops that intersect the ground or the top of a forest canopy are subject to either complete or partial reflection (Dumbauld et al., 1976). With these assumptions, the dosage for an instantaneous volume source is given by the expression

$$D_V\{x,y,z\} = \frac{Q_V}{2\pi\,\sigma_y\sigma_z\bar{u}} \left\{\exp\left[-\frac{1}{2}\left(\frac{y}{\sigma_y}\right)^2\right]\right\}$$

$$\sum_{j=1}^{J} f_j \left\{ \sum_{i=0}^{\infty} \left[\gamma_j^{\,i} \exp\left[-\frac{1}{2}\left(\frac{2iH_m - H' + z + V_j x/\bar{u}}{\sigma_z}\right)^2\right] \right.\right. \quad \text{(B-1)}$$

$$\left.\left. + \gamma_j^{\,i+1} \exp\left[-\frac{1}{2}\left(\frac{2iH_m + H' + z - V_j x/\bar{u}}{\sigma_z}\right)^2\right]\right]\right.$$

$$+ \sum_{i=1}^{\infty} \left[\gamma_j^{\,i} \exp\left[-\frac{1}{2} \left(\frac{2iH_m + H' - z - V_j x/\bar{u}}{\sigma_z} \right)^2 \right] \right. \qquad \text{(B-1)}$$

(Continued)

$$\left. + \gamma_j^{\,i-1} \exp\left[-\frac{1}{2} \left(\frac{2iH_m - H' - z + V_j x/\bar{u}}{\sigma_z} \right)^2 \right] \right] \Bigg\}$$

where

Q_V = source strength of the volume source

σ_y = standard deviation of the crosswind spray distribution

σ_z = standard deviation of the vertical spray distribution

x,y,z = the alongwind, crosswind and vertical coordinates of the point at which the dosage is calculated

and the remaining parameters are defined on pages 10 and 11 of the main text. For convenience in writing Equation (B-1), 0^0 is defined to be equal to unity.

We assume that the lateral and vertical growth of the spray cloud due to turbulent mixing is rectilinear. The expressions for σ_y and σ_z are

$$\sigma_y = \sigma_A' (x + x_V) \qquad \text{(B-2)}$$

$$\sigma_z = \sigma_E' (x + x_V) = \frac{1}{k} \sigma_A' (x + x_V) \qquad \text{(B-3)}$$

where σ_A', σ_E', x_V and k are defined on page 10. The amount of spray material deposited on the ground or entering the forest canopy through gravitational

settling is obtained from the expression

$$Dep_V = \frac{Q_V}{\sqrt{2\pi}\,\sigma_y}\left\{\exp\left[-\frac{1}{2}\left(\frac{y}{\sigma_y}\right)^2\right]\right\}\sum_{j=1}^{J}\left\{\frac{d}{dx}\left[\frac{1}{\sqrt{2\pi}\,\sigma_z}\int_{-\infty}^{o} A\{z\}dz\right]\right\}$$

where $A\{z\}$ is the term following the first summation sign in Equation (B-1). After substituting Equations (B-2) and (B-3) for σ_y and σ_z into the equation for deposition and performing the indicated differentiation and integration, the deposition equation takes the form

$$Dep_V = \frac{k\,Q_V}{2\pi(\sigma'_A)^2\,(x+x_V)^3}\left\{\exp\left[-\frac{1}{2}\left(\frac{y}{\sigma'_A(x+x_V)}\right)^2\right]\right\} \tag{B-4}$$

$$\sum_{j=1}^{J} f_j\,(1-\gamma_j)\left\{M + N\right\}$$

where

$$M = \left\{H' + (V_j\,x_V/\bar{u})\right\}\left\{\exp\left[-\frac{k^2}{2}\left(\frac{H'-(V_j x/\bar{u})}{\sigma'_A(x+x_V)}\right)^2\right]\right\} \tag{B-5}$$

$$N = \sum_{i=1}^{\infty}\gamma_j^{\,i-1}\left\{\left[2iH_m - H' - (V_j x_V/\bar{u})\right]\left[\exp\left(-\frac{k^2}{2}\left(\frac{2iH_m - H' + (V_j x/\bar{u})}{\sigma'_A\,(x+x_V)}\right)^2\right)\right]\right. \tag{B-6}$$

$$\left. + \gamma_j\left[2iH_m + H' + (V_j x_V/\bar{u})\right]\left[\exp\left(-\frac{k^2}{2}\left(\frac{2iH_m + H' - (V_j x/\bar{u})}{\sigma'_A\,(x+x_V)}\right)^2\right)\right]\right\}$$

Expressions similar to Equations (B-1) and (B-6) have been used successfully for several years to predict the dosage and deposition downwind

from nearly instantaneous sources in work performed for the U. S. Army (Cramer, et al., 1972; Dumbauld, Rafferty and Cramer, 1976).

The expressions for drift and deposition downwind from a line source oriented at an arbitrary angle θ with the wind direction are derived through consideration of the line source geometry shown in Figure B-1, which is similar to Figure 2-1 on page 7. In Figure B-1, a finite line source of length L is directed along the δ coordinate at height H' with one end of the line source at the point (ε=0, δ=0, z=H'). From the geometry shown in Figure B-1,

$$x = x'-g = x'-\delta'\sin\theta \tag{B-7}$$

$$x' = (\varepsilon+\delta\tan\theta)\cos\theta \tag{B-8}$$

$$y = \frac{\delta'+m-\delta}{\cos\theta} = \delta'\cos\theta+x'\tan\theta-(\delta/\cos\theta) \tag{B-9}$$

When Equations (B-7), (B-8) and (B-9) are substituted for x,x' and y in Equations (B-1) and (B-4), the dosage at point R downwind from the line source is

$$D_\ell = \int_o^L D_V \, d\delta' \tag{B-10}$$

and the deposition at point R is

$$Dep_L = \int_o^L Dep_V \, d\delta' \tag{B-11}$$

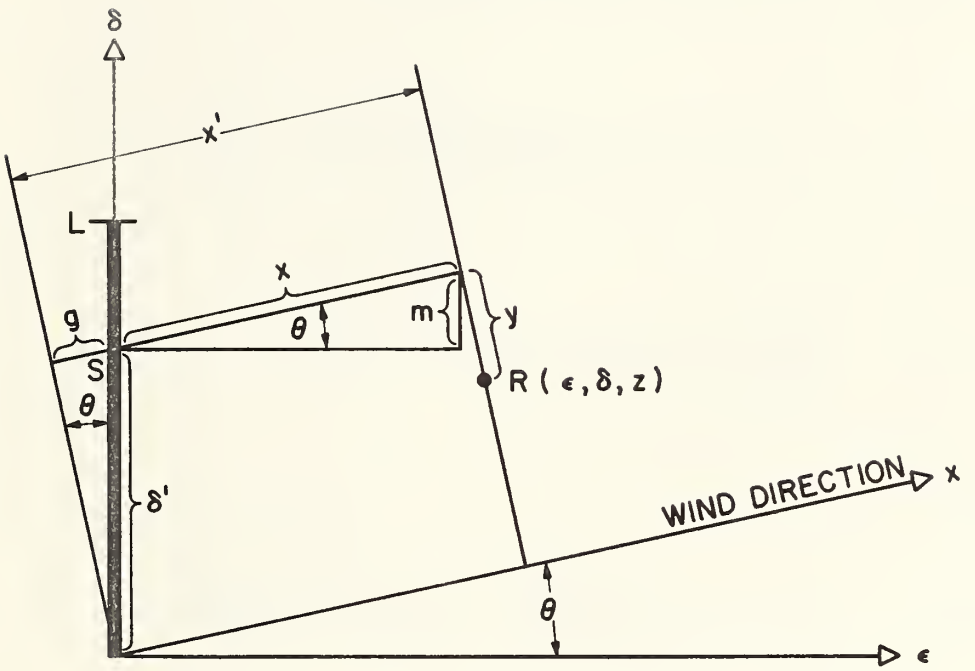

FIGURE B-1. Line source geometry

As an example of the procedures used in performing the required integration over L to obtain dosage and deposition at the point R, the derivation for deposition downwind from the line source is outlined below. Substituting for y and x in Equations (B-4), (B-5) and (B-6) we obtain

$$Dep_L = \int_o^{\ell} \frac{k\,Q}{L\,2\pi\,(\sigma_A')^2\,(x'-\delta\sin\theta+x_V)^3}$$

$$\left\{ \exp\left[-\frac{1}{2}\left(\frac{\delta'\cos\theta+x'\tan\theta-(\delta/\cos\theta)}{\sigma_A'\,(x'-\delta'\sin\theta+x_V)} \right)^2 \right] \right\} \qquad \text{(B-12)}$$

$$\sum_{j=1}^{J} \left\{ f_j\,(1-\gamma_j) \left[M_L\{j\} + N_L\{j\} \right] \right\} d\delta'$$

where

$$M_L\{j\} = \left\{ H'+(V_j x_V/\bar{u}) \right\} \left\{ \exp\left[-\frac{k^2}{2} \left(\frac{H'-\left(\frac{V_j(x'-\delta'\sin\theta)}{\bar{u}}\right)}{\sigma_A'\,(x'-\delta\sin\theta+x_V)} \right)^2 \right] \right\} \qquad \text{(B-13)}$$

$$N_L\{j\} = \sum_{i=1}^{\infty} \gamma_j^{\,i-1} \left\{ \left[2iH_m - H' - (V_j x_V/\bar{u}) \right] \right. \qquad \text{(B-14)}$$

$$\left. \left[\exp\left(-\frac{k^2}{2} \left(\frac{2iH_m - H' + \left(\frac{V_j(x'-\delta'\sin\theta)}{\bar{u}}\right)}{\sigma_A'\,(x'-\delta'\sin\theta+x_V)} \right)^2 \right) \right] + \right.$$

$$+\gamma_j \left[2iH_m + H' + (V_j x_V/\bar{u}) \right] \qquad \text{(B-14) (Continued)}$$

$$\left[\exp\left(-\frac{k^2}{2} \left(\frac{2iH_m + H' - \left(\frac{V_j (x' - \delta' \sin\theta)}{\bar{u}} \right)}{\sigma'_A \, (x' - \delta' \sin\theta + x_V)} \right)^2 \right) \right]$$

$Q = L\,Q_V$ = total source strength

$$\ell = \begin{cases} \delta + \varepsilon \cot\theta; & \delta + \varepsilon \cot\theta \leq L \\ L \quad\quad ; & \delta + \varepsilon \cot\theta > L \end{cases} \qquad \text{(B-15)}$$

Let: $S = \dfrac{Qk}{2\pi L}$

$$A = \sqrt{2}\,\sigma'_A \,(x' - \delta' \sin\theta + x_V) \qquad \text{(B-16)}$$

$$B = H' + (V_j x_V/\bar{u}) \qquad \text{(B-17)}$$

$$C = 2iH_m - H' - (V_j x_V/\bar{u}) \qquad \text{(B-18)}$$

$$D = 2iH_m + H' + (V_j x_V/\bar{u}) \qquad \text{(B-19)}$$

Equation (B-12) can be restated in the form

$$\mathrm{Dep}_L = \frac{-2S}{\sin\theta}\sum_{j-1}^{J}\left\{ f_j(1-\gamma_j)\int_a^b \frac{1}{A^3}\left\{\left\{ \exp\left[-\frac{1}{A^2}\left(x'\cot\theta + x_V\cot\theta - \frac{A\cot\theta}{\sqrt{2}\,\sigma'_A} + x'\tan\theta - \frac{\delta}{\cos\theta}\right)^2\right]\right\}\right.\right.$$

$$\left\{ B\exp\left[-\frac{k^2}{A^2}\left(H' + \frac{V_j x_V}{\bar{u}} - \frac{V_j A}{\sqrt{2}\,\sigma'_A\,\bar{u}}\right)^2\right]\right. \qquad \text{(B-20)}$$

$$+\sum_{i=j}^{\infty}\gamma_j^{\,i-1}\left\{ C\exp\left[-\frac{k^2}{A^2}\left(2iH_m - H' - \frac{V_j x_V}{\bar{u}} + \frac{V_j A}{\sqrt{2}\,\sigma'_A}\right)^2\right]\right.$$

$$\left.\left.\left.\left. + \gamma_j\, D\exp\left[-\frac{k^2}{A^2}\left(2iH_m + H + \frac{V_j x_V}{\bar{u}} - \frac{V_j A}{\sqrt{2}\,\sigma'_A\,\bar{u}}\right)^2\right]\right\}\right\}\right\} dA\right\}$$

or,

$$\mathrm{Dep}_L = \frac{-2S}{\sin\theta}\sum_{j=1}^{J}\left\{ f_j(1-\gamma_j)\left\{\int_a^b \frac{B}{A^3}\exp\left[-k^2\left(\frac{B}{A} - p\right)^2\right]\exp\left[-\left(\frac{N}{A} - q\right)^2\right] dA\right.\right.$$

$$+\sum_{i=1}^{\infty}\int_a^b \gamma_j^{\,i-1}\left\{\frac{C}{A^3}\exp\left[-k^2\left(\frac{C}{A} + p\right)^2\right]\exp\left[-\left(\frac{N}{A} - q\right)^2\right]\right. \qquad \text{(B-21)}$$

$$\left.\left.\left. + \frac{\gamma_j D}{A^3}\exp\left[-k^2\left(\frac{D}{A} - p\right)^2\right]\exp\left[-\left(\frac{N}{A} - q\right)^2\right]\right\} dA\right\}\right\}$$

where

$$N = (x'+x_V)\cot\theta + x'\tan\theta - \frac{\delta}{\cos\theta}$$

$$p = V_j/(\sqrt{2}\,\sigma_A'\,\bar{u})$$

$$q = \cot\theta/(\sqrt{2}\,\sigma_A')$$

$$a = \sqrt{2}\,\sigma_A'\,(x'+x_V)$$

$$b = \sqrt{2}\,\sigma_A'\,(x'+x_V-\ell\,\sin\theta)$$

Squaring the arguments of the exponentials and collecting terms, we obtain the following restatement of Equation (B-21):

$$\mathrm{Dep}_L = \frac{-2S}{\sin\theta}\sum_{j=1}^{J}\left\{f_j(1-\gamma_j)\left\{\int_a^b \frac{B}{A^3}\exp\left[-\left(\frac{F}{A^2}-\frac{G}{A}+P\right)\right]dA\right.\right.$$

$$+\sum_{i=1}^{\infty}\gamma_j^{\,i-1}\left\{\int_a^b \frac{C}{A^3}\exp\left[-\left(\frac{I}{A^2}-\frac{J}{A}+P\right)\right]dA\right. \qquad \text{(B-22)}$$

$$\left.\left.\left.+\int_a^b \frac{\gamma_j D}{A^3}\exp\left[-\left(\frac{E}{A^2}-\frac{K}{A}+P\right)\right]dA\right\}\right\}\right\}$$

where

$$F = k^2B^2 + N^2$$

$$G = 2\left[pBk^2 + Nq\right]$$

$$P = p^2k^2 + q^2$$

$$I = k^2C^2 + N^2$$

$$J = -2\left[pCk^2 - Nq\right]$$

$$E = k^2D^2 + N^2$$

$$K = 2\left[pDk^2 + Nq\right]$$

Completing the squares for the three exponential terms in Equation (B-22), we obtain the expression

$$\begin{aligned} Dep_L = \frac{-2S}{\sin\theta} \sum_{j=1}^{J} \Bigg\{ f_j(1-\gamma_j) \Bigg\{ \int_a^b \frac{B}{A^3} \exp\left[-F\left(\frac{1}{A} - \frac{G}{2F}\right)^2 \right] \exp\left[\frac{G^2}{4F} - P \right] dA \\ + \sum_{i=1}^{\infty} \gamma_j^{\,i-1} \Bigg\{ \int_a^b \frac{C}{A^3} \exp\left[-I\left(\frac{1}{A} - \frac{J}{2I}\right)^2 \right] \exp\left[\frac{J^2}{4I} - P \right] dA \\ + \int_a^b \frac{\gamma_j D}{A^3} \exp\left[-E\left(\frac{1}{A} - \frac{K}{2E}\right)^2 \right] \exp\left[\frac{K^2}{4E} - P \right] dA \Bigg\} \Bigg\} \Bigg\} \end{aligned} \qquad \text{(B-23)}$$

If we let

$$R' = \sqrt{F}\left(\frac{1}{A} - \frac{G}{2F}\right)$$

$$S' = \sqrt{I}\left(\frac{1}{A} - \frac{J}{2I}\right)$$

$$T' = \sqrt{E}\left(\frac{1}{A} - \frac{K}{2E}\right)$$

Equation (B-23) becomes

$$Dep_L = \frac{2S}{\sin\theta} \sum_{j=1}^{J} \Bigg\{ f_j (1-\gamma_j) \Bigg\{ \frac{B}{\sqrt{F}} \exp\left[\frac{G^2}{4F} - P\right] \Bigg(\int_{a'}^{b'} \frac{R'}{\sqrt{F}} \exp\left[-R'^2\right] dR' +$$

$$+ \frac{G}{2F} \int_{a'}^{b'} \exp\left[-R'^2\right] dR' \Bigg) + \sum_{i=1}^{\infty} \gamma_j^{i-1} \Bigg\{ \frac{C}{\sqrt{I}} \exp\left[\frac{J^2}{4I} - P\right]$$

$$\times \Bigg(\int_{a''}^{b''} \frac{S'}{\sqrt{I}} \exp\left[-S'^2\right] dS' + \int_{a''}^{b''} \frac{J}{2I} \exp\left[-S'^2\right] \Bigg)$$

$$+ \frac{\gamma_j D}{\sqrt{E}} \exp\left[\frac{K^2}{4E} - P\right] \Bigg(\int_{a'''}^{b'''} \frac{T'}{\sqrt{E}} \exp\left[-T'^2\right] dT' + \int_{a'''}^{b'''} \frac{\dot{K}}{2E} \exp\left[-T'^2\right] dT' \Bigg) \Bigg\} \Bigg\} \Bigg\}$$

where

$$a' = \sqrt{F}\left(\frac{1}{a} - \frac{G}{2F}\right)$$

$$a'' = \sqrt{I}\left(\frac{1}{a} - \frac{J}{2I}\right)$$

$$a''' = \sqrt{E}\left(\frac{1}{a} - \frac{J}{2E}\right)$$

$$b' = \sqrt{F}\left(\frac{1}{b} - \frac{G}{2F}\right)$$

$$b'' = \sqrt{I}\left(\frac{1}{b} - \frac{J}{2I}\right)$$

$$b''' = \sqrt{E}\left(\frac{1}{b} - \frac{K}{2E}\right)$$

Finally, performing the integration using the definition of an error function, the analytic solution is

$$\text{Dep}_L = \frac{2S}{\sin\theta} \sum_{j=1}^{J} \Bigg\{ f_j (1-\gamma_j) \Bigg\{ \frac{B}{2F} \exp\left(\frac{G^2}{4F} - P\right) \left(\exp\left[-(a')^2\right] - \exp\left[-(b')^2\right] \right)$$

$$+ \frac{GB\sqrt{\pi}}{4F^{3/2}} \exp\left(\frac{G^2}{4F} - P\right) \left(\text{erf } b' - \text{erf } a' \right) + \sum_{i=1}^{\infty} \gamma_j^{\,i-1} \Bigg\{ \frac{C}{2I} \exp\left[\frac{J^2}{4I} - P\right]$$

$$\left(\exp\left[-(a'')^2\right] - \exp\left[-(b'')^2\right] \right) + \frac{JC\sqrt{\pi}}{4I^{3/2}} \exp\left[\frac{J^2}{4I} - P\right] \qquad \text{(B-24)}$$

$$\left(\text{erf } b'' - \text{erf } a'' \right) + \frac{\gamma_j D}{2E} \exp\left[\frac{K^2}{4E} - P\right]$$

$$\left(\exp\left[-(a''')^2\right] - \exp\left[-(b''')^2\right] \right) + \frac{KD\sqrt{\pi}\,\gamma_j}{4E^{3/2}} \exp\left[\frac{K^2}{4E} - P\right]$$

$$\left(\text{erf } b''' - \text{erf } a''' \right) \Bigg\} \Bigg\} \Bigg\} \Bigg\}$$

which is identical to Equation (2-24) in the main body of the report. A similar procedure can be used to derive Equation (2-1) for drift downwind from a line source.